Targeting the DNA damage response protein ATR kinase in pancreatic cancer

Charles Ross Dunlop

Darwin College

Cancer Research UK Cambridge Institute

University of Cambridge

This dissertation is submitted for the degree of

Doctor of Philosophy

May 2020

DECLARATION

This thesis is the result of my own work and includes nothing which is the outcome of work done in collaboration except as declared in the preface and specified in the text.

It is not substantially the same as any work that has already been submitted before for any degree or other qualification except as declared in the preface and specified in the text.

It does not exceed the prescribed 60,000 word limit for the Clinical Medicine and Clinical Veterinary Medicine Degree Committee.

ABSTRACT

Name: Charles Ross Dunlop

Title: Targeting the DNA damage response protein ATR kinase in pancreatic cancer

Therapeutic targeting of the DNA damage response (DDR), coupled with the implementation of personalised treatment strategies, has the potential to improve the poor survival outcomes of pancreatic ductal adenocarcinoma (PDAC). Many common genetic alterations in PDAC augment replication-associated DNA damage, or replication stress (RS), which increases reliance on the RS-response factor, Ataxia Telangiectasia and Rad3-related (ATR) kinase. Furthermore, many chemotherapies used in the treatment of PDAC increase RS, leading to ATR activation which limits the efficacy of these therapies. Therefore, there is good rationale for targeting ATR as a strategy for treatment of patients with PDAC. In this thesis, I report on investigations into the therapeutic potential of combining the ATR inhibitor, AZD6738, with DNA-damaging drugs and DDR-targeted agents in preclinical models of PDAC. My primary focus was on maximising the efficacy of combined ATR inhibition and gemcitabine (ATRi/gem). I hypothesised that ATRi/gem would most likely benefit specific sub-groups of patients with pre-existing aberrations in DDR pathways (i.e. a precision medicine approach to patient selection). Accordingly, I investigated the potential for deficiency in the double-strand-break master-regulator, Ataxia Telangiectasia Mutated (ATM), to sensitise PDAC models to ATRi/gem. I found that complete loss of ATM function - through kinase inhibition or through CRISPR knockout, but not ATM depletion by RNA interference - sensitised to ATRi and ATRi/gem in PDAC models. Using flow cytometry and quantitative image-based cytometry, I gained insight into the mechanisms by which AZD6738 and gemcitabine synergise, finding evidence for replication catastrophe that was significantly augmented in ATM-deficient cells. *In vivo*, I demonstrated that low-dose gemcitabine can be used to sensitise to AZD6738, much more effectively in an ATM-deficient setting. My results suggest that ATM-deficiency augments the replication catastrophe-mediated cell death induced by ATRi/gem, thus ATM-loss could predict response to this combination. The preclinical assessments of AZD6738 and gemcitabine that formed part of this project have led to the launch of a phase-I clinical trial (ATRiUM; NCT03669601). My data indicate that ATM status should be carefully assessed in tumours from patients with PDAC, since the distinction between ATM-low and ATM-null could be crucial in maximising the success of trials using ATM expression as a predictive biomarker. In this dissertation, I also present my investigations into the combination of AZD6738 with the poly(ADP-ribose) polymerase (PARP) inhibitor, olaparib. While AZD6738 and olaparib synergistically inhibited the growth of PDAC cells proficient in homologous recombination (HR) *in vitro*, I identified no anti-tumour effect in HR-proficient *in vivo* models. This could indicate that a DDR deficiency would be necessary for this combination to be most effective in PDAC, a hypothesis that will be tested in the clinic in the Precision-Panc trial, PRIMUS-004.

ACKNOWLEDGEMENTS

Firstly, I would like to thank Professor Duncan Jodrell and Dr Frances Richards for giving me the opportunity to work in the Pharmacology & Drug Development Group at the Cancer Research UK Cambridge Institute, and for providing excellent supervision over the four years. Thank you to all members of the Jodrell lab, past and present, for your support. A special thanks in particular to Dr Yann Wallez, your mentorship when I first started was invaluable and I am extremely grateful for the guidance you provided me with in the early days of my PhD. I have been very lucky to work in a well-resourced institute, and owe a massive thanks to the Core Facility teams who make it such an excellent place to do research. Thank you to the funders Cancer Research UK and Pancreatic Cancer UK for making this research possible. Thanks also to those within AstraZeneca who I had the opportunity to collaborate with during my time here. Outside of the lab I must also thank my housemates plus all my fellow crew and committee members at Darwin College Boat Club, for making my time as a Cambridge student such an enjoyable experience. Thank you to my parents for supporting me for all these years. And finally, to Magda. The most generous person I know, your kindness and support has meant the world to me over these past years. Thank you.

CONTENTS

ABBREVIATIONS

5-FU	5-fluorouracil
A-T	Ataxia-telangiectasia
ATM	Ataxia Telangiectasia Mutated
ATR	Ataxia Telangiectasia and Rad3-related
ATRi/gem	Combined ATR inhibition and gemcitabine
BER	Base excision repair
DDR	DNA damage response
dFdC	2',2'-difluoro 2'-deoxycytidine = gemcitabine
dFdCDP	Gemcitabine diphosphate
dFdCTP	Gemcitabine triphosphate
DNA-PKcs	DNA-dependent Protein Kinase catalytic subunit
dNTP	Deoxynucleoside triphosphate
DSB	Double-strand break
FdUMP	Fluorodeoxyuridine monophosphate
FdUTP	Fluorodeoxyuridine triphosphate
FUTP	Fluorouridine triphosphate
GEMM	Genetically engineered mouse model
HR	Homologous recombination
IHC	Immunohistochemistry
IR	Ionising radiation
KAP1	KRAB-associated protein 1
KPC mouse	Lox-Stop-Lox (LSL)-*Kras*^{G12D}; LSL-*Trp53*^{R172H}; *Pdx1-cre* mouse
mOS	Median overall survival
MRN	MRE11–RAD50–NBS1
MRP	Multidrug resistance protein
NGS	Next-generation sequencing
NHEJ	Non-homologous end-joining
PanIN	Pancreatic intraepithelial neoplasms
PAR	Poly(ADP-ribose)
PARP	Poly(ADP-ribose) polymerase
PBSTT	Phosphate-buffered saline, 0.1% Triton X-100, 0.1% Tween-20
PDAC	Pancreatic ductal adenocarcinoma
PK	Pharmacokinetic
RC	Replication catastrophe
RPA	Replication protein A
RRM2	Ribonucleotide reductase M2
RS	Replication stress
SRB	Sulforhodamine B
SSB	Single-strand break
SSBR	Single-strand break repair
ssDNA	Single-stranded DNA

TCA	Trichloroacetic acid
TGI	Tumour growth inhibition
TME	Tumour microenvironment
TOP1	Topoisomerase I
UPLC-MS/MS	Ultra-performance liquid chromatography - tandem mass spectrometry

CHAPTER ONE: Introduction to pancreatic cancer and the DNA damage response

1.1. Pancreatic cancer biology

Pancreatic cancers can either be exocrine or endocrine, that is, adenocarcinomas of the ductal epithelium or neuroendocrine tumours of the islet cells, respectively. By far the most common of the two is the exocrine disease, pancreatic ductal adenocarcinoma (PDAC), which represents more than 90% of pancreatic cancers (McGuigan et al., 2018; Zhou et al., 2010). A highly lethal malignancy, the mortality rate of PDAC almost matches its incidence, and it is projected to become the second leading cause of cancer death by 2030 (Rahib et al., 2014).

PDAC is caused by the accumulation of genetic mutations. The most frequently mutated gene in PDAC is KRAS, with somatic mutations in >90% of cases (Bailey et al., 2016; Witkiewicz et al., 2015) (**Table 1.1**). The majority of these mutations affect residue G12 in the KRAS GTPase protein (Forbes et al., 2017), which causes constitutive activity and in turn aberrant stimulation of the RAF-MEK-ERK axis (Marais et al., 1995) as well as other pathways that promote proliferation. The tumour suppressor gene CDKN2A, which encodes $p16^{INK4a}$, is inactivated in over 90% of PDAC through either mutation or transcriptional silencing (Schutte et al., 1997), leading to loss of cell cycle regulation at the G1/S phase border. Additionally, somatic mutations in TP53 occur in 60-70% of cases (Bailey et al., 2016; Witkiewicz et al., 2015) and often abrogate the DNA-binding ability of p53, causing loss of its effector function as a transcriptional activator in response to cellular stresses such as DNA damage and hypoxia (Kern et al., 1992). The fourth most commonly mutated gene in PDAC is SMAD4, another tumour suppressor which, when functional, acts downstream of TGFβ family receptors to activate the expression of genes that promote growth inhibition (Cao et al., 2008; Dai et al., 1998). In addition to these four major drivers, numerous whole-genome-sequencing efforts investigating the genetic landscape of PDAC have identified mutations in hundreds of other genes, but at lower frequencies (Bailey et al., 2016; Biankin et al., 2012; Liu et al., 2018; Singhi et al., 2019). These include axon guidance pathway genes, chromatin remodellers and regulators of the DNA damage response.

Somatic KRAS mutation and loss of CDKN2A are early events during pancreas tumorigenesis, as evidence by their regular presence in low-grade PDAC precursor lesions known as pancreatic intraepithelial neoplasms (PanINs). Conversely, p53 alterations and loss of SMAD4

Pancreatic Adenocarcinoma (QCMG, Nature 2016) Mutated genes (383 profiled samples)		
Gene	#	Freq
KRAS	344	89.80%
TP53	253	66.10%
SMAD4	86	22.50%
CDKN2A	71	18.50%
ARID1A	29	7.60%
LRP1B	22	5.70%
RNF43	21	5.50%
KMT2C	21	5.50%
KMT2D	19	5.00%
TGFBR2	18	4.70%
ATM	14	3.70%
RBM10	14	3.70%
KDM6A	12	3.10%

Pancreatic Adenocarcinoma (TCGA, PanCancer Atlas) Mutated genes (179 profiled samples)		
Gene	#	Freq
KRAS	117	65.40%
TP53	107	59.80%
SMAD4	37	20.70%
CDKN2A	35	19.60%
RNF43	11	6.10%
GNAS	9	5.00%
ARID1A	9	5.00%
ATM	8	4.50%
TGFBR2	8	4.50%
RNF213	8	4.50%
RELN	7	3.90%
KDM6A	7	3.90%
KMT2D	7	3.90%

Table 1.1. The most frequently mutated cancer genes in PDAC. Two separate datasets are displayed. Left = Queensland Centre for Medical Genomics (QCMG) dataset, whole-genome and deep-exome sequencing analysis of 383 PDAC samples (Bailey et al., 2016). Right = The Cancer Genome Atlas (TCGA) dataset, 179 PDAC samples, https://www.cancer.gov/tcga (Liu et al., 2018). Frequency data downloaded from cbioportal.org (Cerami et al., 2012). Genes discussed in this chapter are highlighted in bold.

occur later, at the grade-3 PanIN stage which precedes invasion (**Fig. 1.1**) (Hruban et al., 2000; Kanda et al., 2012; Maitra et al., 2003). Low-grade PanINs (PanIN-1) are common, microscopic lesions that are often undetectable by standard imaging techniques. Meanwhile high-grade PanINs are less common and tend to be detected in pancreata that also have invasive PDAC (Kanda et al., 2012). Histologically, invasive PDAC tumours are characterised by a dense stroma that is made up of extracellular matrix proteins, fibroblasts and immune cells (Karamitopoulou, 2019). These stromal features of the human disease are mimicked in the widely used mouse model for PDAC, the Lox-Stop-Lox (LSL)-*Kras*^{G12D}; LSL-*Trp53*^{R172H}; *Pdx1-cre* (KPC) mouse (Hingorani et al., 2005), which also exhibits the clinical features of advanced disease, including loss of body condition, haemorrhagic ascites and metastases (Gopinathan et al., 2015). The desmoplastic stroma has been associated with therapy failure through a number of mechanisms, including the impairment of drug delivery (Jacobetz et al., 2013; Olive et al., 2009), establishment of immune privilege that abrogates anticancer T-cell responses (Feig et al., 2013) and alteration of host metabolism (Flint et al., 2016).

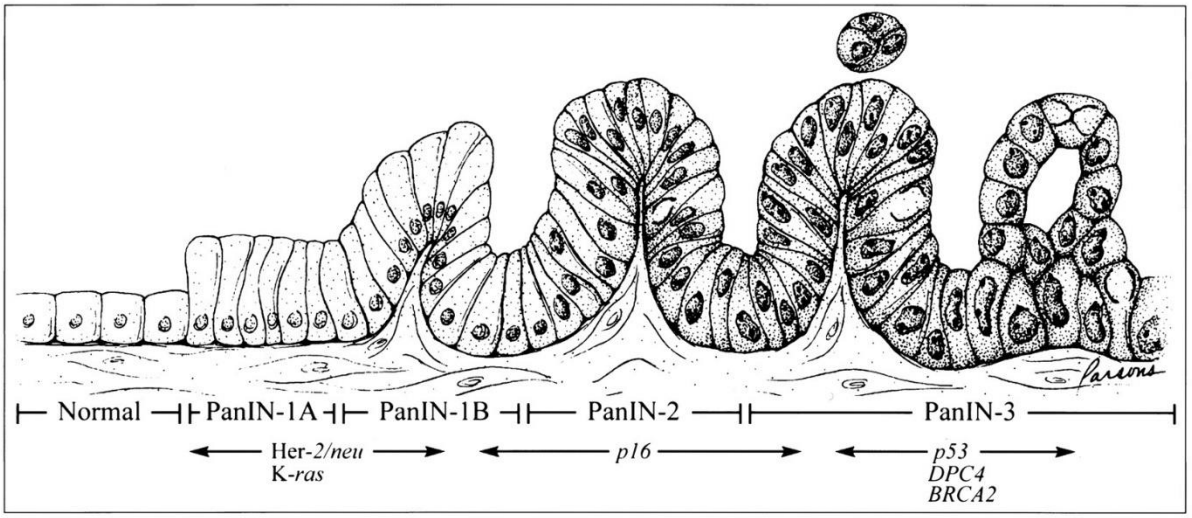

Fig. 1.1. Progression model for PDAC. KRAS mutation and loss of CDKN2A (p16) are early events during pancreas tumorigenesis, while p53 alterations and loss of SMAD4 (DPC4) occur later. Figure from Hruban et al., 2000.

1.2. Clinical management of PDAC

Most cases of PDAC are asymptomatic in the early stages. As a result, diagnoses are often made at a late stage when the main symptoms are abdominal pain and weight loss (Gullo et al., 2001; Kalser et al., 1985). While surgical resection can be curative in some cases, the late emergence of symptoms means that most patients have locally advanced or metastatic disease at presentation and are ineligible for surgery (Vincent et al., 2011). For the 15-20% of patients that do present with operable disease, the majority ultimately relapse with metastases (Griffin et al., 2015). The mainstay of treatment for metastatic PDAC is systemic chemotherapy. Since a 1997 clinical trial which showed that gemcitabine monotherapy outperformed 5-fluorouracil (5-FU) monotherapy in terms of median overall survival (5.65 months vs 4.41 months) (Burris et al., 1997), gemcitabine has been used extensively in the treatment of patients with PDAC. Gemcitabine, or 2',2'-difluoro 2'-deoxycytidine (dFdC), is a nucleoside analogue that requires intracellular phosphorylation for its activity. dFdC is initially phosphorylated by deoxycytidine kinase to give the mono-phosphate, which is sequentially phosphorylated to yield the diphosphate (dFdCDP) and triphosphate (dFdCTP) forms that induce cytotoxicity (Mini et al., 2006). dFdCDP irreversibly inhibits one of the key enzymes that mediates synthesis of deoxyribonucleotides, ribonucleotide reductase, leading to a reduction in the cellular pool of deoxynucleoside triphosphates (dNTPs) (Mini et al., 2006; Montano et al., 2017). dFdCTP is incorporated into nascent DNA to halt chain elongation (Huang et al., 1991; Plunkett et al., 1995). Both mechanisms inhibit DNA synthesis, which underlies the toxicity that gemcitabine

has in highly proliferative tissues such as neoplasms. While the prodrug, dFdC, has a short terminal plasma half-life of 42-94 minutes, the intracellular half-lives of the active metabolites dFdCDP and dFdCTP are reported to be up to 19 hours (GEMZAR FDA label).

In recent years, combinatorial chemotherapy regimens have been incorporated into the clinical management of PDAC, replacing single-agent therapy. The plasticity of pancreatic cancer, and indeed all solid tumours, enables therapeutic adaptation to single-agent treatments, while tumour heterogeneity allows pre-existing, drug-resistant clones to frequently emerge in patients receiving monotherapy. Combination therapy, meanwhile, aims to overcome some of these obstacles. Delivering two or more anticancer agents at once can combat the plasticity that drives therapeutic adaptation and also reduces the likelihood that multi-drug resistant clone will expand from the tumour. In 2011, it was shown that combining gemcitabine with albumin-bound paclitaxel (nab-paclitaxel), an anti-mitotic agent, marginally improved survival in PDAC patients. The combination group showed 8.5 months median overall survival (mOS) compared to 6.7 months in the gemcitabine monotherapy group (Von Hoff et al., 2013). The combinatorial regimen FOLFIRINOX (5-FU, leucovorin, irinotecan and oxaliplatin) was also found to be superior to gemcitabine-alone, giving a mOS of 11.1 months vs 6.8 months (Conroy et al., 2011). One of the advantages of a multi-drug cocktail such as FOLFIRINOX is that, while 5-FU, irinotecan and oxaliplatin are all DNA-damaging agents (and the compounding effect of this additive damage may enhance cell kill) they each have distinct mechanisms of action and therefore may each target distinct cell pools within a heterogenous PDAC tumour (cells which are not killed by the 5-FU may be killed by the oxaliplatin, etc). As for the gemcitabine and nab-paclitaxel combination, preclinical data suggest that the antitumor effect of these drugs is supra-additive (or *synergistic*) since nab-paclitaxel decreases cytidine deaminase levels, stabilising gemcitabine (Frese et al., 2012). Another reason for favouring combination therapy is the possibility to use each drug at lower concentrations, such that toxic side effects are minimised (provided the toxicities of each drug are not overlapping), thereby increasing the therapeutic window. Though combinatorial chemotherapy regimens such as FOLFIRINOX represent an improvement in patient outcome compared to gemcitabine monotherapy, they still only offer a mOS of less than a year, highlighting the need for better therapeutic approaches. This need could be met through more rational drug combinations, that is, using insight into the molecular pathways that contribute to tumour cell survival or therapy response to inform the drug combination (Boshuizen and Peeper, 2020). The majority of chemotherapy currently used in the treatment of PDAC comprises genotoxic agents, thus their

efficacy may be improved by targeting the cellular processes that respond to and repair DNA damage.

1.3. The DNA damage response

DNA in cells is constantly subjected to various forms of damage. From external insults such as UV radiation, to cell-derived stresses such as free radicals, the integrity of the genome is under frequent attack. Consequently, all organisms have evolved cellular mechanisms of DNA damage repair. The DNA damage response (DDR) to a particular insult generally involves recognition of the lesion, followed by cell-cycle arrest (checkpoint activation) and repair. The specific pathways activated depends on the type of damage induced, for example a single-strand break, DNA-strand crosslink, nucleotide mismatch, stalled replication fork or double-strand break (DSB) will all evoke distinct responses. The extent of damage also influences the outcome of DDR activation, since irreparable genotoxic insult may lead to cell death, evolved so as to prevent the passing on to progeny of potentially harmful genome alterations (Jackson and Bartek, 2009).

There is evidence to suggest that a functioning DDR acts as barrier against tumour development. In 2005, two separate research groups demonstrated that replication-associated DNA damage can be induced by oncogene-driven cell division (Bartkova et al., 2005; Gorgoulis et al., 2005). They showed that the DDR was activated in early pre-cancerous lesions and that this activation could be mirrored *in vitro* by the overexpression of oncogenes. A model was proposed whereby hyper-replication in early lesions triggers the DDR, leading to cellular arrest or death as a means to nullify tumour development. This generates a selective pressure for suppression or breakage of the DDR during tumorigenesis, hence why inactivation of core DDR effectors such as p53 is commonplace in almost all cancers (Hollstein et al., 1991). Furthermore, the selection for DDR inactivation leads to one of the hallmarks of cancer, genomic instability, which accelerates cancer evolution (Hanahan and Weinberg, 2011; Negrini et al., 2010).

This model of DDR activation in early lesions is applicable to PDAC progression, since the DNA damage marker phospho- γH2AX (Ser139) has been found to escalate according to grade of PanIN (histological scores of 4.34 for PanIN-1, 6.21 for PanIN-2 and 7.50 for PanIN-3) (Koorstra et al., 2009). Increased γH2AX and elevated DDR activation compared to normal tissue has also been observed in late-stage human PDAC samples (Osterman et al., 2014). This

suggests that PDAC tumours harbour intrinsic DNA damage, which may lead to greater sensitivity to extrinsic genotoxic insult, thus justifying the use of DNA damaging agents as chemotherapies for PDAC. Furthermore, over a third of PDAC cases harbour a somatic mutation in a DDR gene (Aguirre et al., 2018; Bailey et al., 2016; Waddell et al., 2015), most commonly ATM, PALB2, BRCA1 and BRCA2 (the function of these will be discussed further below). In tumours, the inactivation of one or more genes in a particular DDR pathway often creates a dependency on the remaining pathways. Therapeutic targeting of these remaining DDR pathways, whilst simultaneously inducing DNA damage, is therefore an attractive treatment strategy for PDAC.

The following section will outline some of the key members of the DDR, their significance in cancer and their current role as therapeutic targets.

1.3.1. Ataxia Telangiectasia and Rad3-related kinase

Activation of oncogenes such as KRAS can cause hyper-replication of DNA and consequently DNA damage in S-phase (Di Micco et al., 2006; Denko et al., 1994), or replication stress (RS). Broadly, RS refers to events in S-phase that cause slowing or stalling of the replisome machinery. In addition to oncogene-induced hyper-replication, RS can be induced by nucleotide shortages or DNA lesions that physically impede DNA polymerase (Zeman and Cimprich, 2014). Upon stalling of a replication fork, helicase activity continues for a period, which generates stretches of single-stranded DNA (ssDNA) (Byun et al., 2005; Pacek and Walter, 2004). This becomes coated with replication protein A (RPA), and the ssDNA-RPA complex acts as an initial trigger for the cellular response to RS, the core mediator of this response being the serine/threonine kinase, Ataxia Telangiectasia and Rad3-related (ATR).

ATR is a 300 kDa protein belonging to the PIKK family (phosphatidyl inositol 3' kinase-related kinases) that acts as an upstream transducer of DDR signals in response to RS. First, the essential interactor, ATRIP, binds directly to RPA and in turn recruits ATR (Zou and Elledge, 2003). Next, the DNA clamp complex Rad9-Rad1-Hus1 (9-1-1) is recruited to the stalled fork site, where it coordinates checkpoint activation and DNA repair (Majka et al., 2006; Parrilla-Castellar et al., 2004). The allosteric activator of ATR, TOPBP1, binds the ATR-ATRIP complex and this induces ATR kinase activity (Kumagai et al., 2006; Mordes et al., 2008). ATR can phosphorylate hundreds of substrates (Stokes et al., 2007), most notably Chk1 kinase (Guo et al., 2000; Liu et al., 2000), which ATR activates to propagate a global anti-RS signal

throughout the nucleus. When active, Chk1 inhibits replication origin firing to limit any further ssDNA-exposure and thus prevent nuclear exhaustion of RPA (Toledo et al., 2013). Chk1 induces S-phase or G2 arrest by promoting the degradation of the pro-mitotic CDC25 phosphatases which, when active, remove inhibitory CDK phosphorylations that are driven by WEE1 kinase (e.g. P-CDK1-Tyr15) (Sanchez et al., 1997; Sørensen et al., 2003; Xiao et al., 2003). This arrest allows time for attempted restart of any stalled forks and completion of DNA synthesis in the RS-affected regions. In addition to its activation of Chk1, ATR safeguards genome integrity from RS by upregulating the ribonucleotide reductase M2 subunit (RRM2) which increases dNTP pools (Buisson et al., 2015) and by promoting recovery or restart of failed forks (Mutreja et al., 2018; Trenz et al., 2006) through modulation of chromatin remodellers such as SMARCAL1 (Couch et al., 2013), BLM (Davies et al., 2007) and WRN (Pichierri et al., 2003).

ATR/Chk1 function is not only important during periods of high RS but for every round of unperturbed replication, due to their critical regulation of origin firing (Petermann et al., 2006, 2010; Shechter et al., 2004; Syljuåsen et al., 2005). Since ATR and Chk1 are essential for proliferating cells, complete loss of either molecule leads to embryonic lethality in mice (Brown and Baltimore, 2000; Takai et al., 2000). Low levels of ATR protein, a cellular feature of patients with Seckel Syndrome who commonly harbour hypomorphic mutations in ATR, leads to microcephaly, craniofacial deformities and growth retardation (Mokrani-Benhelli et al., 2013; O'Driscoll and Jeggo, 2003). In cancer, total loss of ATR or Chk1 has never been reported. Instead, there is evidence to support an 'oncogene-addiction' model, where hyper-proliferative tumour cells are reliant on RS response factors such as ATR/Chk1 for survival. The upregulation or amplification of Chk1 has been reported in numerous cancer types (Derenzini et al., 2015; Krajewska et al., 2015; Sarmento et al., 2015), while *in vitro* overexpression of Chk1 increases RAS- or MYC-driven transformation (López-Contreras et al., 2012; Ruiz et al., 2015). Furthermore, oncogene activation increases the lethality of ATR or Chk1 targeting (Gilad et al., 2010; Murga et al., 2011; Schoppy et al., 2012). Therefore, there is good rationale for using pharmacological inhibition of ATR/Chk1 as an anticancer strategy.

The first reported chemical inhibitor of ATR was caffeine, but it is not selective since it also inhibits other members of the PIKK family, including fellow DDR kinase ATM (discussed later) (Sarkaria et al., 1999). Next, schisandrin B (Nishida et al., 2009), ETP-46464 (Toledo et al., 2011) and NU6027 (Peasland et al., 2011) were identified as ATR inhibitors, however none

had the required specificity or pharmacokinetic properties to be used clinically. In 2011, Vertex Pharmaceuticals reported the discovery of a series of aminopyrazines that potently and selectively inhibited ATR (Charrier et al., 2011) and described the cellular activity of one of these compounds, VE-821. This molecule induced cell death in several cancer lines and synergised with various genotoxic agents, including cisplatin (Reaper et al., 2011). An analogue with improved pharmacokinetic properties, VE-822, was later reported to radio-sensitise PDAC xenografts (Fokas et al., 2012) and this compound is currently in multiple clinical trials as VX-970 (or M6620, following transfer of the molecule rights to Merck in 2017). AstraZeneca first described a new family of ATR inhibitors in 2013, which included AZ20 (Foote et al., 2013). Though the water solubility and liver enzyme interactions of AZ20 made it unsuitable as clinical candidate, it was optimised to derive AZD6738 (ceralasertib) (Foote et al., 2018) which is now being assessed clinically in a number of trials. Additionally, Bayer have their own ATR inhibitor, BAY1895344, in clinical development (Wengner et al., 2020). While some of these trials are monotherapy assessments, most are combinatorial, with the ATR inhibitors being combined with DNA-damaging agents, other molecularly targeted agents or immunotherapeutics, as recently reviewed by Bradbury and colleagues (Bradbury et al., 2019). Chk1 inhibition is also being explored by a number of groups, the two main clinical candidates being LY2606368 (Prexasertib) from Eli Lily and SRA737 (previously CCT245737) from Sierra Oncology (Rundle et al., 2017).

Several groups have used unbiased screening approaches to identify genetic determinants of ATRi sensitivity. These screens aim to identify *synthetic lethality* between ATR and another gene or protein. In genetics, synthetic lethality is where concurrent loss of two genes causes death, while in oncology it more broadly refers to the situation where a tumour-specific defect creates a vulnerability that can be exploited to induce tumour cell death. In 2014, a siRNA screen using a library of 240 genes involved in DNA repair and replication identified synthetic lethality between ATR and ERCC1, an endonuclease that aids repair of bulky DNA adducts and inter-strand crosslinks (Mohni et al., 2014). The screen was performed using 1 μM VE-821 in the osteosarcoma line, U2OS. The same group used a synthetic lethal screen to ask which pathways sensitise U2OS cells to the combination of ATRi and cisplatin (Mohni et al., 2015). Loss of REV3 (POLZ), the catalytic subunit of the translesion polymerase ζ, was found to increase sensitivity to the combination, as did loss of 53BP1. In 2016, ARID1A was identified as a synthetic lethal partner of ATR. A larger siRNA library of 1,280 genes was used to screen the breast cancer line HCC1143 and also the non-tumour, mammary epithelial line,

MCF12A (Williamson et al., 2016). ARDI1A, which is commonly mutated gene in PDAC (Bailey et al., 2016), is a component of the SWI/SNF chromatin-remodelling complex, which helps modulate the repair, replication and transcription of DNA (Jeggo and Downs, 2014; Roberts and Orkin, 2004). Validation experiments following the siRNA screen suggested that ARID1A-loss caused a reduction in the recruitment of topoisomerase II to chromatin and also accelerated mitotic entry, perhaps explaining the ATRi-sensitising effect. Screening approaches can also be used to identify resistance mechanisms. Notably, in 2016 a genome-wide CRISPR screen found that cells deficient in CDC25A were highly resistant to ATRi, since the ability for ATRi to induce premature mitotic entry and DNA-breakage was CDC25A-dependent (Ruiz et al., 2016). Other genetic determinants of ATRi sensitivity that have been identified include *APEX2*, *ATRIP*, *C16orf72*, *C17orf53*, *KIAA1524* (*CIP2A*), *POLE3*, *POLE4*, *RNASEH2A*, *RNASEH2B*, *RNASEH2C* (Hustedt et al., 2019), *XRCC1* (Sultana et al., 2013), *POLD1* (Hocke et al., 2016), *PARP14* (Dhoonmoon et al., 2020), *PRIM1* (Job et al., 2018), *GLUT1* (Erber et al., 2019) and *STAG2* (Mondal et al., 2019), as well as *ATM* which is discussed in detail in section 1.3.2.

As inhibitors of ATR and Chk1 progress through phase I/II trials, developing a deep understanding of how their potential can be maximised must be a priority for preclinical and clinical scientists. This will require thorough interrogation of their mechanisms-of-action, development of reliable pharmacodynamic assays and validation of predictive biomarkers of response and resistance. The latter is of particular importance, since deficiency in any one DDR pathway may not sensitise a tumour to any and all DDR inhibitors. The application of precision medicine strategies, where therapies are assigned based on patient-specific tumour vulnerabilities, has the potential to improve outcomes for diseases such as PDAC, but a thorough knowledge of disease biology and the therapies in question will be essential for such a tailored approach to succeed. One molecule being proposed as a potential predictive biomarker of response for a range of DDR-related therapies is Ataxia Telangiectasia Mutated kinase, which is discussed in detail below.

1.3.2. Ataxia Telangiectasia Mutated kinase

Ataxia Telangiectasia Mutated (ATM) is a DDR kinase, closely related to ATR, that acts as a master regulator of cellular responses to DSBs (Banin et al., 1998; Canman et al., 1998). These are highly lethal lesions, as evidence by experiments suggesting that a single unrepaired DSB

can be enough to induce cell death (Bennett et al., 1993). There are many potential sources of DSBs, including ionising radiation (IR) or the collapse of a stalled replication fork. The recruitment of ATM to DSB sites is dependent on its physical interaction with NBS1 (Falck et al., 2005; Lee and Paull, 2005), which forms part of the MRE11–RAD50–NBS1 (MRN) complex. MRN creates a physical bridge that traverses DSB ends (Stracker and Petrini, 2011), where it plays an important role in regulating DSB repair. It has been proposed that, upon DSB induction, the usually inactive dimers or multimers of ATM cross-phosphorylate one another on serine 1981, causing a dissociation into active monomers (Bakkenist and Kastan, 2003). However, more recent structural studies indicate that purified dimeric ATM is enzymatically active and can exist in an 'closed' or 'open' state (Baretić et al., 2017). Upon activation, ATM phosphorylates hundreds of substrates including Chk2 which, like Chk1, induces cell cycle arrest (Bartek et al., 2001). Serine 15 on p53 is a target for ATM kinase, the phosphorylation of which increases the transcriptional activity of p53, which can lead to growth arrest or apoptosis (Banin et al., 1998; Kastan et al., 1992; Westphal et al., 1997). Furthermore, ATM phosphorylates many of the factors that have direct roles in DSB repair including CtIP (You et al., 2009), Artemis (Beucher et al., 2009) and all three components of the MRN complex (Di Virgilio et al., 2009; Gatei et al., 2011; Lim et al., 2000). Moreover, ATM mediates chromatin relaxation by targeting regulators of chromatin structure such as KRAB-associated protein 1 (KAP1) (Ziv et al., 2006). Thus, ATM's role in the response to DSBs is multi-layered, in line with its classification as a DSB master-regulator. There is also evidence to suggest that ATM is involved in cellular processes outside of the DDR, including metabolism, oxidative stress and hypoxia responses (Ditch and Paull, 2012).

The two major mechanisms of DSB repair are non-homologous end-joining (NHEJ) and homologous recombination (HR). ATM can contribute to either process depending on cell cycle phase. As its name suggests, NHEJ does not require DNA sequence homology to repair a break and can occur at any stage of the cell cycle. Conversely, HR relies on the presence of a sister chromatid to be used as a homologous template and thus can only occur during late S or G2 phase. In the specific context of IR-induced DSBs outside of S phase, around 80% are repaired by NHEJ in a fast process that does not require ATM (Beucher et al., 2009). PIKK family member DNA-PKcs (discussed in more detail later) coordinates the end-joining process that results in the ligation of DSB ends, but often creates small deletions at the junctions. Meanwhile, 15-20% of these non-S-phase IR-induced breaks are repaired by a slower ATM-dependent re-joining pathway that requires the MRN complex and Artemis (Beucher et al.,

2009; Riballo et al., 2004). Thus, while ATM is not essential for the core processes of NHEJ which operate on directly ligatable ends, there are a subset of breaks in IR-treated G1 cells that are repaired with slower kinetics in an ATM-dependent manner, which may represent un-ligatable ends such as DSBs in heterochromatic regions (Álvarez-Quilón et al., 2014; Goodarzi et al., 2008; Riballo et al., 2004). As for DSBs in S-phase, such as those derived from collapsed replication forks which may be unsuitable for end-joining, these can be repaired by HR. ATM stimulates one of the early events in HR which is resection, where DNA is degraded either side of the break (Jazayeri et al., 2006). MRE11 endonuclease initiates the process by nicking the 5' strand at a distance from the DSB. From here, exonuclease-I resects DNA in the 5' to 3' direction and MRE11 resects from 3' to 5'. This resection process is promoted by BRCA1-dependent recruitment of CtIP (Sartori et al., 2007; Yu and Chen, 2004; Yun and Hiom, 2009) and leaves stretches of ssDNA which becomes coated in RPA (the trigger for ATR activation, thus DSBs can lead to ATR signalling) (Cuadrado et al., 2006). BRCA2 then loads RAD51 onto ssDNA, displacing the RPA (Saeki et al., 2006). The recruitment of BRCA2 to DSBs is promoted by BRCA1 and its partner PALB2 (Sy et al., 2009; Xia et al., 2006; Zhang et al., 2009). Next, RAD51 mediates invasion, where a physical interaction is made between the DNA to be polymerised and the homologous duplex DNA template of the sister chromatid. Finally, DNA is synthesised using the invading 3′-end as a primer (Krejci et al., 2012). Owing to its use of a DNA template, HR is a mostly error-free process, unlike NHEJ which can generate indels. As well as ATM's regulation of resection in the early stages of HR, there is evidence to suggest that ATM is also required for later stages after RAD51-loading (Bakr et al., 2015). Thus, ATM-deficient cells have been reported to show defective HR function (Kirshner et al., 2009; Köcher et al., 2012; Serrano et al., 2013).

Many of the studies that have investigated the role of ATM in DNA repair made use of cells from patients with the hereditary disorder, ataxia-telangiectasia (A-T) syndrome. Homozygous germline mutations in ATM cause A-T, which manifests with a range of symptoms including immunodeficiency, neurodegeneration, cerebellar ataxia, delayed pubertal development and radio-sensitivity (Lavin and Shiloh, 1996; Uhrhammer et al., 1998). Furthermore, patients with A-T have a cancer risk that is around 61 to 184 times higher than the general population (Morrell et al., 1986), which is likely due to defective DNA repair and genomic instability. Heterozygous germline ATM mutations also increase cancer susceptibility around 2-3-fold (Swift et al., 1991). Specifically, germline ATM mutations have been associated with increased

risk of breast cancer, lung cancer, glioma and PDAC (Liu et al., 2014; Shen et al., 2012; Thompson et al., 2005).

One of the first studies to describe ATM as a PDAC susceptibility gene revealed ATM germline mutations at a prevalence of 4.6% in families with high occurrences of PDAC (Roberts et al., 2012). Another study investigating a panel of 32 cancer susceptibility genes in PDAC patients unselected for family history, found germline ATM mutations at a prevalence of 3.3% (Brand et al., 2018). In addition, numerous whole-genome-sequencing studies have identified somatic ATM mutations in PDAC samples, at a rate of around 3-5% (Bailey et al., 2016; Biankin et al., 2012; Liu et al., 2018; Singhi et al., 2019). The authors of a recent review article on ATM-deficiency in PDAC performed a comprehensive literature search that captured 5,234 pancreatic cancer patients. They estimated that the total prevalence of germline or somatic ATM mutations in PDAC was 6.4%, though they uncovered a large range of 1%–34% (Armstrong et al., 2019). They noted that, with ATM being a very large gene (146,619 bases with 66 exons), mutations occur throughout its functional domains with no recurrent hotspot. Many of the ATM mutations found in cancer are missense mutations, the functional consequences of which are not always obvious. If an identified mutation correlates with one known to cause A-T syndrome, then it is likely that it is an inactivating variant (Choi et al., 2016). Otherwise, the functional consequence would have to be evaluated, either experimentally or using a predictive model. Navrkalova et al. took primary chronic lymphocytic leukaemia (CLL) cells from patients with ATM-mutant cancer and used a functional test to assess ATM status, whereby p21 expression was assessed following DNA damage. They used doxorubicin to induce DSBs and the purine analogue fludarabine to induce a broader spectrum of DNA damage, assuming ATM-defective cells would show impaired p21 induction upon treatment with doxorubicin but not fludarabine (while p53 defects should impair p21 induction after exposure to both drugs). All 11 ATM-mutant samples demonstrated ATM dysfunction (Navrkalova et al., 2013). In 2016, Weber et al. used irradiation followed by western blot analysis of ATM autophosphorylation and several downstream targets to assess the ATM activity of 7 lung cancer cell lines with missense ATM mutations. Only 2/7 lines (H23 and H1395) displayed a major functional impairment of ATM, while the missense mutations in the remaining five cell lines appeared to have no or only limited impact on overall ATM function in response to IR (Weber et al., 2016). Thus, the detection of an ATM missense mutation in a patient sample will not always inform functional ATM status.

In patients with PDAC that have a germline ATM mutation, loss of heterozygosity (i.e. a second hit in the tumour) has been reported to occur in 44% of instances (Yurgelun et al., 2019). As well as DNA mutation analysis, ATM status can also be assessed at the protein level using tissue microarrays. These data-sets indicate that low ATM protein expression in PDAC occurs at around 12-17% (Kamphues et al., 2015; Kim et al., 2014), however, there is no consensus for defining ATM "low" by immunohistochemistry (IHC). ATM expression may be downregulated through epigenetic mechanisms such as promoter methylation, which has been reported in breast cancer (Vo et al., 2004), brain cancer (Mehdipour et al., 2015) and head and neck squamous cell carcinoma (Ai et al., 2004), but has yet to be confirmed in PDAC.

The loss of ATM in a proportion of cancer samples supports the concept that inactivation of DDR factors is actively selected for during tumour progression. While ATM deficiency may initially arise in order to escape arrest or apoptosis during periods of oncogene-induced DNA damage, this loss of a key DSB regulator could expose tumours to therapeutic vulnerabilities. The idea that ATM deficiency may sensitise cancer cells to certain DNA-damaging therapies, and thus could be used clinically as a predictive biomarker of response, is an active area of investigation. Preclinical studies have indicated that ATM deficiency can sensitise cancer cells to radiation (Ayars et al., 2017), doxorubicin (Jiang et al., 2009), topoisomerase poisons and antimetabolites (Fedier et al., 2003). Of particular interest is ATR inhibition, since loss of ATM has been shown, in some cancer models, to sensitise to ATR inhibitor monotherapy (Reaper et al., 2011). For example, primary chronic lymphocytic leukaemia cells with ATM defects showed enhanced sensitivity to AZD6738 compared to wild-type or normal cells (Kwok et al., 2016), and when ATM was knocked-down with small interfering RNA (siRNA) in the gastric adenocarcinoma line, SNU-484, AZD6738 IC50 was reduced $\geq$ 2-fold (Min et al., 2017). However, in contrast, when Vendetti et al. used short hairpin RNA (shRNA) to deplete ATM in two lung cancer cell lines, the shATM cells appeared more resistant to AZD6738 monotherapy than control – only when AZD6738 was combined with cisplatin did shATM sensitise (Vendetti et al., 2015). In 2017, Ayars et al. reported that MIA PaCa-2 cells treated with shATM were no more sensitive to the ATR inhibitor, VE-821, than control cells (Ayars et al., 2017). However, work by Perkhofer et al. using mouse models of ATM-deficient PDAC suggested that ATM-loss did confer sensitivity to VE-822 (Perkhofer et al., 2017). With this lack of consistency in the literature, further investigation into the potential utility of ATM loss as a predictive biomarker for ATR inhibition is needed.

Since loss of ATM function has the promise to sensitise tumours to numerous therapies, ATM kinase inhibitors are currently undergoing clinical development. The selective ATM inhibitor AZD0156 (Barlaam and Pike, 2016; Pike et al., 2018) is being assessed in combination with FOLFIRINOX and poly(ADP-ribose) polymerase (reviewed in section 1.3.4) inhibition in advanced solid tumours (NCT02588105), while the brain-penetrant AZD1390 (Durant et al., 2018) is being combined with radiotherapy in patients with brain cancer (NCT03423628). Increased normal tissue toxicity may of course be a concern when administering ATM inhibitors and DNA-damaging therapies, therefore it will be important to monitor the side effects of these compounds as they progress through the clinic.

1.3.3. DNA-dependent Protein Kinase catalytic subunit

Along with ATR and ATM, DNA-PKcs (DNA-dependent protein kinase catalytic subunit) is the third PIKK family member that sits at the heart of the DDR (**Fig. 1.2**). As a catalytic subunit, DNA-PKcs forms the full DNA-PK complex by interacting with Ku70 and Ku80. These Ku proteins recognise and bind the broken DNA ends of a DSB, and recruit DNA-PKcs to the break site (Blier et al., 1993). Here, DNA-PKcs phosphorylates and regulates the activity of NHEJ factors, including Artemis, XRCC4, XLF and DNA ligase IV, which ligates DNA ends during the final stages of NHEJ. Intriguingly, however, none of these individual phosphorylations are independently required for efficient end-joining (Neal and Meek, 2011). That said, complete ablation of DNA-PKcs kinase activity causes inefficient DSB repair (Kurimasa et al., 1999), thus DNA-PKcs is a critical factor for NHEJ. The process of NHEJ often introduces indels which, if occurring within an exonic coding region, can lead to frameshift mutations that essentially inactivate the gene. CRISPR/Cas9 gene knockout technology depends on the Cas9 nuclease introducing a DSB that is processed by NHEJ, leading to gene inactivation (Wang et al., 2013). As well as the direct role for DNA-PKcs in NHEJ, there is also evidence to suggest that, in certain instances, DNA-PKcs may complement ATM and ATR in the activation of checkpoints (Arlander et al., 2008; Li and Stern, 2005; Lin et al., 2014).

While the addiction of cancers to ATR-driven signalling and the frequency of ATM-loss in tumours is fairly well established, the role of DNA-PKcs in cancer is less clear. Deregulated DNA-PKcs expression, either up or down, plus genetic mutations in its gene, PRKDC, have all been observed in a range of cancers, suggesting that the role of DNA-PKcs in tumorigenesis

may depend on the tissue type or cellular context (Evert et al., 2013; Herrero et al., 2015; Hosoi et al., 2004; Lee et al., 2005; Tonotsuka et al., 2006). What remains clear is that, as with ATM inhibition, targeting DNA-PKcs can sensitise preclinical models of cancer to DSB-inducing therapies. Early-generation DNA-PKcs inhibitors, NU7427 and NU7441, sensitised colorectal carcinoma cells to IR and etoposide (Zhao et al., 2006), breast cancer cells to IR and doxorubicin (Ciszewski et al., 2014), non-small cell lung carcinoma cells to irinotecan (Yanai et al., 2017) and B-cell chronic lymphocytic leukaemia cells to the doxorubicin analogue, mitoxantrone (Elliott et al., 2011). While useful tool compounds, the selectivity of these inhibitors for DNA-PKcs over other PIKK family members was not convincing enough for their clinical development. In 2019, AstraZeneca described the discovery of a highly potent and selective DNA-PKcs inhibitor, AZD7648 (Goldberg et al., 2019). They demonstrated that AZD7648 sensitised multiple *in vivo* cancer models to IR, doxorubicin and poly(ADP-ribose) polymerase inhibition (Fok et al., 2019). Consequently, a clinical trial has commenced to assess AZD7648 alone and in combination with other anti-cancer agents in patients with advanced cancers (NCT03907969). Additionally, the Celgene Corporation's dual DNA-PKcs/mTOR inhibitor, CC-115 (Dylgjeri et al., 2019; Tsuji et al., 2017), and Merck's DNA-PKcs inhibitor, M3814 (Damstrup et al., 2016; Sun et al., 2019; Wise et al., 2019), are in multiple clinical trials. As well as combining M3814 with DSB-inducing therapy, Merck are also exploring the possibility of using DNA-PKcs inhibition as a means to limit NHEJ and promote HR following CRISPR/Cas9 DSB-induction, which could be used for gene-therapy purposes (Riesenberg et al., 2019).

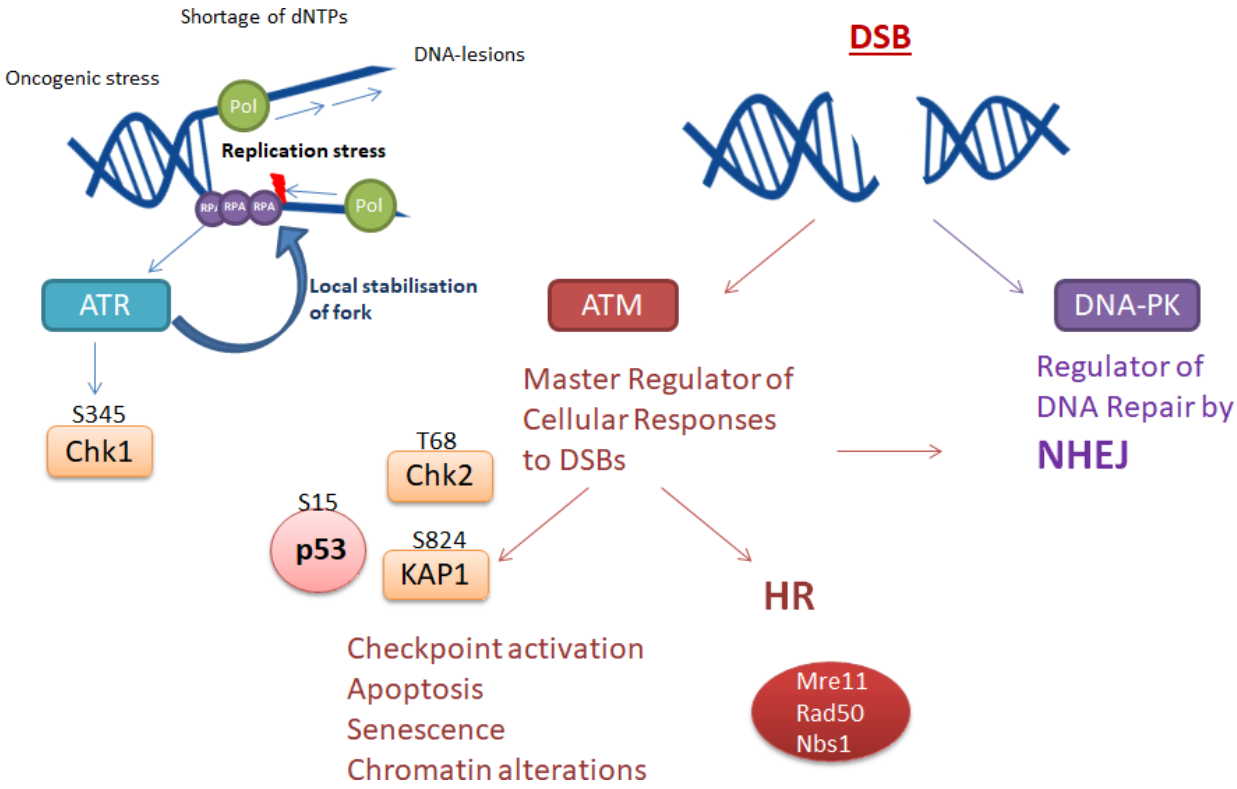

Fig. 1.2. ATM, ATR and DNA-PK: the trinity at the heart of the DNA damage response. The left-hand DNA structure represents a stalled replication fork, induced by sources of replication stress such as oncogene activation, dNTP shortages or DNA-lesions. If ATR fails to resolve a stalled fork (e.g. due to ATR inhibition by AZD6738), the structure may collapse, leading to the induction of a double-strand break (DSB) which is depicted on the right side of the image. DSBs activate ATM and DNA-PK.

1.3.4. Poly(ADP-Ribose) Polymerase

Inhibitors of ATM, ATR and DNA-PKcs are all at relatively early stages of clinical development, in that no regulatory approvals have yet been granted for these compounds. Conversely, the DDR factors that are leading the way as therapeutic targets, with regulatory approvals in multiple indications already granted, are poly(ADP-ribose) polymerases (PARPs). There are 17 PARP family members, the founding member being PARP1 (Gibson and Kraus, 2012). As the name suggests, PARPs are not kinases but polymerase enzymes that catalyse the poly(ADP)-ribosylation (PARylation) of target proteins, using oxidised nicotinamide adenine dinucleotide (NAD^+) as a substrate. The DNA-dependent PARPs, PARP1, PARP2 and PARP3 are activated by DNA lesions, including single-strand breaks (SSBs) (Satoh and Lindahl, 1992). As a DNA damage sensor, PARP1 binds to a SSB and in turn PARylates itself and regions around the break site, leading to the recruitment of PAR-binding, SSB-repair proteins (Fisher et al., 2007; Satoh and Lindahl, 1992) such as XRCC1 (El-Khamisy et al., 2003).

Though PARP1 has been commonly referred to as a base excision repair (BER) protein, this view has been challenged in recent years. The BER process involves the making of a SSB incision, which in turn acts as a substrate for SSB repair (SSBR) involving PARP1; thus, while PARP1 may be recruited to sites of BER, it is not required for base excision directly (Helleday, 2011; Ström et al., 2011). The central role for PARP1 in SSBR means that PARP1-null mice are hypersensitive to DNA-damaging chemotherapies and to IR (de Murcia et al., 1997).

In several cancer types, including breast, colorectal, testicular and malignant melanoma, overexpression of PARP-1 has been observed and is associated with invasiveness and poor clinical prognosis (Mego et al., 2013; Nosho et al., 2006; Rojo et al., 2012; Staibano et al., 2005). PARP mutations are rare in cancer, but may emerge in response to treatment, since some can cause resistance to PARP inhibitor therapy (Pettitt et al., 2018). The first PARP inhibitors developed were analogues of nicotinamide (a by-product of NAD^+ metabolism by PARP, that has weak inhibitory action) (Purnell and Whish, 1980), and in 1980 these early compounds were shown to abrogate DNA repair and improve the cytotoxicity of DNA methylating agents (Durkacz et al., 1980). Later, more potent second-generation inhibitors, PD128763 and NU1025, were developed (Griffin et al., 1995; Suto et al., 1991). These were able to sensitise cells to methylating agents, topoisomerase I poisons and IR (Bowman et al., 2001). In the early 2000s, several third-generation PARP inhibitors with further enhanced potency were developed and characterised, including olaparib, rucaparib, veliparib, niraparib and talazoparib many of which entered clinical development (Malyuchenko et al., 2015).

The first PARP inhibitor to be approved by the FDA and EMA was olaparib (AZD2281, Lynparza™), which inhibits PARP1 and PARP2. Initial approval was for the maintenance treatment of patients with platinum-sensitive relapsed BRCA-mutated (germline and/or somatic) ovarian cancer (Ledermann et al., 2014). The specific selection of a BRCA-mutant population had stemmed from seminal preclinical studies showing that tumours deficient in BRCA1 or BRCA2 were hypersensitive to PARP inhibition (Bryant et al., 2005; Farmer et al., 2005). This synthetic lethality between PARP and BRCA1/2 has been reproduced in multiple model systems and cancer types since the seminal studies in 2005 (Grignani et al., 2020). The precise mechanisms underlying the mode of action of PARP inhibitors and their toxicity in BRCA-deficient cancers have been under frequent debate. Studies suggest that the cytotoxicity caused by PARP inhibition is in part caused by PARP1 being "trapped" on DNA, and this may be more relevant than the abrogation of SSBR function (Murai et al., 2012). Importantly, different PARP inhibitors have varying PARP-trapping abilities (talazoparib >> niraparib ≈

olaparib ≈ rucaparib >> veliparib) which corresponds to their cytotoxic potency (Murai and Pommier, 2015). Trapped PARP1 poses an obstacle to the replication machinery during S-phase. Bypass of this obstacle, or the repair of the ensuing DSB that may arise upon collision and fork collapse, requires HR, a process dependent on BRCA1 and BRCA2. Thus, BRCA-deficient cells are unable to effectively repair these PARP inhibitor-induced DNA lesions, leading to cell death (Dréan et al., 2016; Helleday, 2011).

So far, most clinical approvals for PARP inhibitors have been for monotherapy use in BRCA-deficient tumours, following clinical trials that have demonstrated impressive survival rates in ovarian (Moore et al., 2018), breast (Robson et al., 2017) and pancreatic cancer (Golan et al., 2019). However, combining PARP inhibition with other therapeutic agents also has considerable promise. In the case of olaparib, at the time of writing (Spring 2020) there are 260 studies listed on ClincalTrials.gov that involve olaparib; 43 are monotherapy studies, while the rest are assessments of combinations. For example, olaparib is being combined with cisplatin, irinotecan, temozolomide, paclitaxel and radiotherapy, as well as with targeted agents such as inhibitors of PI3K, AKT, mTORC1/2 , WEE1, Chk1 and ATR (Dréan et al., 2016).

The aforementioned significance of PARP trapping (Murai et al., 2012) and its ensuing effects on DNA replication have made olaparib and ATR inhibition a particularly attractive therapeutic option. The physical obstacles to the replisome that trapped PARP creates may lead to the stalling of replication forks, which would require ATR activity to be resolved. In 2012, Huehls et al. reported that siRNA depletion of ATR sensitised the BRCA1-methylated cell line OVCAR-8 to the PARP inhibitor veliparib (ABT-888), whereas depletion of ATM, Chk1, and Ku80 did not sensitise (Huehls et al., 2012). The same research group subsequently showed that the ATR inhibitor, VE-821, sensitised ovarian cancer cells to veliparib, independent of BRCA status (Huntoon et al., 2013). The lab of Yves Pommier later demonstrated that ATR inhibition can overcome a specific resistance mechanism to PARP inhibitors, the inactivation of the helicase SLFN11. They took four cancer cell lines with high SLFN11 (prostate DU145, leukaemia CCRF-CEM and MOLT4, and Ewing's sarcoma EW8) and found that VE-821 enhanced the efficacy of olaparib and talazoparib in all 4 lines, even after PARP inhibitor resistance had been induced through the CRISPR/Cas9 deletion of SLFN11 (Murai et al., 2016). Furthermore, Lee Zou and colleagues cultured the BRCA1-mutant ovarian cell line, UWB1.289, in 1.0 μM olaparib for 45 days to derive lines resistant to PARP inhibition, and found that VE-821 broadly overcame the resistance (Yazinski et al., 2017). As for HR-

proficient PDAC models, before this PhD project commenced, published data on the efficacy of combined ATR and PARP inhibition in this setting was lacking.

1.4. Project aims

In this introductory chapter, I have described how targeting the DDR is being pursued as a therapeutic strategy in the oncology field. In particular, there is good rationale for using this approach in pancreatic cancer, since over a third of PDAC cases harbour a mutation in a DDR gene (ATM, PALB2, BRCA1 and BRCA2). Furthermore, many common genetic alterations in PDAC (KRAS, CDKN2A, TP53) augment replication-associated DNA damage, which increases reliance on the RS-response factor, ATR. Pharmacological inhibition of ATR is likely to be most effective when used in combination with other agents, thus identifying the most synergistic combinations and understanding how their efficacy could be optimised needs to be explored.

In this thesis, I report on investigations into the therapeutic potential of combining the ATR inhibitor, AZD6738, with DNA-damaging drugs and DDR-targeted agents in preclinical models of PDAC. My first aim was to compare a panel of such agents in terms of their ability to synergise with AZD6738 in human and mouse PDAC cell lines. These data are presented in **Chapter 3,** a short introductory results chapter where I complete an existing dataset and then comment on the varying degrees of synergy. AZD6738 and gemcitabine was one of the most synergistic combinations. This led to the primary focus of my PhD, which concerned the determinants of sensitivity to ATR inhibition and gemcitabine (ATRi/gem) treatment. I hypothesised that ATRi/gem would most likely benefit specific sub-groups of patients with pre-existing aberrations in DDR pathways (i.e. a precision medicine approach to patient selection). Accordingly, I aimed to investigate the potential for deficiency in the DSB master-regulator, ATM, to sensitise PDAC models to ATRi/gem. These data, evaluating ATM as a potential predictive biomarker of response for the novel combination, are presented in **Chapter 4**, along with an assessment of the tractability of dual ATM and ATR inhibition as a therapy option. Finally, I also aimed to investigate the combination of AZD6738 and the PARP inhibitor, olaparib, in HR-proficient PDAC models. These experiments are outlined in **Chapter 5**.

CHAPTER TWO: Materials and methods

2.1. Cell culture and chemicals

All human cell lines were purchased from ATCC. MIA PaCa-2, PANC-1 and HPAF-II were cultured in Dulbecco's Modified Eagles Medium (ThermoFisher #41966029) plus 10% FBS (ThermoFisher #10270106). AsPC-1 were cultured in RPMI-1640 Medium (ThermoFisher #21875034) plus 10% FBS. The genetic status of ATM and ATR in these human lines is shown below (**Fig. 2.1**) as well as other genes known to contribute to ATRi sensitivity (as described in section 1.3.1) The murine cell lines K8484 and DT8082 were previously established from KPC mice of the mixed 129/SvJae/C57Bl/6 background (Olive et al., 2009) and were grown in DMEM with 5% FBS. All cell lines were subjected to regular STR fingerprinting and mycoplasma tests, performed by the CRUK-CI Biorepository Core Facility.

AZD6738, AZD0156, AZD7648, AZD1775 and AZD2281 (olaparib) were kindly provided by AstraZeneca. These agents, plus gemcitabine hydrochloride (Tocris #3259), 5-fluorouracil (Sigma #F6627), oxaliplatin (Sigma #O9512), SN38 (7-Ethyl-10-hydroxycamptothecin, Sigma #H0165) and MK8776 (Selleckchem #S2735) were dissolved in DMSO, kept at -20°C, and used within 3 months. Final DMSO concentrations (0.2%) were kept constant in all experiments.

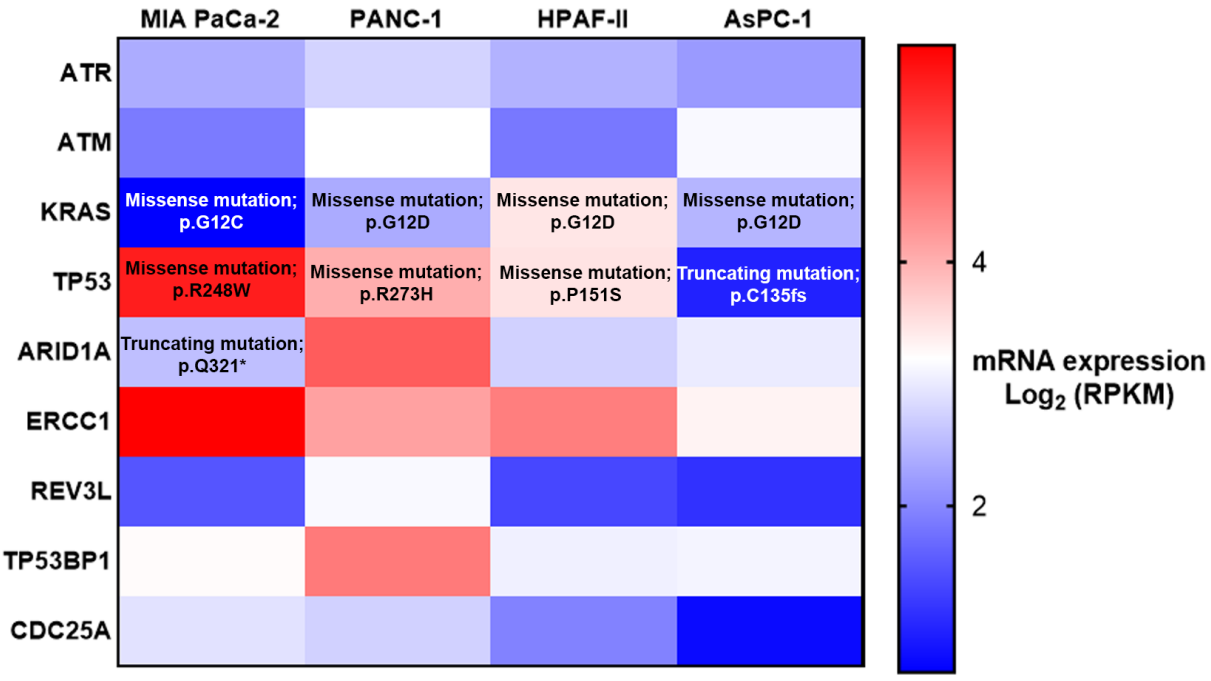

Fig. 2.1. mRNA expression of ATR and genes known to contribute to ATRi sensitivity in four PDAC human cell lines. Mutation data is also overlaid on the plot (a rectangle without text indicates that the gene is not mutated in this cell line). Data source is the Cancer Cell Line Encyclopaedia, accessed via cBioPortal. RPKM = Reads Per Kilobase Million.

2.2. siRNA transfection

ON-TARGETplus-SMARTpool siRNAs targeting ATM were purchased from Dharmacon (#L-003201-00-0005), as well as a Non-Targeting-Control-Pool (#D-001810-10-05). Reverse transfection was achieved using Lipofectamine RNAiMax reagent (Invitrogen#13778/150), as per manufacturer's instructions. Briefly, lipofectamine-siRNA mixture was incubated in a 100mm dish, before cells were seeded on top (final siRNA concentration = 25nM). 48-hours later, cells were split and seeded for drug sensitivity assays or immunoblotting.

2.3. CRISPR/Cas9 gene editing

For generation of ATM knockout MIA PaCa-2 cells, a previously validated all-in-one guide-RNA-Cas9-GFP plasmid (pAiO-WT-ATM), the human ATM-specific guide-RNA sequence, GTTGGTTACATACTTGGACT, cloned into the BbsI site, was kindly provided by Professor Stephen Jackson of the Wellcome Trust/CRUK Gurdon Institute, University of Cambridge, UK (Balmus et al., 2019). Transfection of the plasmid into MIA PaCa-2 cells was achieved using Lipofectamine 3000 Reagent (Invitrogen, #L3000015) as per the manufacturer's instructions for forward transfections in 6-well plate format. 48 hours post-transfection, cells were split and single-cell sorted (BD FACS Aria), specifically for the top 3% of GFP-positive cells, to enrich for cells that had been positively transfected. Single cell clones were left to grow in 96 well plates, before being split into 24 well plates. At the point where clones were being split and transferred to 6 well plates, half of each sample was taken for genomic DNA extraction (QIAamp DNA Micro Kit #56304). From genomic DNA, the region around the sgATM-Cas9 target site was amplified by PCR and sent for Sanger nucleotide sequencing (Eurofins LightRun). Sequencing chromatograms were deconvoluted using the Synthego ICE web tool (ice.synthego.com). Absence of ATM protein was confirmed by immunoblotting.

2.4. Immunoblotting

Following media removal and a PBS wash, cell lysis was performed on 60mm dishes using 50Mm Tris HCl plus 2% SDS, with phosphatase and protease inhibitors (Roche#04906837001, Roche#04693159001). Cells were scraped and boiled at 95 °C for 5 minutes, before NanoDrop™ 8000 (A280) protein quantification. Proteins were resolved using the SDS-PAGE gel system (Life Technologies), detected using IRDye secondary antibodies (LI-COR) and

visualised on the Odyssey CLx imaging system (LI-COR). Primary antibodies used were obtained from Abcam (ab) or Cell Signaling Technology (CST), unless otherwise stated: ATM (ab78), P-ATM-Ser1981 (ab81292), DNA-PKcs (ab44815), P-DNA-PKcs-Ser2056 (ab18192), KAP1 (ab22553), P-KAP1-Ser82 (ab133440), P-CDK1-Tyr15 (ab76146), RPA32 (ab2175), RAD50 (ab89), P-Chk2-Thr68 (ab3501), Chk2 (CST3440), P-Rad50-Ser635 (CST14223S), Chk1 (CST2360), P-Chk1-Ser345 (CST2348), H2AX (CST7631), P-HH3-Ser10 (CST3377), HH3 (CST9715), cleaved-PARP-Asp214 (CST9544), β-Actin (CST4970), β-Tubulin (CST2146), Lamin B1 (CST12586), Vinculin (CST13901), GAPDH (CST5174), ATR (Santa Cruz Biotechnology#SC-1887), P-ATR-Thr1989 (Genetex#GTX128145), γH2AX-Ser139 (Millipore#05-636), P-RPA32-Ser4/8 (Bethyl#A300-245A).

2.5. Fractionation

Fractionation, to derive cytoplasmic and nuclear fractions, was performed as described by Warren and Eastman in 2019 (Warren and Eastman, 2019).

2.6. SRB assay

Cells were seeded in Corning black flat-bottom 96-well plates, 24 hours before drug treatment. For single-agent and combinatorial drug sensitivity assays, cells were treated for 72 hours unless otherwise stated. Following the allotted drug treatment, medium was aspirated and the cells washed once with phosphate-buffered saline (PBS), before the addition of 100 µL of 3% trichloroacetic acid (TCA) to each well. After incubation at 4°C for 1 hour, the TCA was removed and each well was washed once with 100 µL of cold water. 50 µL of 0.057% Sulforhodamine B (SRB) solution (Sigma-Aldrich, #230162) in 1% acetic acid was added to each well to allow staining at room temperature for 30 minutes. Plates were rinsed four times with 1% acetic acid using an automated plate washer (Biotek Elx405 Select CW). After drying, 200 µL of 10 mM Tris base solution (pH 10.5) was added to each well and the solubilisation of protein-bound dye was achieved by placing plates on a gyratory shaker for 5 minutes. The SRB signal was measured at excitation and emission wavelengths of 488 nm and 585 nm respectively, using a PHERAstar FS plate reader (BMG Labtech). The fluorometric signal values were used as surrogates for cell number. For combination studies, synergy was assessed

using Combenefit software (Di Veroli et al., 2016). Combenefit uses Bliss and Loewe additivity models, which use the following definitions:

Synergy distribution

With the hypothetical combination of two agents A and B at concentrations *a* and *b* respectively, the effectiveness of a drug combination can be assessed in terms of the amount of "extra-effect" that is obtained when combining the drugs. Thus, effects can be described as following:

$$E(a,b) = R(a,b) + S(a,b)$$

or

$$S(a,b) = E(a,b) - R(a,b)$$

E(a,b) is the observed effect, i.e. what is actually measured during the experiment.
R(a,b) is the reference effect (model prediction), i.e. a baseline which should be obtained in an experiment when the combination does *not* amplify or reduce cell kill.
S(a,b) is the amount of extra-effect, also termed synergistic effect (when this extra-effect is negative, it is termed antagonistic).

In order to identify synergy or antagonism, the combined reference effect *R(a,b)* is first derived based on single agent dose-response curves. Reference surfaces depend on the mathematical model which is used to define non-synergistic effects.

Bliss model

For the Bliss model, the reference effect for the combination *(a,b)* is obtained by taking the product of the effects at these concentrations:

$$R_{AB\_Bliss}(a,b) = E_A(a) \cdot E_B(b)$$

Loewe model

For the Loewe model, the reference effect for the combination *(a,b)* is calculated by finding two doses a_U and b_U such that:

$$E_A(a_u) = E_B(b_u)$$

And for which the isobole equation was verified:

$$\frac{a}{a_U} + \frac{b}{b_U} = 1$$

These two equations are solved numerically for (a_u,b_u). The numerical solution is used to define the reference effect as:

$$R_{AB\_Loewe}(a,b) = E(a_u) = E_B(b_u)$$

2.7. Clonogenic assay

5 hours prior to treatment, cells were plated at 300 cells/well in 6-well plates. Following 24 hours of drug treatment, the medium was replaced and the cells left to grow for 7 more days after the washout. Cells were then fixed and stained with SRB (as above but with TCA and SRB volumes increased 10-fold). Colonies were imaged and quantified using the GelCount (Oxford Optronix). Plating efficiency was calculated as the ratio of the number of colonies in the control well to the number of cells seeded. The number of colonies that arose after treatment was expressed as surviving fraction (SF). SF was calculated as the ratio of the number of colonies formed after treatment to the number of cells seeded, multiplied by plating efficiency of the control.

2.8. IncuCyte time lapse imaging

96 well plates were placed in the IncuCyte® ZOOM System (Essen Bioscience) with 10X objective, which captured images of cells every 3 hours. Average cell confluence was calculated from 3 fields of view per well using the IncuCyte in-built algorithm. Cell death was measured by adding YOYO™-3 Iodide (Invitrogen #Y3606) to each well at 100 nM final concentration.

2.9. Flow cytometry

Cells were plated in a Corning 60mm dishes 24 hours prior to drug treatment. At the designated timepoint the cell culture media was collected, the plates washed with PBS, cells trypsinised and then combined with the collected media and the wash. Samples were centrifuged, the resulting cell pellets washed with PBS, then cells were fixed with 1 mL ice-cold 70% ethanol overnight at -20°C. For DNA content analysis, fixed cells were centrifuged, washed once with PBS, then resuspended in 0.5 mL of blocking solution (PBS, 2% BSA, 0.1% Tween-20, 0.1% Triton X100) for 1 hour to increase membrane permeability. Finally, cells were treated with 0.5mL FxCycle Violet Stain (Invitrogen #F10347), prepared in blocking solution at 1:1000 dilution, and transferred to FACS tubes. Samples were run on the BD Biosciences LSRFortessa™ flow cytometer, and the resulting data analysed using FlowJo® V10 software.

2.10. Quantitative image-based cytometry

Cells were seeded in Corning black flat-bottom 96-well plates 24 hours before drug treatment. At the designated timepoint, cells were fixed with 4% paraformaldehyde for 10 minutes, then washed twice with PBS. Permeabilisation was achieved by incubating with 0.1% Triton X-100, 0.1% Tween-20, 1xPBS (PBSTT) for 10 minutes at room temperature. Cells were blocked for 30 minutes with blocking solution, PBSTT + 2% Bovine Serum Albumin (Roche #10735094001). Primary antibody in blocking solution was added for 1 hour at room temperature (mouse anti-γH2AX S139, Millipore #05-636, 1:2000 and rabbit anti-phospho-RPA32 S4/8, Bethyl #A300-245A, 1:1000), then wells were washed with PBSTT three times. Secondary antibody (Alexa Fluor 488 goat anti-rabbit, Invitrogen #A11034, 1:500 and Alexa Fluor 568 goat anti-mouse, Invitrogen #A11019, 1:500) plus Hoechst 33342 (Invitrogen #H3570, 1:10,000) in blocking solution was added for 1 hour at room temperature. Plates were washed once with PBSTT and a further two times with PBS. Images were acquired using the Operetta CLS High-Content Analysis System and analysis performed using Harmony 4.5 software. The resulting CSV files from these analyses were loaded into RStudio™ for reshaping of the tabular data, then exported as FlowJo-compatible CSV files which were imported into FlowJo® V10 software to generate pseudo-colour plots.

2.11. Animal experiments

All mouse experiments were carried out in the CRUK Cambridge Institute BRU, in accordance with the UK Animals (Scientific Procedures) Act 1986, with approval from the CRUK Cambridge Institute Animal Ethical Review and Welfare Body. Subcutaneous xenografts of MIA PaCa-2 cells were formed by implanting $5x10^6$ cells (in 0.2 ml 1:1 matrigel: PBS) in the right flank of 7-9-week old female NSG or BALB/c Nude mice (Charles River). Mice with established tumours were randomised into treatment groups. AZD6738 (AstraZeneca) was dissolved to 5 mg/mL or 10 mg/ml in 10% DMSO, 40% Propylene Glycol, 50% de-ionised sterile water and dosed at 5 ml/kg by oral gavage to give 25 mg/kg or 50 mg/kg. Gemcitabine (LKT Laboratories, from Cambridge Bioscience) was dissolved in a saline solution (Vetivex) to 10 mg/mL and given to mice at 50 mg/kg intraperitoneally. Olaparib (AstraZeneca) was prepared to 5mg/mL or 10 mg/mL in 10% v/v DMSO / 50% v/v of 60% w/v HP-B-CD (Kleptose) in purified water and dosed at 10 ml/kg by oral gavage to give 50 mg/kg or 100 mg/kg. AZD0156 (AstraZeneca) was formulated at 1 mg/ml in 10% DMSO, 30% Captisol

(Astra Zeneca), and dosed orally at 10 ml/kg to give 10 mg/kg. AZD1390 (AstraZeneca) was formulated by preparing a stock suspension at 5 mg/ml in vehicle (0.5% HPMC/ 0.1% Tween 80), then diluted to working formulation of 0.5 mg/ml or 1 mg/ml with the same vehicle. These were dosed orally at 10 ml/kg to give 5 mg/kg or 10 mg/kg. Xenografts were measured twice a week using callipers.

2.12. Immunohistochemistry

Formalin-fixed, paraffin-embedded sections were immuno-stained after heat-induced epitope retrieval by sodium citrate at 100°C for 10-20 minutes, using Bond Polymer Refine Detection kit on the automated Bond system according to manufacturer's instructions (Leica). Slides were mounted using Leica CV5030 Coverslipper Workstation and scanned using a ScanScopeXT (Aperio Technologies). Quantification was performed using the Halo software (Indica Labs). Primary antibody used on human xenograft tissue – phospho-Histone H2A.X (Ser139) Rabbit, Cell Signaling Technology, #9718. Primary antibody used on mouse tissue (guts) – anti-gamma H2A.X (phospho S139) Rabbit, Abcam, #ab195190.

2.13. Ultra-performance liquid chromatography - tandem mass spectrometry (UPLC-MS/MS)

For plasma bioanalysis, each plasma sample (25 µL) was prepared using an appropriate dilution factor, and compared against an 11-point standard calibration curve (1-10000 nM) prepared in DMSO and spiked into blank plasma. Acetonitrile (100 µL) was added with the internal standard, followed by centrifugation at 3000 rpm for 10 minutes. Supernatant (50 µL) was then diluted in 300 µL water and analysed via UPLC-MS/MS.

For tumour bioanalysis, tumour was weighed into fast preparation tubes containing Lysing Matrix A (MP Biomedicals UK). Water was added as a base for homogenisation (2 times w/v). Homogenisation was carried out in FastPrep-24 5G (MP Biomedicals USA) at 6m/s for 30 seconds, twice. Each tumour homogenate sample (25 µL) was compared against an 11-point standard calibration curve (1-10000 nM) prepared in DMSO and spiked into blank tumour homogenate. Acetonitrile (100 µL) was added with the internal standard, followed by centrifugation at 3000 rpm for 10 minutes. Supernatant (50 µL) was then diluted in 300 µL water and analysed via UPLC-MS/MS. Analysis was performed by Aaron Smith, AstraZeneca.

2.14. PAR ELISA

PARylation was analysed using the HT PARP in vivo Pharmacodynamic Assay II ELISA 2nd generation ELISA Kit (Trevigen #4520-096-K) as per the manufactures' instructions, and as described in details by Riches et al. in 2019 (Riches et al., 2019). Samples were run by Anna Staniszewska, AstraZeneca.

CHAPTER THREE: Comparison of anti-cancer agents that synergise with the ATR inhibitor, AZD6738, in PDAC cell lines

3.1. Background

Before this project began, the Jodrell lab had begun to test combinations of the ATR inhibitor, AZD6738, with a range of cytotoxic drugs and DDR-targeted agents in a panel of PDAC cell lines (Dr Yann Wallez). The aim was to identify synergistic combinations that could then be taken forward for more in-depth mechanistic and *in vivo* studies. The DNA-damaging agents assessed were gemcitabine and three components of the combinatorial regimen FOLFIRINOX; 5-FU, oxaliplatin and SN38 (the active metabolite of topoisomerase I inhibitor, irinotecan). The DDR-targeted agents assessed were AZD1775 (WEE1i), MK8776 (Chk1i) and olaparib (PARPi). Up to this point, all of these compounds had demonstrated synergism with AZD6738, but most had only been tested in KPC mouse cell lines, as a prelude to studies in the KPC *in vivo* models, but not in any human lines. To complete this dataset (**Table 3.1**), and to allow the synergy to be compared and ranked, I aimed to assess the remaining combinations in human MIA PaCa-2 and PANC-1 cells.

	AZD6738 in combination with:						
	DNA-damaging agents				DDR-targeted agents		
	Gemcitabine	5-FU	Oxaliplatin	SN38	AZD1775 (Wee1i)	MK8776 (CHK1i)	Olaparib (PARPi)
K8484 (mouse, KPC)	✓	✓	✓	✓	✓	✓	✓
DT8082 (mouse, KPC)	✓	✓	✓	✓	✓	✓	✓
TB32048 (mouse, KPC)	✓	✓	✓	✓	✓	✓	✓
TB31456 (mouse, KPC)	✓	✓	✓	✓	✓	✓	✓
KPCFT79653 (mouse, KPCB)	✓	✓	✓	✓	✓	✓	✓
MIA PaCa-2 (human)	✓						✓
PANC-1 (human)	✓						✓

Table 3.1. Table of combinations to be assessed in PDAC cell lines. Those that had been tested before my arrival, by Dr Yann Wallez, are marked in green with a tick. Those assessed by me and presented in this chapter are blank. KPCB denotes a BRCA-mutant mouse cell line.

3.2 Synergy evaluation of AZD6738-based combinations in human PDAC cell lines

I first performed growth inhibition assays, with TCA-fixation and SRB staining after 72 hours of drug incubation, combining AZD6738 with the individual FOLFIRINOX components 5-FU, oxaliplatin and SN38 (**Figs. 3.1-3.3**). I used Combenefit software (Di Veroli et al., 2016) to quantify the drug interactions. Combenefit takes the observed growth inhibition data and compares them to a model prediction which assumes no interaction between the two agents.

Two widely used models are Bliss independence and Loewe additivity. As described by Yadav et al. - *the Bliss independence model utilises probabilistic theory to model the effects of individual drugs in a combination as independent yet competing events, while the Loewe additivity model defines the expected effect as if a drug was combined with itself* (Yadav et al., 2015) (see Methods section 2.6. for full Bliss and Loewe equations). A combination is classified as synergistic when the actual drug response observed is greater than the model prediction, while antagonism is when a lesser effect than expected is observed. There is no consensus on whether Bliss independence or Loewe additivity is a more robust model, given their differing assumptions, thus I have displayed both throughout this chapter. Many groups use the combination-index isobologram method for combination assays, which is based on the median effect principle (Chou, 2010). This permits only the analysis of fixed dose ratios of the two agents in question. The key feature of Combenefit software is its flexibility in determining the expected interaction for any combination of agent concentrations, as well as its scalability (numerous experiments all analysed at once).

While synergy between 5-FU and AZD6738 had previously been observed in KPC mouse cell lines, I observed no synergy with this combination in the human MIA PaCa-2 and PANC-1 (**Fig. 3.1**). Oxaliplatin displayed modest synergy with AZD6738 in the human lines, but at low AZD6738 concentrations (100 - 300 nM) I observed an antagonistic interaction with oxaliplatin in PANC-1 (**Fig. 3.2**). Of the three genotoxic agents tested, the topoisomerase I (TOP1) inhibitor, SN38, demonstrated the most convincing synergy with AZD6738 in MIA PaCa-2 (Bliss maximum synergy score = 37; Loewe maximum synergy score = 38) and PANC-1 (Bliss maximum synergy score = 23; Loewe maximum synergy score = 33) (**Fig. 3.3**).

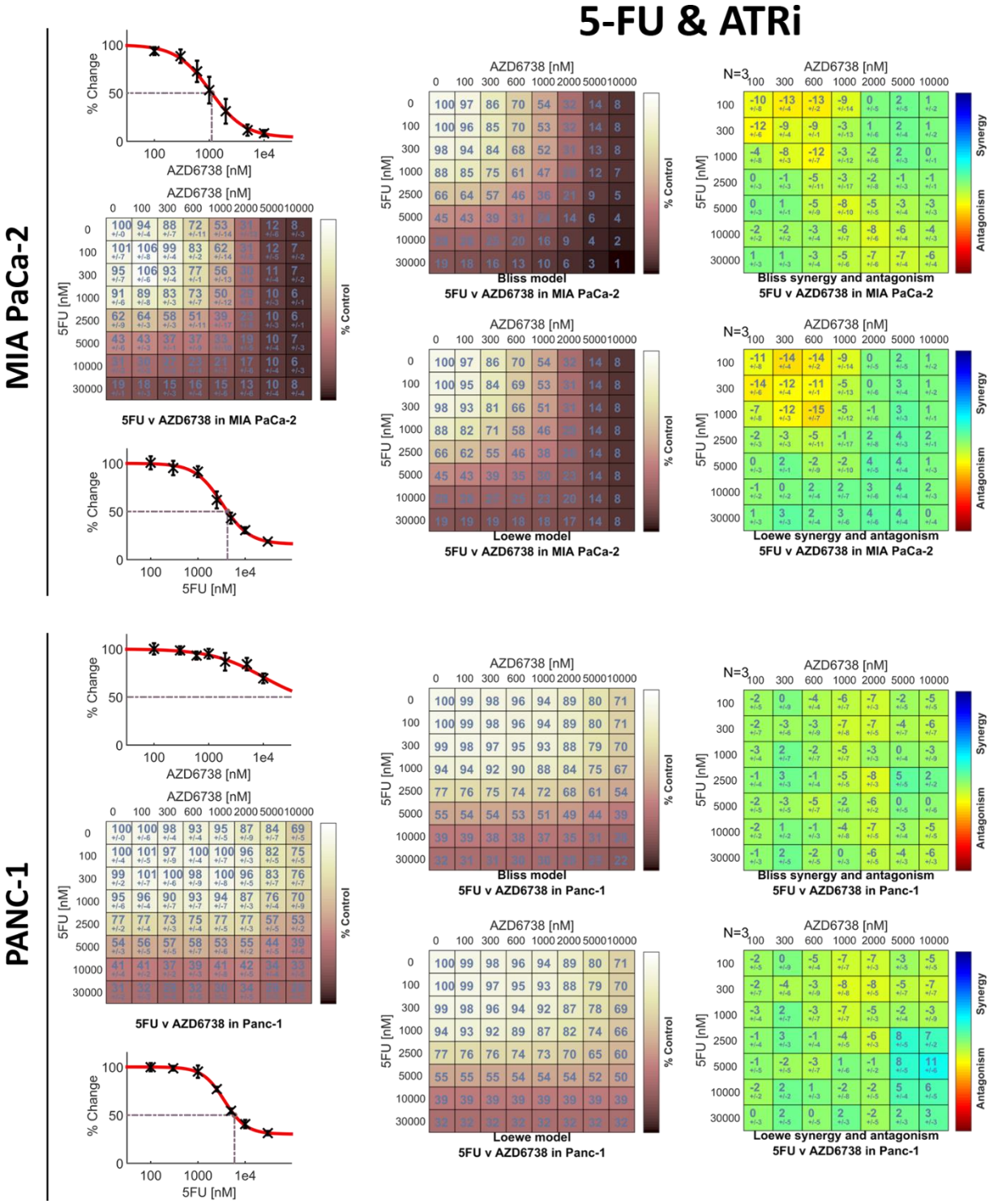

Fig. 3.1. MIA PaCa-2 and PANC-1 were treated with increasing concentrations of AZD6738 and 5-FU for 72 hours. Cell number at endpoint was determined by measuring total protein content using the SRB assay. Left = growth as % of solvent control. Data, mean ± SD, n=3. Middle = Bliss and Loewe model prediction. Right = Combenefit synergy score. Data, mean ± SD, n=3. The greater the difference between the experimental values and the model prediction, the greater the synergy score.

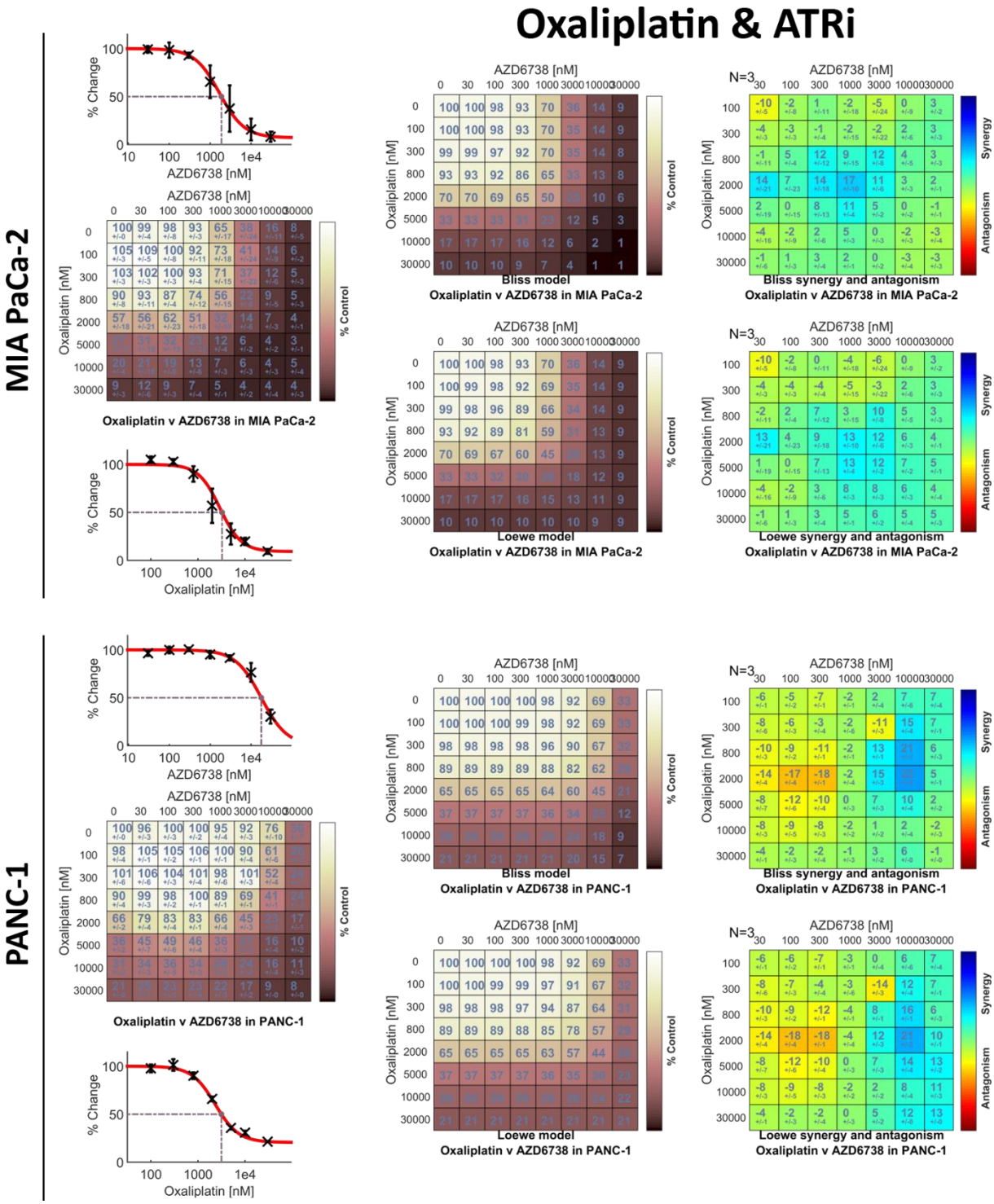

Fig. 3.2. MIA PaCa-2 and PANC-1 were treated with increasing concentrations of AZD6738 and oxaliplatin for 72 hours. Cell number at endpoint was determined by measuring total protein content using the SRB assay. Left = growth as % of solvent control. Data, mean ± SD, n=3. Middle = Bliss and Loewe model prediction. Right = Combenefit synergy score. Data, mean ± SD, n=3. The greater the difference between the experimental values and the model prediction, the greater the synergy score.

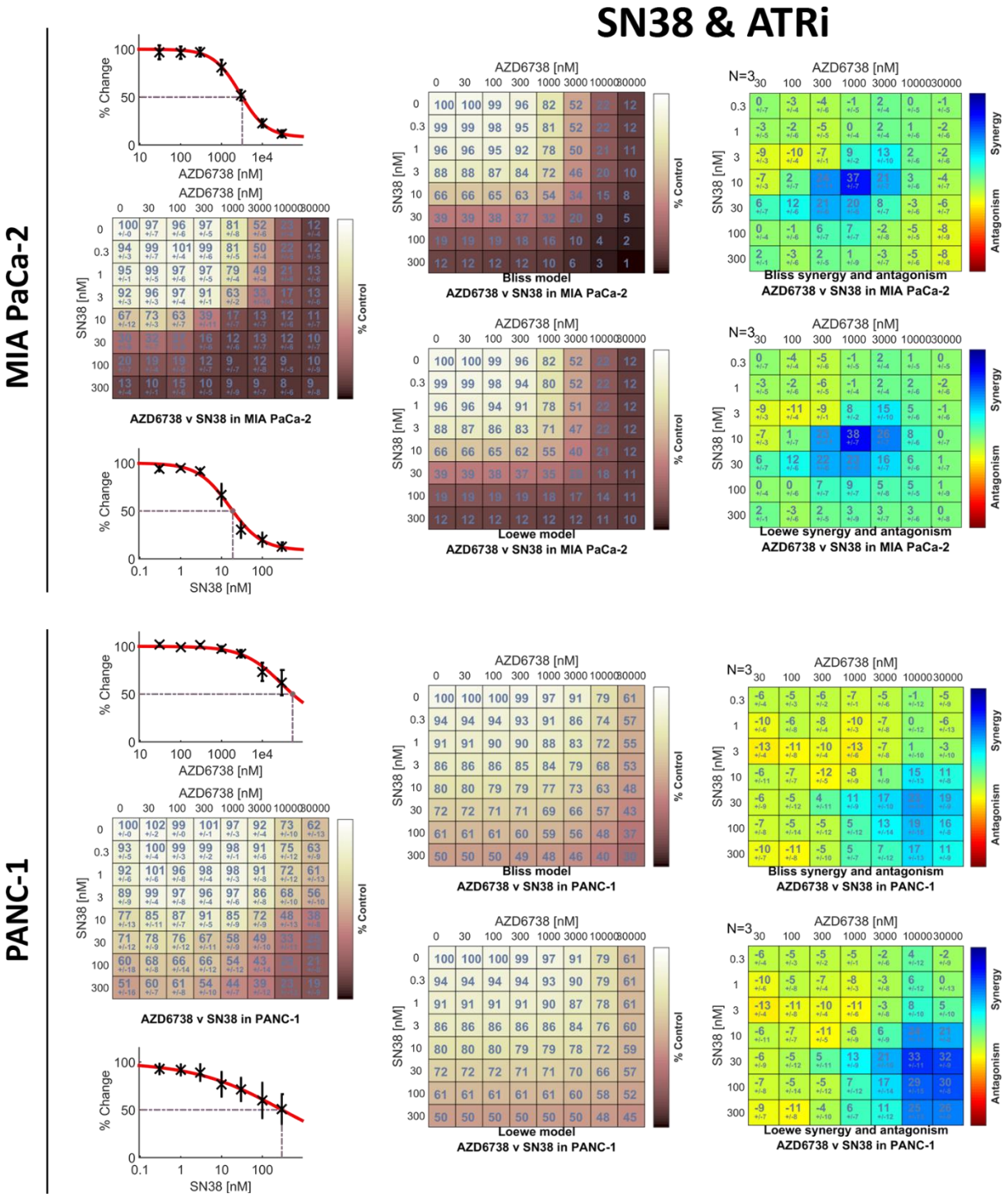

Fig. 3.3. MIA PaCa-2 and PANC-1 were treated with increasing concentrations of AZD6738 and SN38 (the active metabolite of TOP1 inhibitor, irinotecan) for 72 hours. Cell number at endpoint was determined by measuring total protein content using the SRB assay. Left = growth as % of solvent control. Data, mean ± SD, n=3. Middle = Bliss and Loewe model prediction. Right = Combenefit synergy score. Data, mean ± SD, n=3. The greater the difference between the experimental values and the model prediction, the greater the synergy score.

The DDR-targeted agents assessed in MIA PaCa-2 and PANC-1 were the WEE1 inhibitor, AZD1775, and the Chk1 inhibitor, MK8776. WEE1 inhibition demonstrated high synergy scores with AZD6738 in MIA PaCa-2 (Bliss maximum synergy score = 34; Loewe maximum synergy score –=31) and PANC-1 (Bliss maximum synergy score = 26; Loewe maximum synergy score = 27) (**Fig. 3.4**), but inhibition of Chk1 was mostly antagonistic in both cell lines (**Fig. 3.5**).

3.3 Comparison of all cytotoxic and DDR-targeted drugs tested across human and mouse cell lines

Completing these combinatorial assays enabled me to a perform broad comparison of the agents in question, in terms of their ability to synergise with AZD6738 in human and mouse PDAC cell lines. Using the *Batch Analysis* program of Combenefit, which quantifies the sum of synergy and antagonism for a given combination, I was able to rank the DNA-damaging agents and DDR-targeted agents respectively (**Fig. 3.6**). Of the chemotherapies tested, gemcitabine and oxaliplatin had the highest average synergy scores across the 7 cell lines. Meanwhile, AZD1775 and olaparib were the two targeted therapies with strongly positive synergy scores, unlike MK8776 (Chk1 inhibitor) which exhibited antagonism with AZD6738 in multiple cell lines, resulting in a low average score.

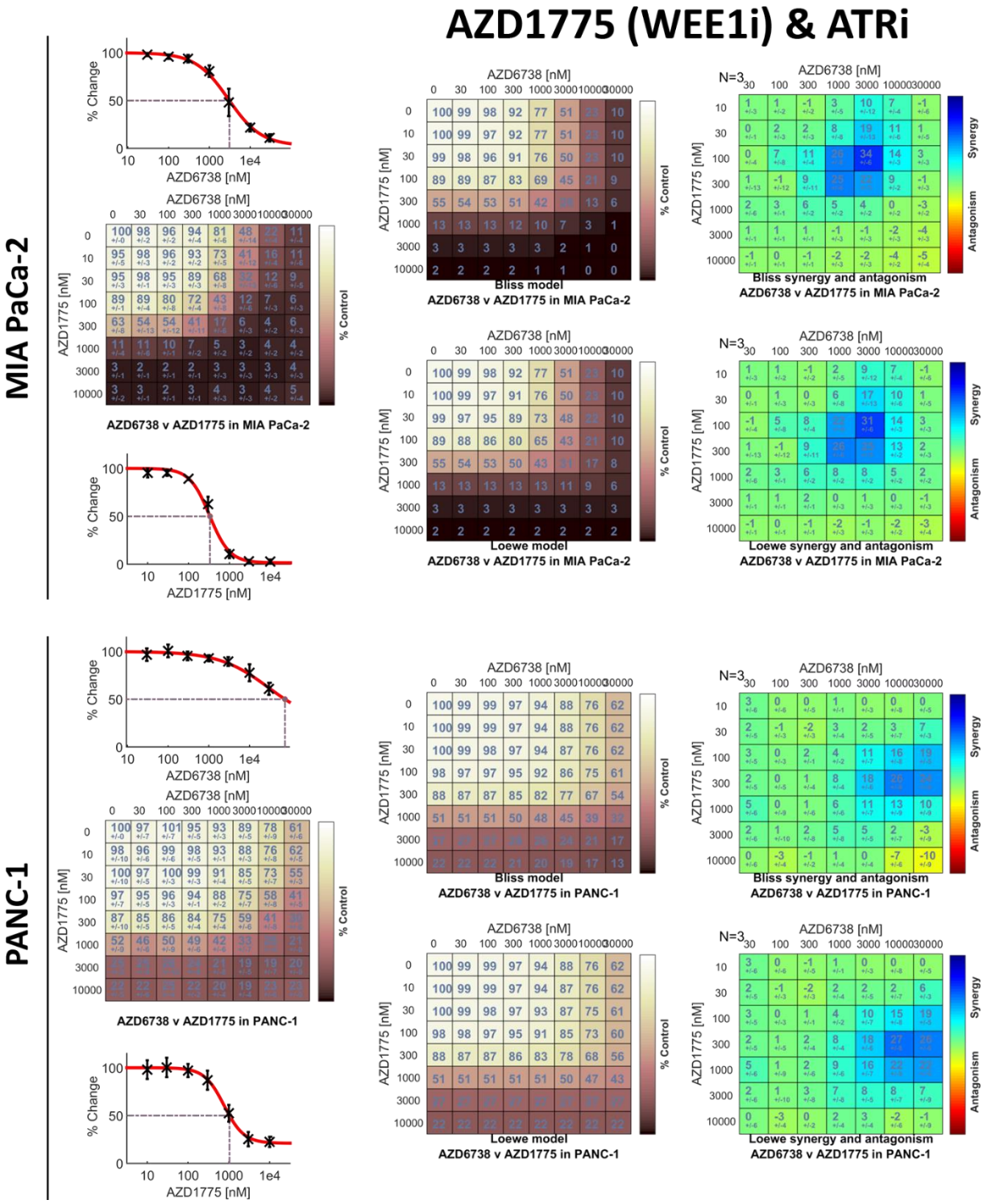

Fig. 3.4. MIA PaCa-2 and PANC-1 were treated with increasing concentrations of AZD6738 and AZD1775 (WEE1 kinase inhibitor) for 72 hours. Cell number at endpoint was determined by measuring total protein content using the SRB assay. Left = growth as % of solvent control. Data, mean ± SD, n=3. Middle = Bliss and Loewe model prediction. Right = Combenefit synergy score. Data, mean ± SD, n=3. The greater the difference between the experimental values and the model prediction, the greater the synergy score.

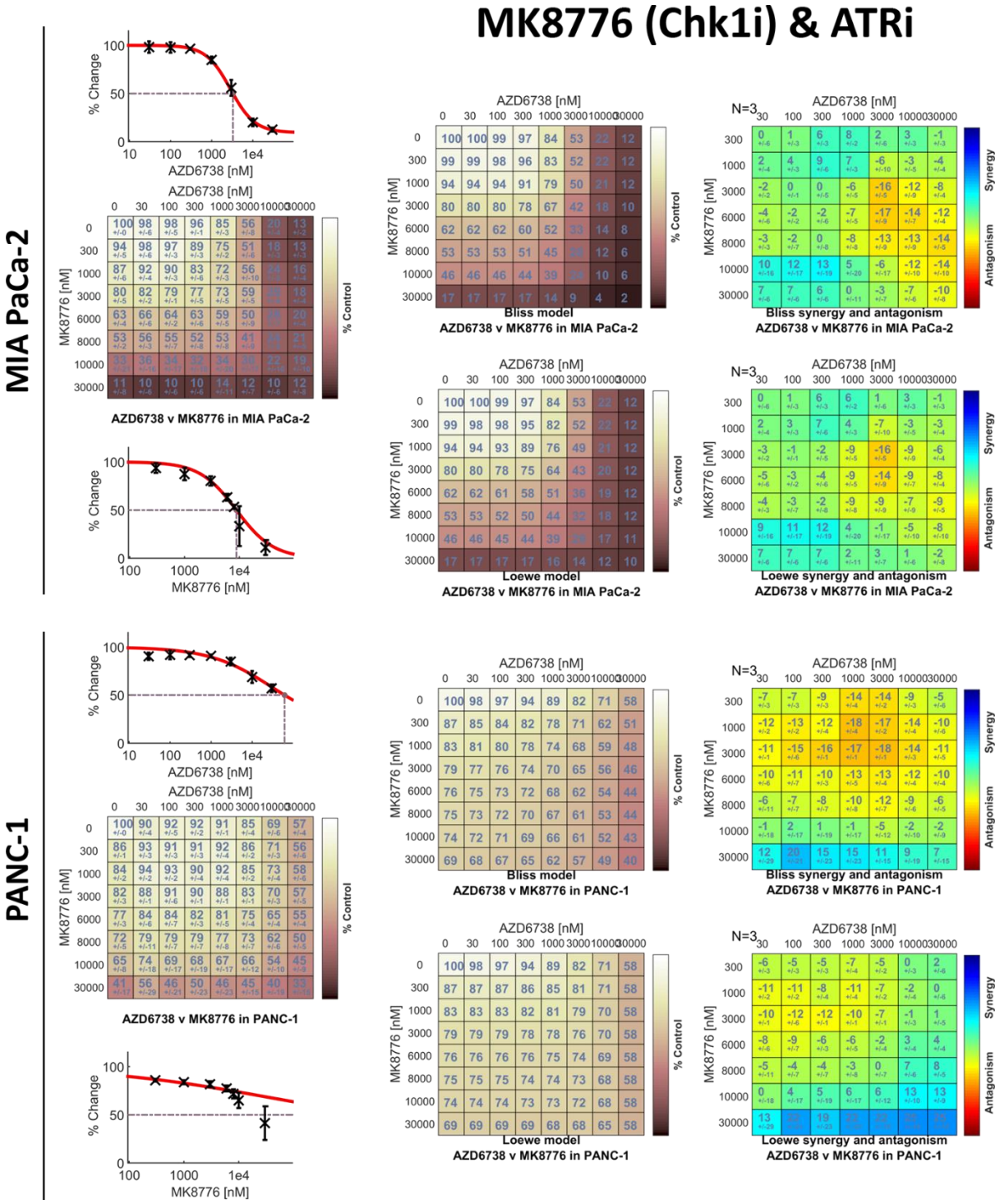

Fig. 3.5. MIA PaCa-2 and PANC-1 were treated with increasing concentrations of AZD6738 and MK8776 (Chk1 inhibitor) for 72 hours. Cell number at endpoint was determined by measuring total protein content using the SRB assay. Left = growth as % of solvent control. Data, mean ± SD, n=3. Middle = Bliss and Loewe model prediction. Right = Combenefit synergy score. Data, mean ± SD, n=3. The greater the difference between the experimental values and the model prediction, the greater the synergy score.

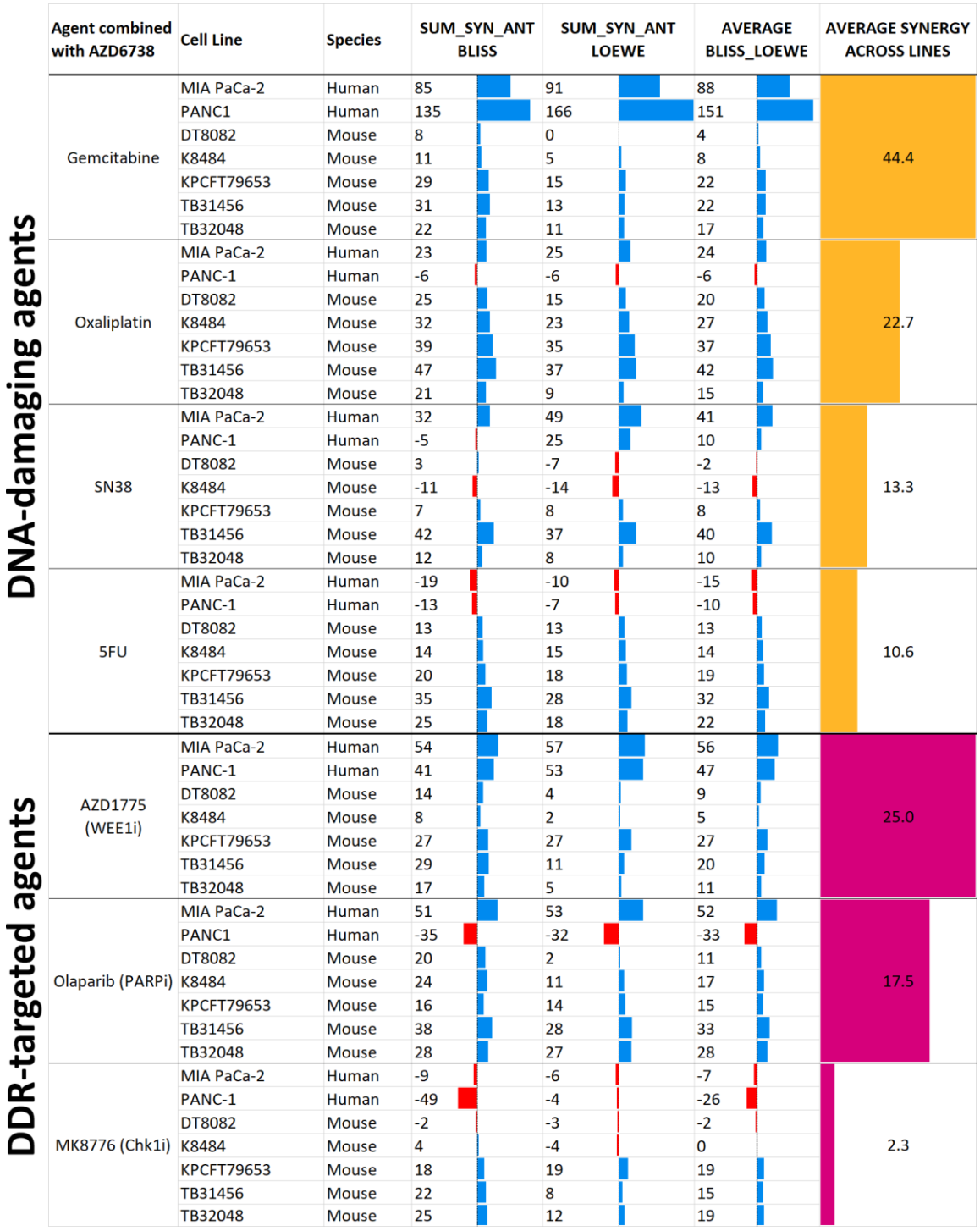

	Agent combined with AZD6738	Cell Line	Species	SUM_SYN_ANT BLISS	SUM_SYN_ANT LOEWE	AVERAGE BLISS_LOEWE	AVERAGE SYNERGY ACROSS LINES
DNA-damaging agents	Gemcitabine	MIA PaCa-2	Human	85	91	88	44.4
		PANC1	Human	135	166	151	
		DT8082	Mouse	8	0	4	
		K8484	Mouse	11	5	8	
		KPCFT79653	Mouse	29	15	22	
		TB31456	Mouse	31	13	22	
		TB32048	Mouse	22	11	17	
	Oxaliplatin	MIA PaCa-2	Human	23	25	24	22.7
		PANC-1	Human	-6	-6	-6	
		DT8082	Mouse	25	15	20	
		K8484	Mouse	32	23	27	
		KPCFT79653	Mouse	39	35	37	
		TB31456	Mouse	47	37	42	
		TB32048	Mouse	21	9	15	
	SN38	MIA PaCa-2	Human	32	49	41	13.3
		PANC-1	Human	-5	25	10	
		DT8082	Mouse	3	-7	-2	
		K8484	Mouse	-11	-14	-13	
		KPCFT79653	Mouse	7	8	8	
		TB31456	Mouse	42	37	40	
		TB32048	Mouse	12	8	10	
	5FU	MIA PaCa-2	Human	-19	-10	-15	10.6
		PANC-1	Human	-13	-7	-10	
		DT8082	Mouse	13	13	13	
		K8484	Mouse	14	15	14	
		KPCFT79653	Mouse	20	18	19	
		TB31456	Mouse	35	28	32	
		TB32048	Mouse	25	18	22	
DDR-targeted agents	AZD1775 (WEE1i)	MIA PaCa-2	Human	54	57	56	25.0
		PANC-1	Human	41	53	47	
		DT8082	Mouse	14	4	9	
		K8484	Mouse	8	2	5	
		KPCFT79653	Mouse	27	27	27	
		TB31456	Mouse	29	11	20	
		TB32048	Mouse	17	5	11	
	Olaparib (PARPi)	MIA PaCa-2	Human	51	53	52	17.5
		PANC1	Human	-35	-32	-33	
		DT8082	Mouse	20	2	11	
		K8484	Mouse	24	11	17	
		KPCFT79653	Mouse	16	14	15	
		TB31456	Mouse	38	28	33	
		TB32048	Mouse	28	27	28	
	MK8776 (Chk1i)	MIA PaCa-2	Human	-9	-6	-7	2.3
		PANC-1	Human	-49	-4	-26	
		DT8082	Mouse	-2	-3	-2	
		K8484	Mouse	4	-4	0	
		KPCFT79653	Mouse	18	19	19	
		TB31456	Mouse	22	8	15	
		TB32048	Mouse	25	12	19	

Fig. 3.6. Sum of synergy and antagonism scores across all 7 cell lines and all 7 combinations tested, calculated using the *Batch Analysis* program of Combenefit software. Red bars denote a negative sum score (antagonism), blue bars denote a positive sum score (synergy).

3.4. Discussion

In this introductory results chapter, I have presented Combenefit synergy data, assessing the interactions of AZD6738 with DNA-damaging agents and DDR-targeted agents. My first finding was that 5-FU demonstrated no synergy with AZD6738 in MIA PaCa-2 and PANC-1, despite having synergised in KPC mouse cell lines. Like gemcitabine (dFdC), 5-FU is an antimetabolite, however its mechanism of action is different to dFdC. There are 3 active metabolites of 5-FU, these are (1) fluorodeoxyuridine monophosphate (FdUMP), which inhibits the *de novo* synthesis of deoxythymidine monophosphate (dTMP) by thymidylate synthetase (TS), leading to dNTP pool imbalance and DNA damage, (2) fluorodeoxyuridine triphosphate (FdUTP), which mis-incorporates into DNA and (3) fluorouridine triphosphate (FUTP), which mis-incorporates into RNA, disrupting normal RNA processing and function (Longley et al., 2003). Of these mechanisms, TS inhibition by FdUMP and DNA mis-incorporation of FdUTP are the most likely to activate the ATR pathway and explain the synergy seen in the KPC cell lines. One hypothesis for why 5-FU demonstrated no synergy with AZD6738 in the human cells could be that, in these cell lines, conversion to FUTP may be more dominant leading to RNA-processing disruption that, while toxic, would not induce ATR activation. To test this, the proportion of each 5-FU metabolite in KPC mouse lines vs human cell lines could be assessed by liquid chromatography with tandem-mass spectrometry. However, this is not the direction I chose to take for this project, choosing instead to focus on combinations that demonstrated consistent synergy, as I explain at the beginning of the next chapter.

The two additional DNA-damaging agents that constitute FOLFIRINOX, oxaliplatin and irinotecan (SN38), did demonstrate synergy with AZD6738 in MIA PaCa-2 and PANC-1 cells. Both these agents cause physical obstacles to form on DNA that impede the replication machinery, leading to fork stalling which will activate ATR. Oxaliplatin creates adducts by forming intra-strand and inter-strand cross-links (Graham et al., 2004), while TOP1 inhibition causes catalytic intermediates called TOP1 cleavage complexes to accumulate on DNA (Pommier et al., 2010). Potentiation of cisplatin by AZD6738 in lung cancer modes has been reported before (Vendetti et al., 2015), however the ability for oxaliplatin to also synergise with ATR inhibition has not been previously described. As for combined ATR and TOP1 inhibition, the Pommier group have assessed VE-821 and VX-970 (M6620) in combination with camptothecin (analogues of camptothecin include irinotecan and topotecan) and novel non-camptothecin TOP1 inhibitors, LMP400 and LMP776, in preclinical models of breast and

colon cancer (Coussy et al., 2020; Jossé et al., 2014), but not in pancreatic models. They have since demonstrated in a phase I trial that ATR inhibition using M6620 plus the maximum dose of topotecan is tolerable in patients (Thomas et al., 2017). The data I have presented indicate that the combination of AZD6738 and irinotecan may be effective in PDAC.

The two DDR-targeted agents that I assessed in combination with AZD6738 were the WEE1 inhibitor, AZD1775, and the Chk1 inhibitor, MK8776. WEE1 inhibition synergised with AZD6738 in both human cell lines. Though this was not a combination that I explored further during my PhD, in 2018 and 2019 two groups using preclinical breast cancer models demonstrated efficacy using this approach, citing forced mitotic entry of cells with DNA damage and mitotic catastrophe as the mechanism of cell death (Bukhari et al., 2019; Jin et al., 2018). As for Chk1, I found that the AZD6738 and MK8776 combination was mostly antagonistic in MIA PaCa-2 and PANC-1. To some extent, this contradicts the findings reported by the Helleday group. They concluded that combined ATR and Chk1 inhibition synergistically inhibited growth in U2OS and MCF-7 cells (in their view, because ATR would be required for survival during the uncontrolled origin firing induced upon Chk1 inhibition) (Sanjiv et al., 2015). However, they were combining the ATR inhibitor (VE-821) with AZD7762, which is in fact a dual inhibitor of Chk1 and Chk2, unlike the Chk1-specifc MK8776. The use of different inhibitors, as well as the different model systems (i.e. the differing genetic backgrounds of the cancer models assessed), may explain the contrasting results. Additionally, they primarily used clonogenic survival assays (72-hour drug treatment in sparsely seeded 10cm plates, followed by fresh media replacement and further incubation for 5–8 days before fixation, staining with methylene blue and manual colony counting) to assess the combination *in vitro*, as opposed to my shorter 72-hour SRB assays in a 96-well format. To investigate why AZD6738 antagonises MK8776 in MIA PaCa-2 and PANC-1, I would have to look at the changes in DDR signalling (e.g. markers such as P-ATR-T1989, P-Chk1-S345, P-Chk2-T68, P-CDK1-Y15, γH2AX-S139) and cell-cycle alterations that occur upon single agent versus combination treatment. It has been reported that in some KRAS-driven mouse models of PDAC, Chk1 inhibition monotherapy does not induce any detectable increase in γH2AX or apoptosis (Murga et al., 2011). The growth inhibition I observed with MK8776 alone may not represent cell death, conceivably, the increase in origin firing induced by Chk1-inhibiton may cause an ATR-dependent growth arrest (e.g. via ATR-driven activation of Chk2 (Pabla et al., 2008; Wang et al., 2006)), which may be prevented in the presence of AZD6738.

One of the potential limitations of this chapter is the lack of a clear positive control for calling synergy. The 5-FU and ATRi combination seemingly displayed no synergy, but to be sure of this result one of the combinations from Table 3.1 already know to be synergistic in MIA PaCa-2 and PANC-1 (e.g. gemcitabine and ATRi) could have been included alongside this set of experiments. Another potential limitation is that all experiments used 72-hour drug treatments, and it is possible that some of the combinations tested may require longer-term treatments for their full effect (i.e. DNA-damage induction and ATR activation) to be observed. If I were to repeat this set of experiments, I would perhaps try longer drug treatments for those combinations that displayed no synergy.

Primarily, the reason for adding more MIA PaCa-2 and PANC-1 data to the AZD6738 combination dataset (**Figs. 3.1-3.5**) was to be able to compare and rank the respective synergy scores (**Fig. 3.6**). AZD6738 and gemcitabine was ranked as the most synergistic combination which was reassuring, since this combination was already being progressed in the Jodrell lab into *in vivo* studies. My own investigations into the AZD6738 and gemcitabine combination form the basis of Chapter 4. Meanwhile, the synergy between AZD6738 and olaparib was also followed up by myself and others in the lab, as I will explain in detail in Chapter 5.

CHAPTER FOUR: ATM-loss as a predictive biomarker of response for combined ATR inhibition and gemcitabine in PDAC

4.1. Background

At the time that I started this project, the Jodrell lab had identified AZD6738 and gemcitabine (ATRi/gem) as a synergistic combination, which was demonstrating impressive efficacy in *in vitro* and *in vivo* PDAC models, such that a phase-I clinical trial was proposed (2017), and eventually launched (2019) as the ATRiUM trial (NCT03669601) (Wallez et al., 2018). I hypothesised that ATRi/gem would most likely benefit specific sub-groups of patients with pre-existing aberrations in DDR pathways. I further hypothesised that deficiency in the double-strand-break master-regulator, ATM, would sensitise tumours to ATRi/gem.

As discussed in Chapter 1, germline or somatic ATM mutations in PDAC occur at a prevalence of around 6.4%, (Armstrong et al., 2019), while tissue microarray data-sets indicate that low ATM protein expression in PDAC occurs at around 12-17% (Kamphues et al., 2015; Kim et al., 2014). The loss of ATM in a proportion of PDAC samples, plus the central role it plays in DSB repair make ATM a primary candidate for a potential predictive biomarker of response for ATRi/gem therapy. In Chapter 1, I described how ATM-deficiency has been linked previously, in some cancer models, to greater sensitivity to ATRi. However, there is a lack of consistency in the literature, not only in the conclusion but in terms of cancer model assessed, ATR inhibitor used, combination tested and the experimental method of ATM depletion employed. Synthetic lethal interactions are not always universal and often depend highly on the genetic background in which they are studied (Ryan et al., 2018). This led me to undertake an assessment of how ATM status affects ATRi sensitivity in PDAC cells, specifically using AZD6738 with and without gemcitabine, in alignment with the ATRiUM trial.

4.2. Pharmacological inhibition of ATM sensitises to ATR inhibition in PDAC cell lines

First, to assess the degree of sensitisation to ATR inhibition associated with loss of ATM function in PDAC cells, I used the selective and potent ATM kinase inhibitor, AZD0156 (Barlaam and Pike, 2016; Hickson et al., 2018; Pike et al., 2018), in combination with the ATR inhibitor, AZD6738 (Foote et al., 2018). The key advantage of using pharmacologic ATM inhibition initially was the ability to screen multiple lines relatively quickly, as opposed to genetic perturbation with can be timely and less scalable. I confirmed full target engagement

of AZD0156 in PDAC cells at low nanomolar concentrations (≥10 nM), as assessed by abrogation of ATM auto-phosphorylation in response to irradiation (IR) in MIA PaCa-2 (**Fig. 4.1A**). In the absence of extrinsic damage, AZD0156 exposure had minimal effect on human or mouse PDAC cell growth when used at concentrations ≤100 nM (**Fig. 4.1B**), at which off-target activity is minimised.

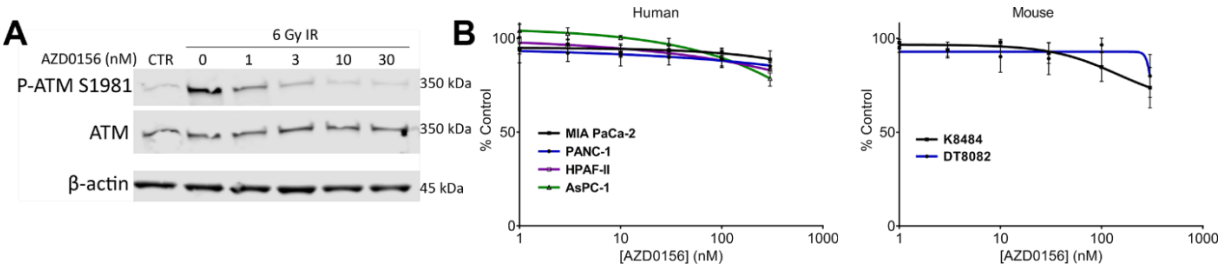

Fig. 4.1 (A) MIA PaCa-2 were incubated with AZD0156 for 1 hour before exposure to 6 Gy of γ-irradiation (IR). 30 mins post-IR, cells were harvested for immunoblot analysis. (**B)** Human and mouse cell lines were exposed to AZD0156 for 72 hours to generate dose-response curves using the SRB assay. Each point represents the mean of three independent experiments ± SEM.

I next evaluated the degree of growth inhibition induced by AZD6738 (ATRi) across a range of AZD0156 (ATMi) concentrations. ATMi sensitised all 6 of the human and mouse PDAC lines tested to ATR inhibition (**Fig. 4.2**). Calculation of Bliss and Loewe synergy scores using Combenefit software (Di Veroli et al., 2016) showed that the ATRi/ATMi combination synergistically inhibited growth in all 6 of these lines, albeit modestly in the ATRi-resistant PANC-1 (GI_{50} > 30 μM).

To assess the long-term proliferation capacity of cells exposed to a 24-hour pulse of AZD6738, I then performed clonogenic assays. In this assay, ATMi strikingly sensitised MIA PaCa-2 to ATRi (**Fig. 4.3**).

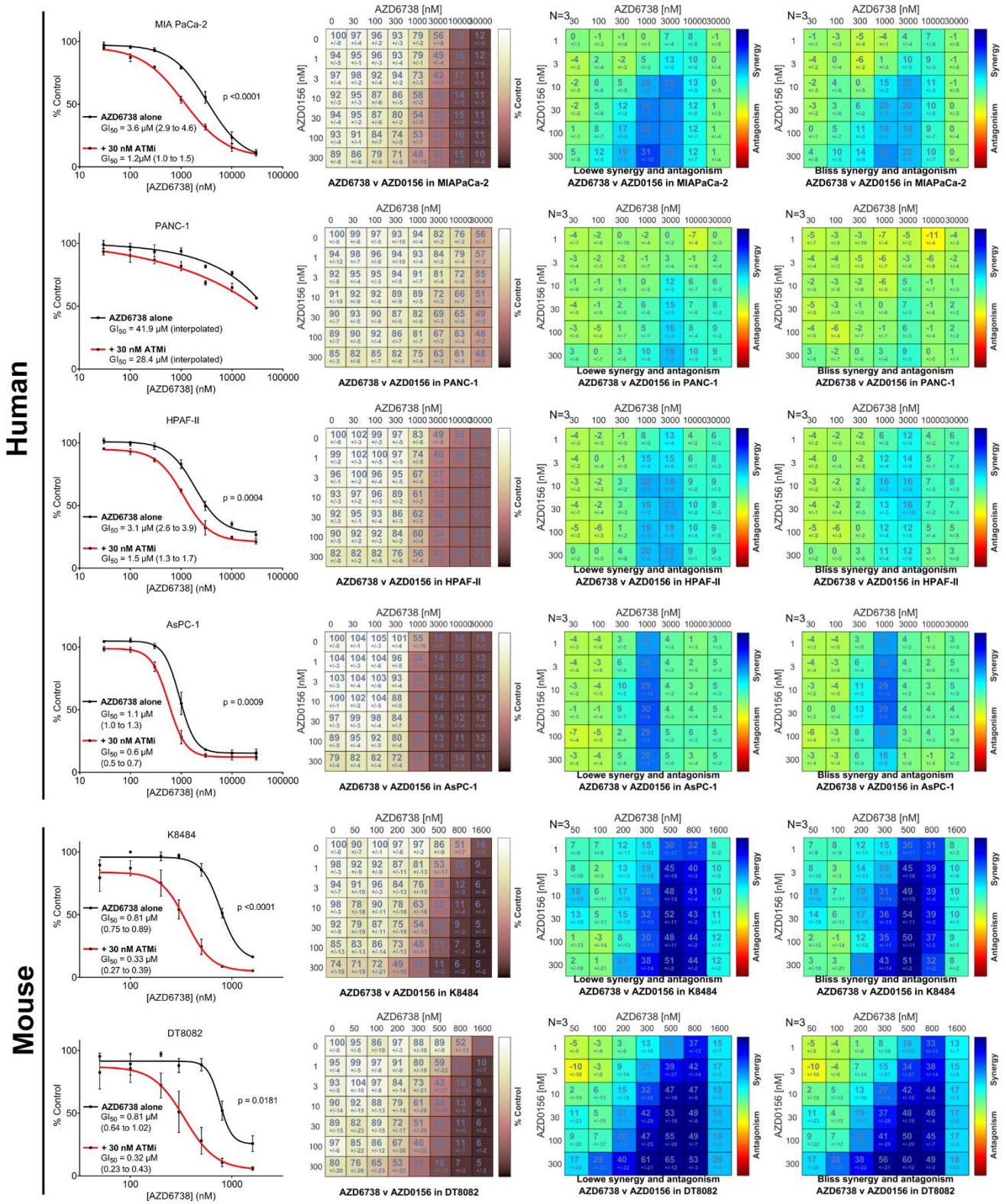

Fig. 4.2. Human and mouse lines were treated with increasing concentrations of AZD6738 and AZD0156 for 72 hours. Left = AZD6738 dose response curve with and without 30 nM AZD0156, mean ± SEM, n=3, with GI_{50} plus 95% confidence intervals shown, plus *p* value of curve comparison (Extra sum-of-squares F test). Middle = Full dose ranges, growth as % of solvent control (as assessed by SRB assay), mean ± SD, n=3. Right = Combenefit synergy score (Loewe and Bliss).

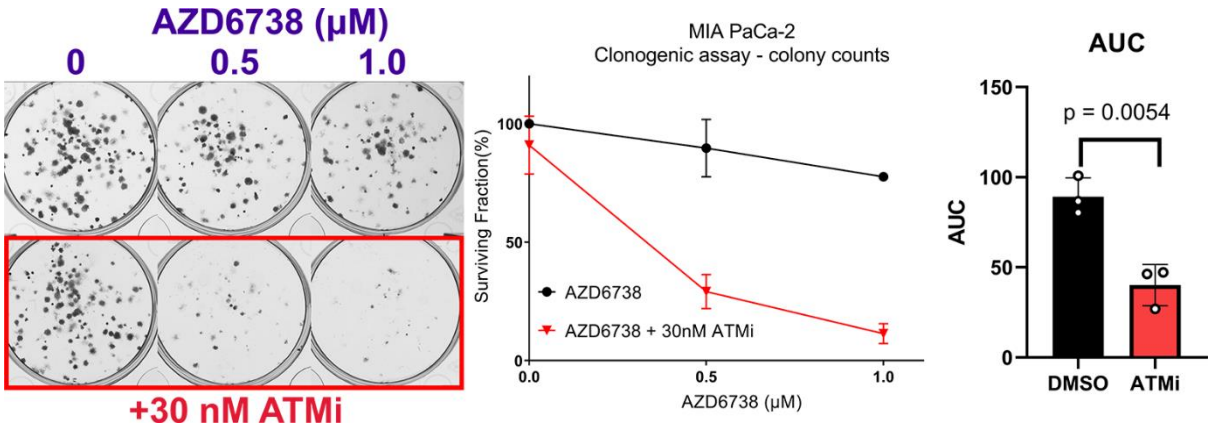

Fig. 4.3. Clonogenic survival of MIA PaCa-2 cells plated at low density and exposed to the indicated drug combinations for 24 hours before washout. Cells were left to grow for 7 days after washout. Left = representative image of wells. Middle = surviving fraction values quantified using the GelCount. Each point represents the mean of three independent experiments ± SEM. Right = the area of the curve (AUC) for AZD6738 and AZD6738 + 30 nM ATMi AUC were generated using GraphPad Prism 7. Bars represent mean ±SD.; p = result of two-tailed Student's t test.

4.3. ATM protein depletion by siRNA knockdown does not sensitise PDAC cells to ATR inhibition

Having identified that pharmacological inhibition of ATM in PDAC cell lines can sensitise to ATRi, I next evaluated the potential for siRNA knockdown of ATM to confer ATRi sensitivity in three human cell lines – MIA PaCa-2, PANC-1 and HPAF-II. Despite achieving durable ATM knockdown (average 88% knockdown efficiency across 3 lines) (**Fig. 4.4A**), this did not significantly sensitise any of the 3 cell lines to 72-hour exposure to AZD6738 (**Fig. 4.4B**). Due to this disparity between kinase inactivation (ATMi) and protein depletion (siATM), I hypothesised that reduced expression of ATM may be insufficient to sensitise cells to AZD6738.

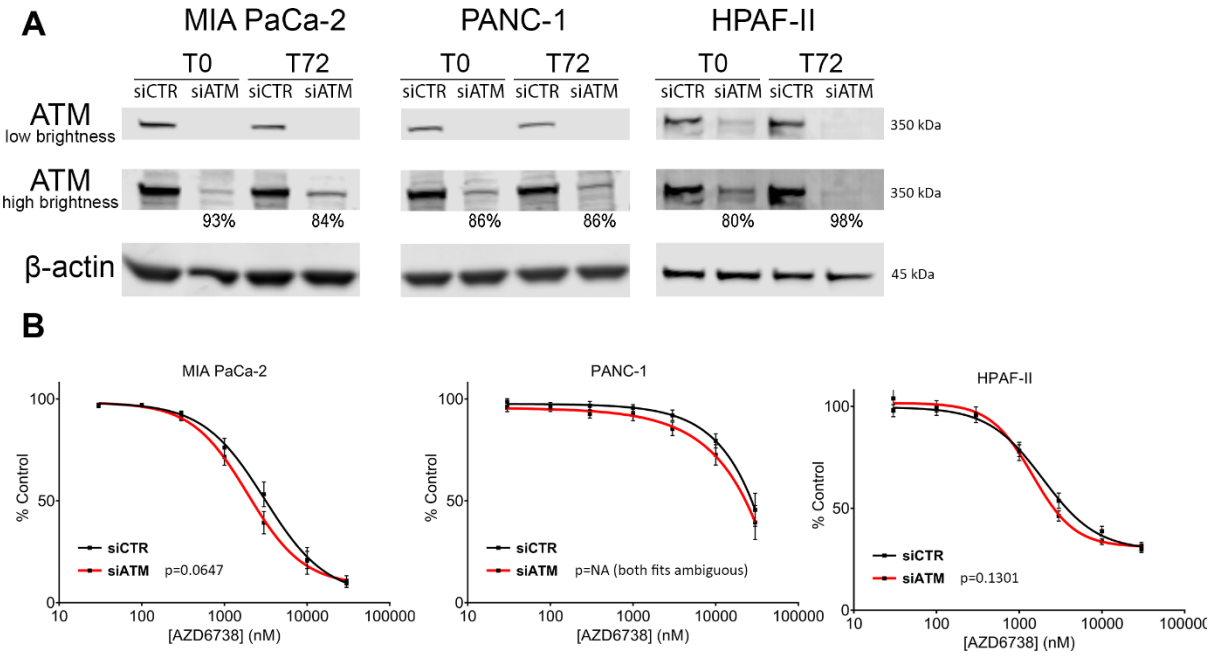

Fig. 4.4 (A) ATM protein expression in human cell lines at the start (T0) of the drug sensitivity assay (3 days post-transfection) and at the 72-hour assay endpoint (6 days post-transfection). Two different "exposures" of the ATM blot are shown (by adjusting brightness of the IRDye image in LiCor Image Studio). Percentage knockdown values versus siCTR are displayed, derived using LiCor Image Studio quantification software. **(B)** AZD6738 dose-response curves of human lines, having been transfected with either a non-targeting siRNA control pool (siCTR) or with an ATM-targeting siRNA pool (siATM). Assay duration was 72-hours. Each point represents the mean of three independent experiments ± SEM. *p* values of curve comparisons (Extra sum-of-squares F test) are also shown.

4.4. Deletion of ATM using CRISPR/Cas9 does significantly sensitise PDAC cells to ATR inhibition

Having observed a sensitisation effect with the ATMi, but not with siATM, I next used CRISPR/Cas9 technology to generate ATM knockout (KO) MIA PaCa-2 single cell clones. By Sanger sequencing (**Fig. 4.5**) and immunoblotting, I identified three clones that did not express detectable ATM and showed no phospho-ATM S1981 upon irradiation (**Fig. 4.6A**).

These three ATM-null clones were 7-fold more sensitive to AZD6738 than wild-type (WT) MIA PaCa-2 cells (mean ATM-null cells GI_{50} = 0.37 µM; mean ATM-positive cells GI_{50} = 2.73 µM) (**Fig. 4.6B-C**). As sensitisation occurred upon ATM knock-out, but not knock-down with siRNA, this suggests that complete loss of ATM function, not just depletion, is necessary to sensitise PDAC cells to ATRi monotherapy.

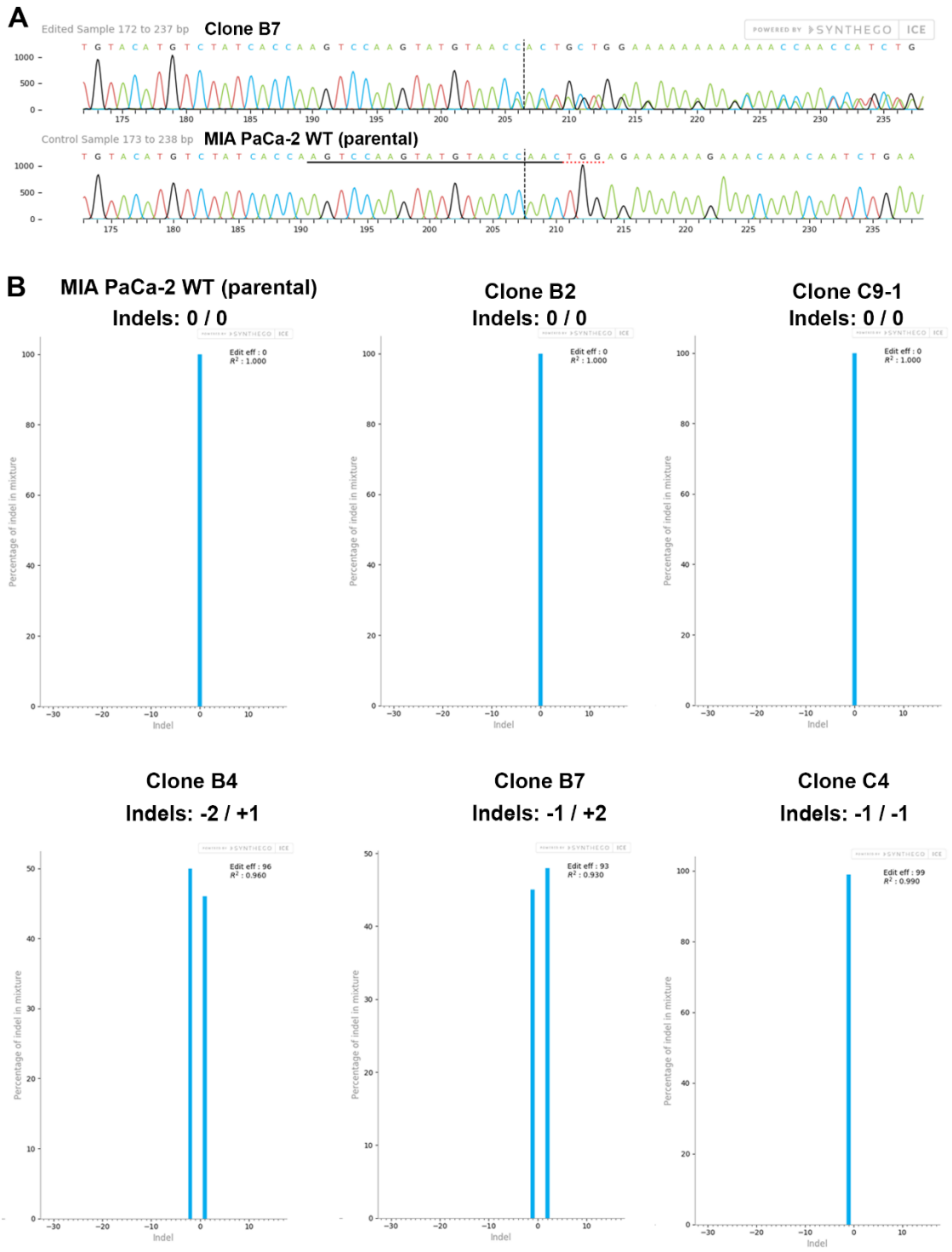

Fig.4.5 (A) Genetic characterisation of sgATM-Cas9-transfected MIA PaCa-2 single cell clones. From genomic DNA, the region around the sgATM-Cas9 target site (in exon 59) was amplified by PCR and sent for Sanger nucleotide sequencing. Example trace for clone B7 is shown, with the guide RNA sequence (black line) and the NGG protospacer adjacent motif (dotted red line) highlighted. **(B)** Chromatograms were deconvoluted using the Synthego ICE web tool (ice.synthego.com) which generated plots showing the relative prevalence of indels in each sample (i.e. in each clone). All indels identified were small insertions or deletions, occurring at Valine-2862, in the kinase domain of ATM (e.g. Indels: -1/+2 for clone B7. Allele 1 has a single nucleotide deletion, c.8972delC, and allele 2 has a two-nucleotide insertion, c.8971_8972insXX).

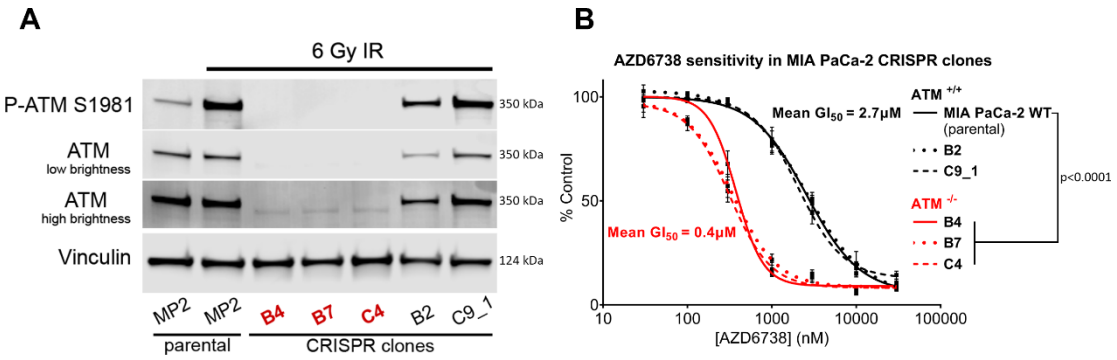

C

		(nM)		
Clone name	**ATM status**	**AZD6738 GI_{50}**	**95% confidence interval**	**Mean GI_{50}**
WT (parental)	positive	2819	2486 to 3227	2728
B2	positive	2909	2412 to 3582	
C9_1	positive	2458	2106 to 2911	
B4	null	405	362 to 477	372
B7	null	373	325 to 430	
C4	null	337	287 to 398	

Fig. 4.6 (A) 30 mins post 6 Gy of γ-irradiation (IR), MIA PaCa-2 single cell clones from a CRISPR/Cas9 ATM knockout pool were harvested for immunoblot analysis to determine the ATM status. Clones B4, B7 and C4 were confirmed ATM-null. **(B)** AZD6738 dose-response curves of MIA PaCa-2 CRISPR clones. Assay duration was 72-hours. Each point represents the mean of three independent experiments ± SEM. *p* value denotes curve comparison (Extra sum-of-squares F test) of ATM-KO curves vs MIA PaCa-2 WT **(C)** AZD6738 GI_{50} values (the concentration that inhibits growth by 50% relative to control) for MIA PaCa-2 CRISPR clones.

4.5. ATM loss of function sensitises to the combination of AZD6738 and gemcitabine

I next tested whether reduced ATM function could sensitise to the combination of AZD6738 and gemcitabine (ATRi/gem). Kinase inhibition of ATM conferred sensitivity to 72-hour ATRi/gem exposure in MIA PaCa-2 (**Fig. 4.7A**) but siRNA depletion did not (**Fig. 4.7B**). While siATM induced no shift in the AZD6738 dose response curve in neither the presence nor the absence of gemcitabine, genetic deletion of ATM did sensitise MIA PaCa-2 cells to ATRi/gem (**Fig. 4.7C**) and caused a 2.6-fold shift in the mean gemcitabine GI_{50} (**Fig. 4.7D-E**).

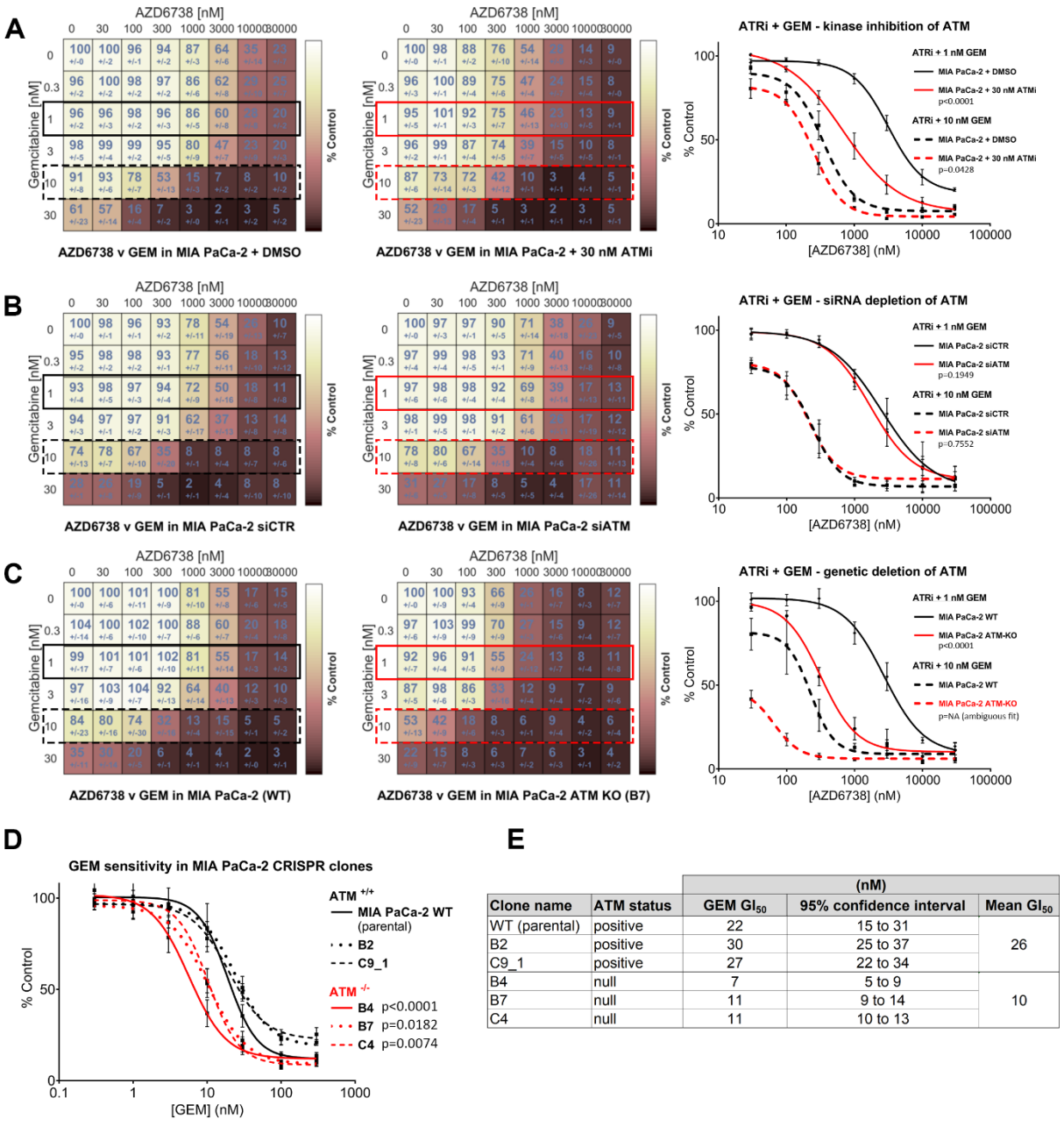

E

		(nM)		
Clone name	ATM status	GEM GI_{50}	95% confidence interval	Mean GI_{50}
WT (parental)	positive	22	15 to 31	26
B2	positive	30	25 to 37	
C9_1	positive	27	22 to 34	
B4	null	7	5 to 9	10
B7	null	11	9 to 14	
C4	null	11	10 to 13	

Fig. 4.7 (A) The effect of ATM kinase inhibition by AZD0156 on ATRi (AZD6738) & gemcitabine sensitivity in MIA PaCa-2. **(B)** The effect of ATM depletion by siRNA on AZD6738 & gemcitabine sensitivity in MIA PaCa-2**. (C)** The effect of ATM deletion by CRISPR/Cas9 on AZD6738 & gemcitabine sensitivity in MIA PaCa-2. In all three panels (A-C), MIA PaCa-2 in the conditions listed were treated with increasing concentrations of AZD6738 and gemcitabine for 72 hours. Left = Matrices displaying growth as % of solvent control (as assessed by SRB assay), mean ± SD, n=3. Right = AZD6738 dose response curves in the presence of 1 nM or 10 nM gemcitabine, mean ± SEM, n=3. *p* values denote curve comparisons (Extra sum-of-squares F test) between black and red curves **(D)** Gemcitabine dose-response curves of MIA PaCa-2 CRISPR clones. Assay duration was 72-hours. Each point represents the mean of three independent experiments ± SEM. *p* values denote curve comparisons (Extra sum-of-squares F test) of ATM-KO curves vs MIA PaCa-2 WT **(E)** Gemcitabine GI_{50} values (the concentration that inhibits growth by 50% relative to control) for MIA PaCa-2 CRISPR clones.

The ATM-KO hypersensitivity to ATRi/gem was particularly evident in assays where the ATRi/gem was pulsed for 24-hours with observation of subsequent cell growth by time-lapse imaging. A 24-hour pulse of 500 nM AZD6738 and 10 nM gemcitabine had no effect on the growth ability of the WT line (growth as percentage of solvent control = 96% +/-7) but maintained durable growth inhibition for at least 4 days in the ATM-KO cells (growth as percentage of solvent control = 7% +/-1) (**Fig. 4.8A-B**), with a parallel increase in cell death, quantified by YoYo-3 staining (**Fig. 4.8A**).

Though the combination of ATRi/gem had a more profound effect in ATM-KO cells, the shift in the dose-response curve (between WT vs KO) with gemcitabine was not any greater than the shift seen with single agent ATRi (**Fig. 4.7C, right**). Thus, more mechanistic studies plus *in vivo* experiments were needed to elucidate whether ATM-loss would be a suitable predictive biomarker of response to ATRi/gem in patients with PDAC.

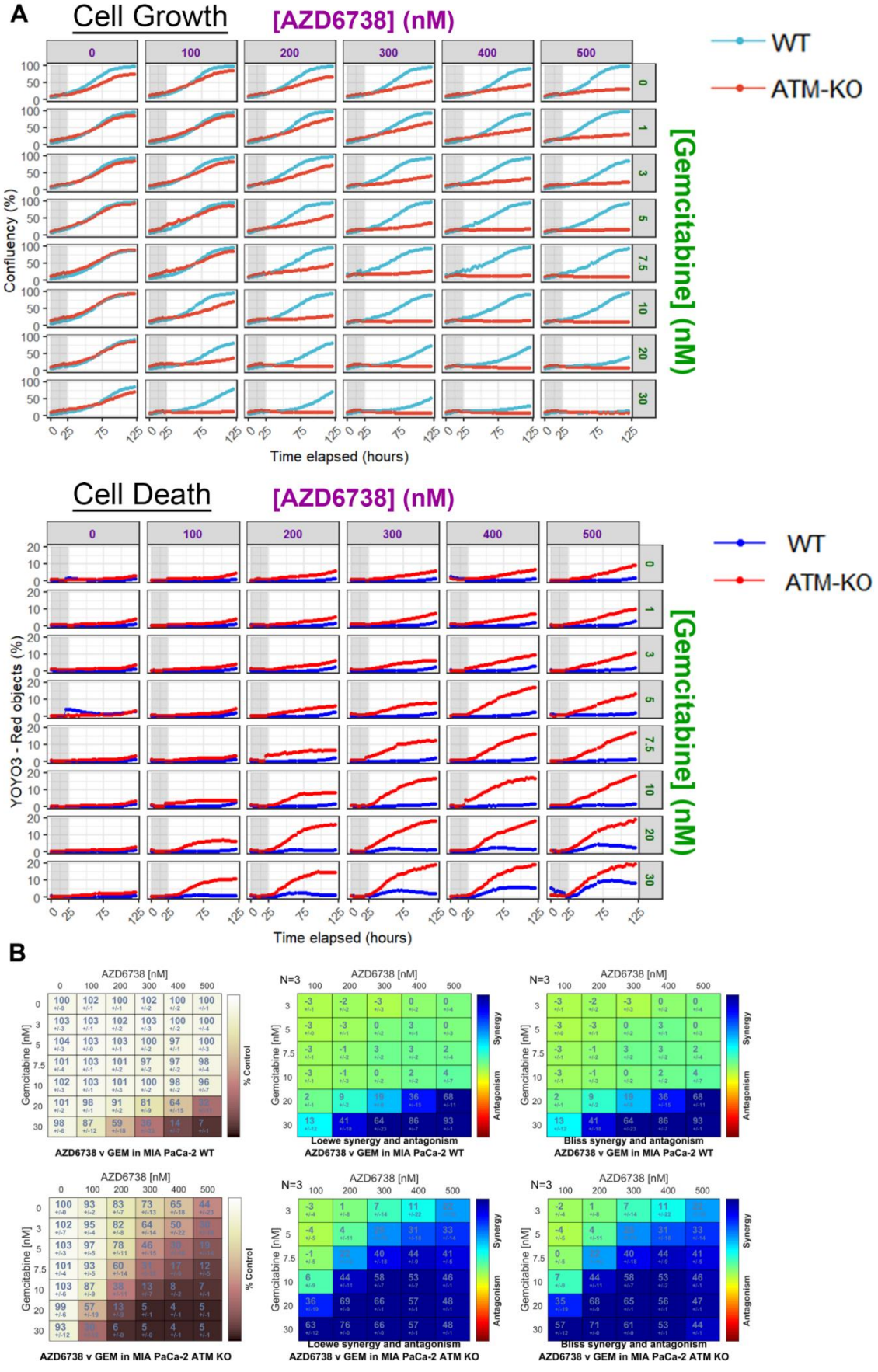

Fig. 4.8 (A) MIA PaCa-2 WT and MIA PaCa-2 ATM-KO (clone B7) cells in medium containing the YOYO-3 Iodide cell-impermeant dye were treated with AZD6738 and gemcitabine in a 6 × 8 concentration grid for 24 hours (grey bar denotes…

…period of drug treatment). The drugs were washed out and replaced with fresh YOYO-3-containing medium. Three fields per sample were imaged by IncuCyte time lapse microscopy every 3 hours for 125 hours. Phase Object Confluence was quantified as the percentage of the image area occupied by cells (upper). Cell death accumulation (lower) was quantified by measuring Red Object Confluence, and expressed as a percentage of the total Object Confluence. Each curve is a representative of three independent experiments. **(B)** The same cells from the IncuCyte experiment in (A) were fixed in TCA after 125 hours and the relative growth was assessed by SRB assay. Left = growth as % of solvent control, mean ± SD, n=3 independent experiments. Right = Combenefit synergy score (Loewe and Bliss).

4.6. ATRi/gem-induced DDR activation persists in the absence of ATM function, due to DNA-PK activity

Having found that targeting ATM, by either pharmacological inhibition or by genetic deletion, can sensitise PDAC cells to the combination of AZD6738 and gemcitabine, I next investigated the DDR signalling pathways activated by ATRi/gem, in the presence or absence of ATM function. 24 hour exposure of MIA PaCa-2 cells to 2000 nM ATRi and 30 nM gemcitabine (concentrations known to be synergistic in this line (Wallez et al., 2018)) induced phosphorylation of ATM and its downstream targets RAD50, KAP1 and Chk2 (**Fig. 4.9A**). Unexpectedly, because they are reported to be ATM kinase targets, the phospho-ATM S1981, phospho-KAP1 S824 and phospho-Chk2 T68 persisted, even in the presence of ATMi (AZD0156) (**Fig. 4.9A**). This persistence was specific to ATRi/gem, since irradiation-induced activation of these markers was prevented by 10 nM ATMi (**Fig. 4.9A & 4.1A**). In the ATRi/gem treated samples, I did observe ATMi dose-dependent abrogation of phospho-RAD50 S635 (**Fig. 4.9A**), a biomarker of ATM activity (Gatei et al., 2011; Jones et al., 2018), suggesting that the ATMi was acting on-target. Therefore, the persistence of phospho-Chk2 T68 and others could be due to the activity of another kinase, the most likely candidate being DNA-PKcs.

Indeed, the phospho-KAP1 and phospho-Chk2 induced by ATRi or ATRi/gem treatment was abrogated by the selective DNA-PKcs inhibitor, AZD7648 (Fok et al., 2019) (**Fig. 4.9B**). Along with phospho-ATM, these phosphorylations were only fully prevented upon combined ATMi and DNA-PKcsi. I also probed for ATR and its downstream partner Chk1. Gemcitabine-induced phospho-ATR T1989 persisted in the presence of ATRi due to ATM-dependent phosphorylation (**Fig. 4.9B**). Meanwhile, phospho-Chk1 S345 was only abrogated upon DNA-PKcs inhibition (**Fig. 4.9B**). Thus, I revealed that much of the downstream DDR activation induced by ATRi or ATRi/gem was not prevented by ATMi (besides phospho-RAD50 and phospho-ATR), because of phosphorylation by DNA-PKcs.

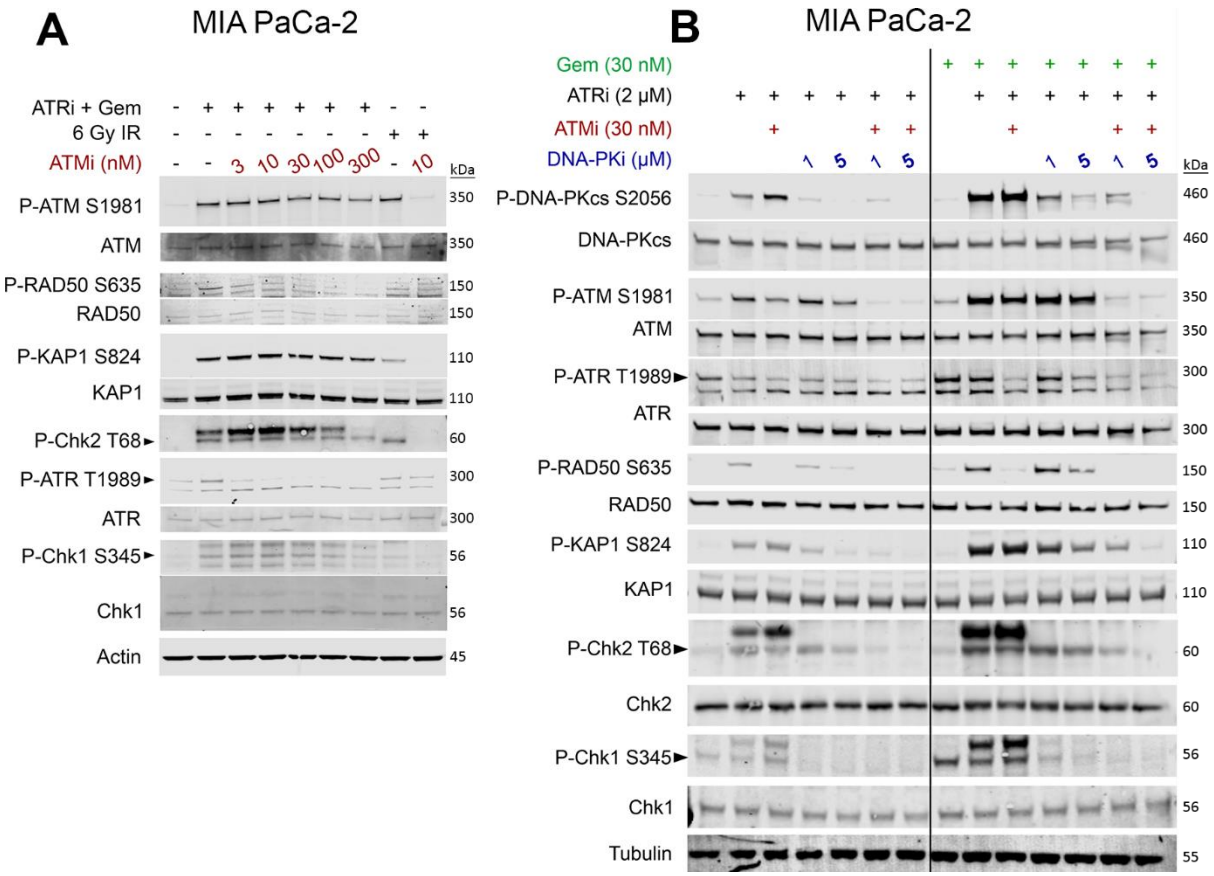

Fig. 4.9 (A) Immunoblot analysis of MIA PaCa-2 cells. Cells which received 6 Gy of γ-irradiation (IR) were harvested 30 mins post-IR. All other samples were harvested after 24 hours of drug exposure. ATRi + GEM denotes 2 μM AZD6738 and 30 nM gemcitabine. ATMi is AZD0156 and was either applied concurrently with ATRi/gem, or administered one hour prior to IR, in the case of the two IR samples. (**B)** Immunoblot analysis of MIA PaCa-2 cells. Cells were harvested after 24 hours of drug exposure. ATRi is AZD6738, ATMi is AZD0156, DNA-PKi is AZD7648.

Next, I repeated these immunoblotting experiments in HPAF-II and found the same DNA-PKcs-dependency for ATR/gem-induced phospho-KAP1, phospho-Chk2 and phospho-Chk1 (**Fig. 4.10**), confirming that this was not a phenotype specific to MIA PaCa-2.

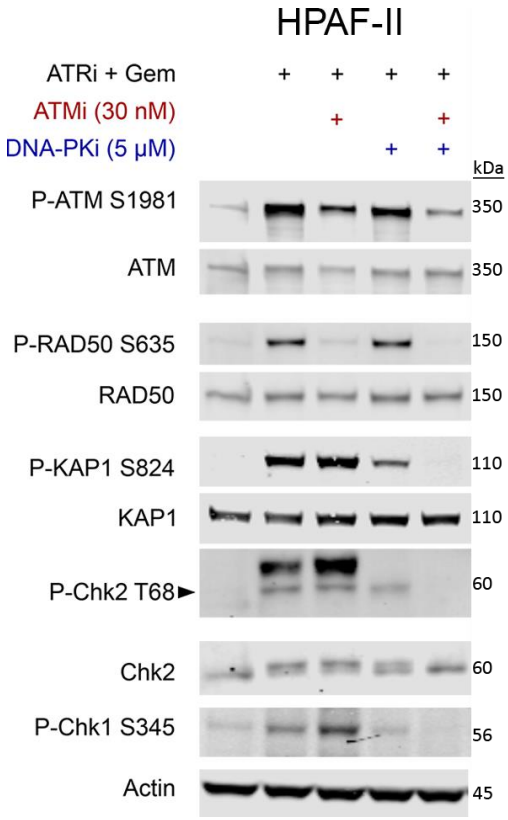

Fig. 4.10. Immunoblot analysis of HPAF-II cells. Cells were harvested after 24 hours of drug exposure. ATRi + GEM denotes 2 µM AZD6738 and 30 nM gemcitabine. ATMi is AZD0156, DNA-PKi is AZD7648.

I next interrogated DDR pathway activation in ATM-KO MIA PaCa-2 cells. Once again, ATRi/gem treatment upregulated phospho-Chk2, phospho-KAP1 and phospho-Chk1 in both the presence and the absence of ATM function (**Fig. 4.11**). These phosphorylations were DNA-PKcs driven, as evidenced by their abrogation by AZD7648 (**Fig. 4.11**). The low baseline levels of phospho-RAD50 S635 in untreated ATM-KO MIA PaCa-2 cells appeared to be ATR-dependent, consistent with recent findings that in ATM-deficient models ATR can phosphorylate RAD50 (Jones et al., 2018). Unlike with Chk2 and KAP1, the ability for the ATM-KO cells to upregulate phospho-RAD50 S635 upon ATRi/gem was significantly impaired in comparison to ATM-WT. The modest phospho-RAD50 S635 that was induced by ATRi/gem was DNA-PKcs-dependent (**Fig. 4.11**). Meanwhile, phosphorylation of ATR T1989 appeared to be ATR- and ATM-dependent, but not DNA-PKcs-dependent (**Fig. 4.11**).

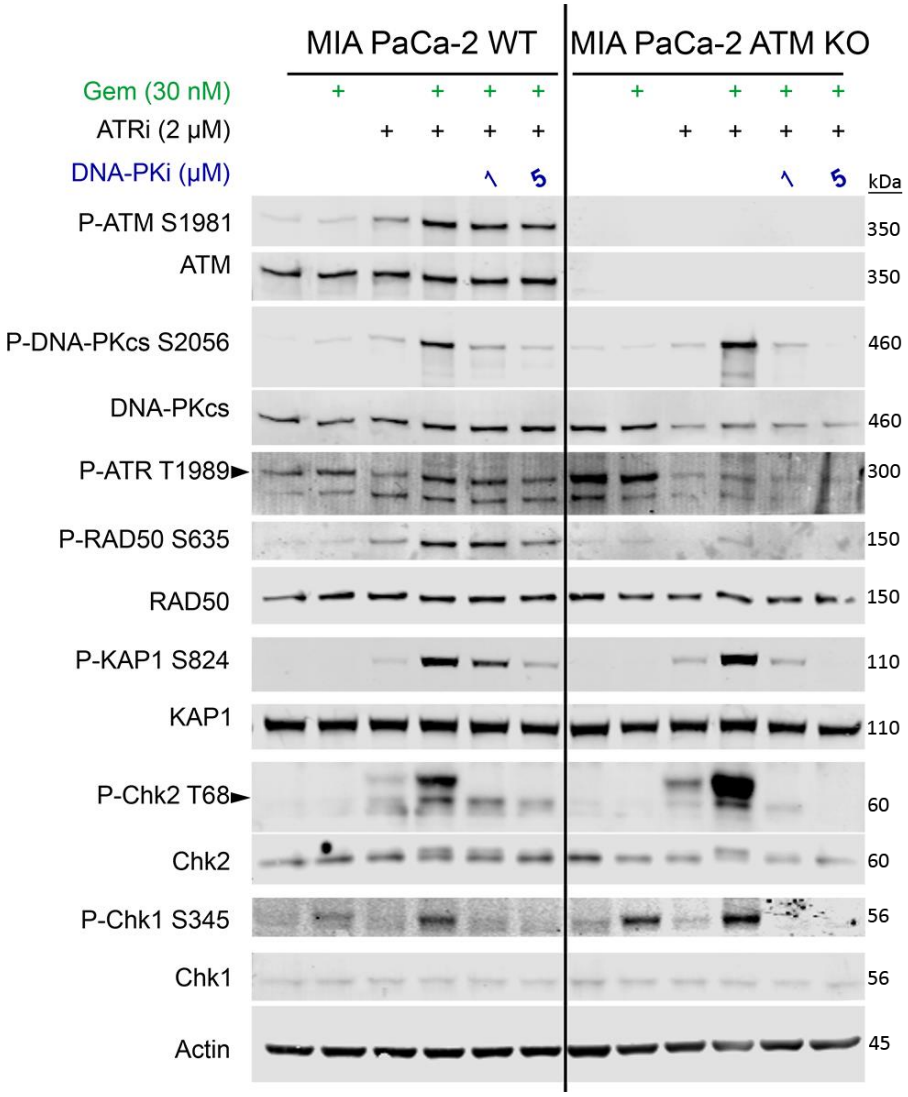

Fig. 4.11. Immunoblot analysis of MIA PaCa-2 WT and MIA PaCa-2 ATM-KO cells (clone B7). Cells were harvested after 24 hours of drug exposure. ATRi is AZD6738, DNA-PKi is AZD7648.

Despite the contribution of DNA-PKcs to many of the DDR phosphorylations in ATRi-treated cells, Bliss and Loewe cytotoxicity synergy scores showed consistently less synergy for the AZD6738 and AZD7648 (DNAPKi) combination than for AZD6738 and AZD0156 (ATMi) across human and mouse PDAC cell lines (**Fig. 4.12 & 4.13**).

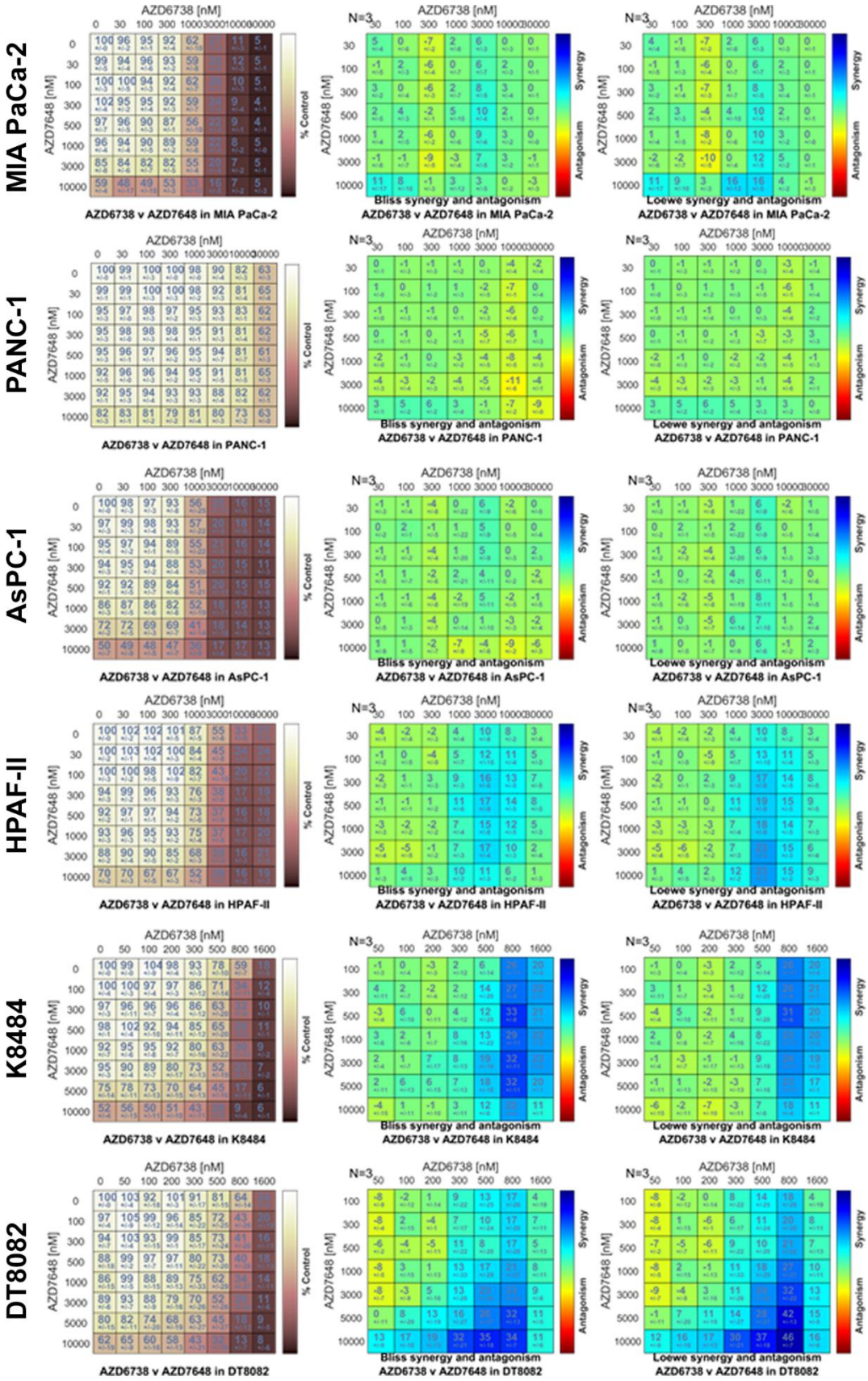

Fig. 4.12. Cells were treated with increasing concentrations of AZD6738 (ATRi) and AZD7648 (DNA-PKi) for 72 hours. Left = growth as % of solvent control (as assessed by SRB assay), mean ± SD, n=3. Right = Combenefit synergy score (Bliss and Loewe).

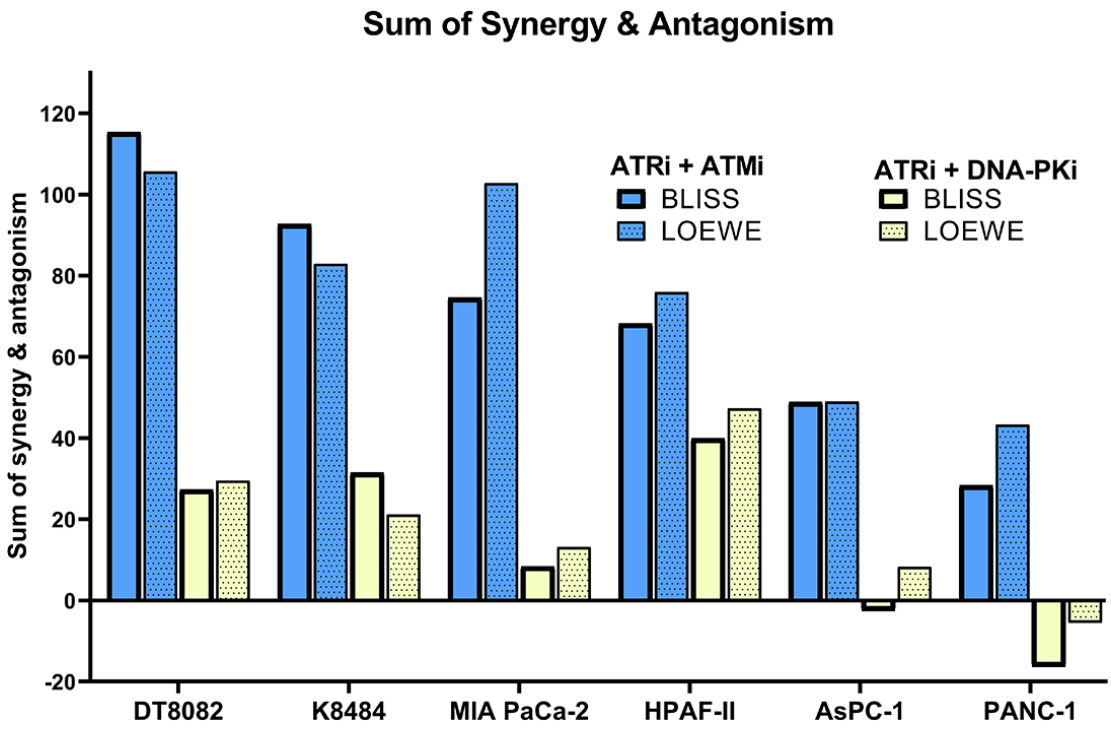

Fig. 4.13. Synergy comparison of the AZD6738 & AZD0156 combination (ATRi + ATMi, see Fig. 1C & 1D) vs the AZD6738 & AZD7648 combination (ATRi + DNAPKi). Combenefit software was used to calculate the sum of synergy and antagonism across the dose ranges tested.

Furthermore, in triple combination SRB experiments, the addition of DNA-PKcsi to ATRi/gem led to only moderate sensitisation compared to ATMi (**Fig. 4.14A-B**). As with MIA PaCa-2 WT, DNA-PKcsi also had minimal effect on the sensitivity of ATM-KO MIA PaCa-2 to ATRi or ATRi/gem (**Fig. 4.14D-E**). This suggests that ATM function is more critical to cell survival during ATRi or ATRi/gem exposure than DNA-PKcs activity. It also implies that the Chk1/Chk2 phosphorylations that arise through DNA-PKcs activity do not play a major protective role in ATRi/gem-exposed PDAC cells. To test this one could carry out genetic experiments where Chk1/Chk2 are deleted or downregulated before assessing response to ATRi/gem, or using Chk1/Chk2 inhibitors.

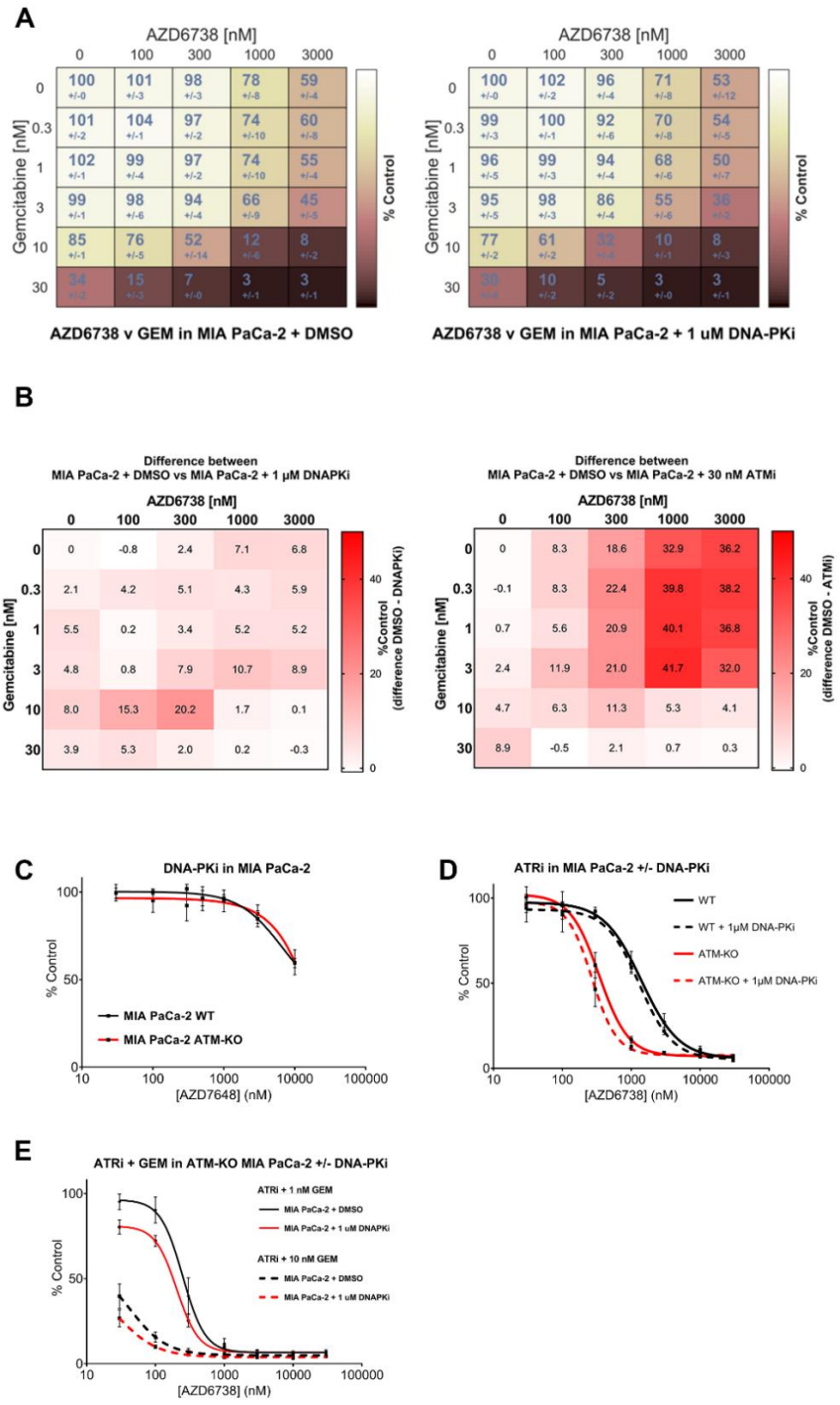

Fig. 4.14 (A) The effect of DNA-PK inhibition on AZD6783 & gemcitabine sensitivity in MIA PaCa-2. Values denote growth as % of solvent control (as assessed by SRB assay), mean ± SD, n=3. **(B)** Visualisation of how much more effect ATM inhibition has compared to DNA-PKcs inhibition, on the growth of ATRi/gem-treated MIAPaCa-2. Left = the *%Control* values of the *MIA PaCa-2 + 1 µM DNA-PKi* matrix from Fig. 4.13 (A) were subtracted from those of the *MIA PaCa-2 + DMSO* matrix from Fig. 4.13 (A). Right = the *%Control* values of the *MIA PaCa-2 + 30 nM ATMi* matrix from Fig. 4.7 (A) were subtracted from those of the *MIA PaCa-2 + DMSO* matrix from Fig. 4.7 (A). **(C)** AZD7648 (DNA-PKi) dose response curves in WT and ATM-KO MIA PaCa-2 (clone B7). (**D)** Effect of DNA-PKi on ATRi sensitivity in WT and ATM-KO MIA PaCa-2. **(E)** Effect of DNA-PKi on ATRi/gem sensitivity in ATM-KO MIA PaCa-2. Assay duration was 72-hours. Each point represents the mean of three independent experiments ± SEM.

4.7. ATRi/gem-induced replication catastrophe is augmented in ATM-null PDAC cells

I next investigated the effect of AZD6738 and gemcitabine treatment on the cell cycle profile of ATM-proficient and ATM-deficient PDAC cells. Treatment with 500 nM AZD6738 and 10 nM gemcitabine for 24 hours had little-to-no effect on the cell cycle profile of WT MIA PaCa-2 cells. Conversely, 10 nM gemcitabine induced intra-S accumulation in the ATM-KO MIA PaCa-2, along with a reduction in the G2-M proportion (**Fig. 4.15A**). This was augmented by the addition of 500 nM AZD6738, which also increased the sub-G1 fraction, indicating induction of cell death. When the higher concentration of 2000 nM AZD6738 was used, I observed modest intra-S accumulation with ATRi-monotherapy, which was specific to the ATM-null cells, while addition of 30 nM gemcitabine could induce S-phase arrest in both the ATM-WT and ATM-KO cells (**Fig. 4.15B**).

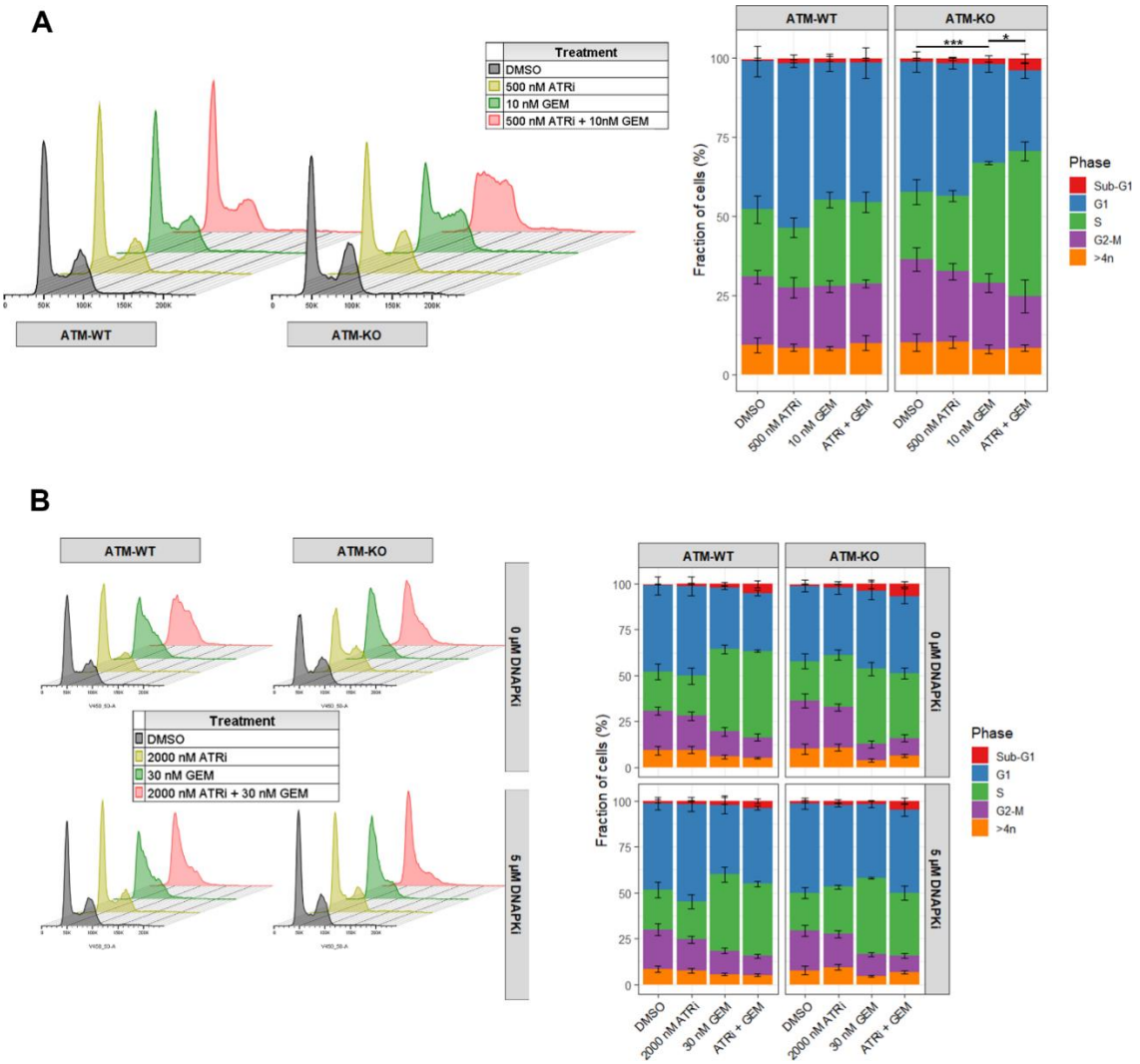

Fig. 4.15 (A) DNA content of MIA PaCa-2 WT and MIA PaCa-2 ATM-KO (clone B7) cells following 24-hour exposure of the indicated drugs. 500 nM AZD6738 and 10 nM gemcitabine are synergistic concentrations in ATM-KO MIA PaCa-2 (see Fig. 4.8B). Left = Representative DNA content histograms, x = FxCycle Violet fluorescence (DNA content), y = cell count…

…Right = cell cycle distribution. Each bar represents the mean of 3 independent experiments ± SD. A one-way ANOVA analysis, comparing the % S phase fractions, was performed with Tukey's multiple comparisons tests, * indicates $p \leq 0.05$, ** $p \leq 0.01$, *** $p \leq 0.001$. **(B)** DNA content of MIA PaCa-2 WT and MIA PaCa-2 ATM-KO cells following 24-hour exposure of the indicated drugs. 2000 nM AZD6738 and 30 nM gemcitabine are synergistic concentrations in both WT and ATM-KO MIA PaCa-2 (see Fig. 4.8B). Left = Representative DNA content histograms, x = FxCycle Violet fluorescence (DNA content), y = cell count. Right = cell cycle distribution. Each bar represents the mean of 3 independent experiments ± SD.

Through immunoblotting I had found that treatment with 2000 nM AZD6738 and 30 nM gemcitabine induced DNA-PKcs-driven activation of the checkpoint proteins, Chk1 and Chk2. However, co-treating with the DNA-PKi AZD7648 did not alter the cell cycle profiles in any of the ATRi/gem conditions (**Fig. 4.15B**), indicating that the intra-S phase arrests I observed were independent of checkpoint activation. An alternative reason for the intra-S accumulation, independent of a checkpoint, could be induction of replication catastrophe. This is defined as the widespread breakage of multiple replication forks, resulting from a global exhaustion of RPA and subsequent degradation of unprotected ssDNA at stalled forks (Toledo et al., 2017, 2013; Warren and Eastman, 2019). I found that 500 nM AZD6738 and 10 nM gemcitabine caused RPA32 to deplete from the cytosol and accumulate in the nucleus over time, with a parallel increase in nuclear γH2AX S139, in the ATM-KO MIA PaCa-2 (**Fig. 4.16**).

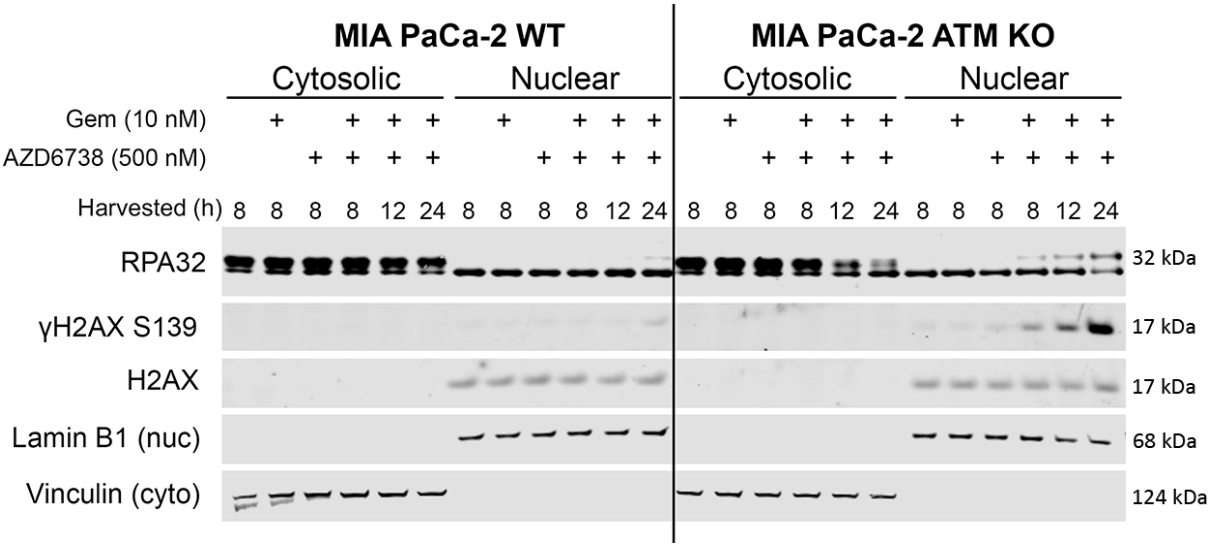

Fig. 4.16 Immunoblot analysis of MIA PaCa-2 WT and MIA PaCa-2 ATM-KO cells treated as indicated, separated by cytosolic and nuclear fractions.

Next, using quantitative image-based cytometry (**Fig. 4.17**), I assessed the degree of replication catastrophe induced by ATRi and ATRi/gem in ATM-WT vs ATM-KO, by quantifying the emergence of cells with pan-nuclear γH2AX S139 and pan-nuclear phospho-RPA32 S4/8 (**Fig. 4.18**). After 24–hour exposure to 500 nM AZD6738 alone, 1.4% of WT MIA PaCa-2 cells were pan-nuclear for both markers, compared to 8.7% of ATM-KO cells (**Fig. 4.18A**).

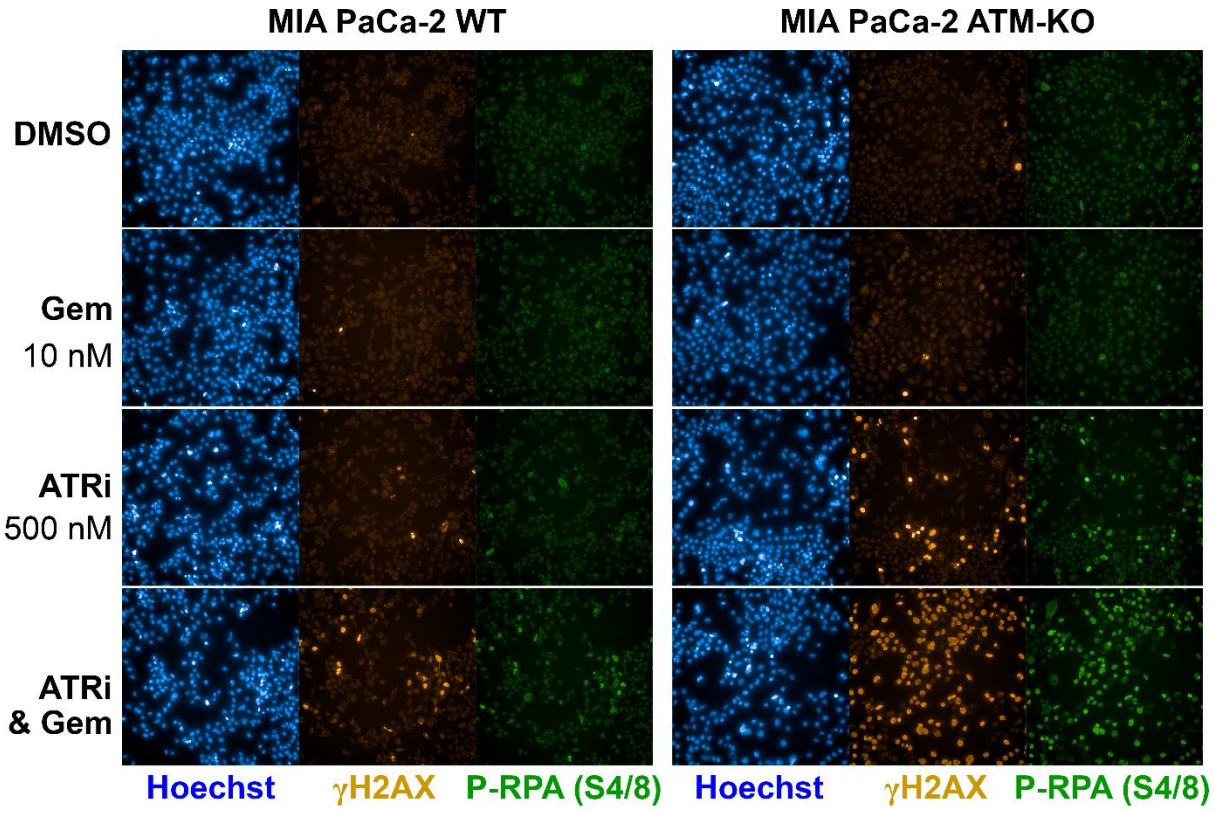

Fig. 4.17. Representative images showing the pan-nuclear emergence of γH2AX S139 and phospho-RPA32 S4/8 upon 24-hour exposure to 500 nM AZD6738 and 10 nM gemcitabine.

The combination of 500 nM AZD6738 and 10 nM gemcitabine induced pan-nuclear γH2AX S139 and phospho-RPA32 in both cell types, but much more extensively in the ATM-KO cells (9.9% WT double-positive vs 58.2% ATM-KO double-positive after 24 hours) (**Fig. 4.18B**). Hoechst quantification indicated that cells with pan-nuclear damage typically had DNA contents between 2n and 4n, consistent with S-phase failure (**Fig. 4.19**). This observation of increased replication catastrophe in the ATM-KO cells suggests that ATM protects against nuclear-wide fork collapse during ATRi/gem treatment.

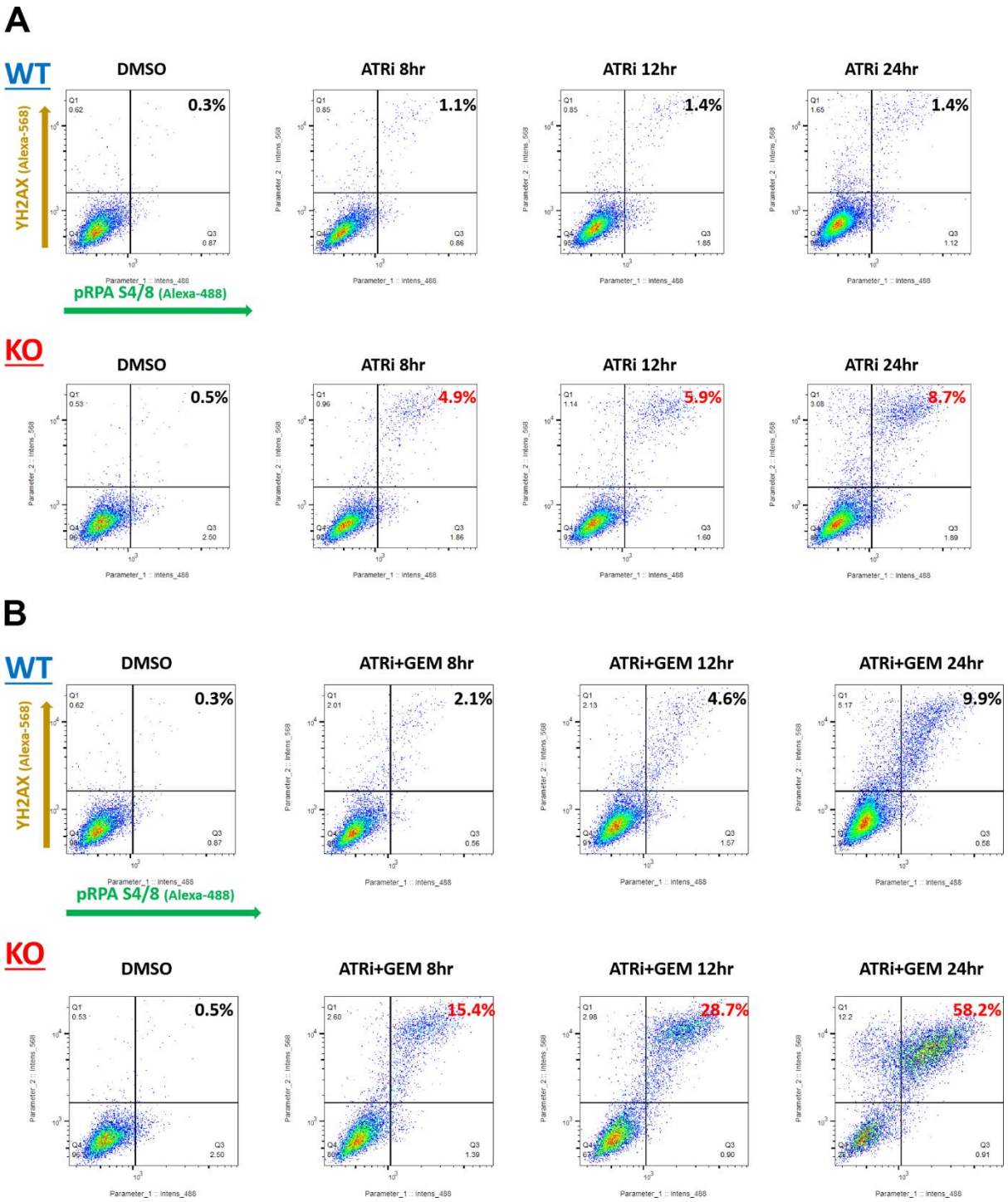

Fig. 4.18. Quantitative image-based cytometry to determine the proportion of cells pan-nuclear for both γH2AX S139 and phospho-RPA32 S4/8, at the timepoints indicated. Images were acquired using the Operetta CLS High-Content Analysis System and analysis performed using Harmony 4.5 software. The resulting data were imported into FlowJo as CSV files to generate the pseudo-colour plots shown. Percentages of double-positive cells are shown. **(A)** ATRi = 500 nM AZD6738. **(B)** ATRi = 500 nM AZD6738, GEM = 10 nM gemcitabine.

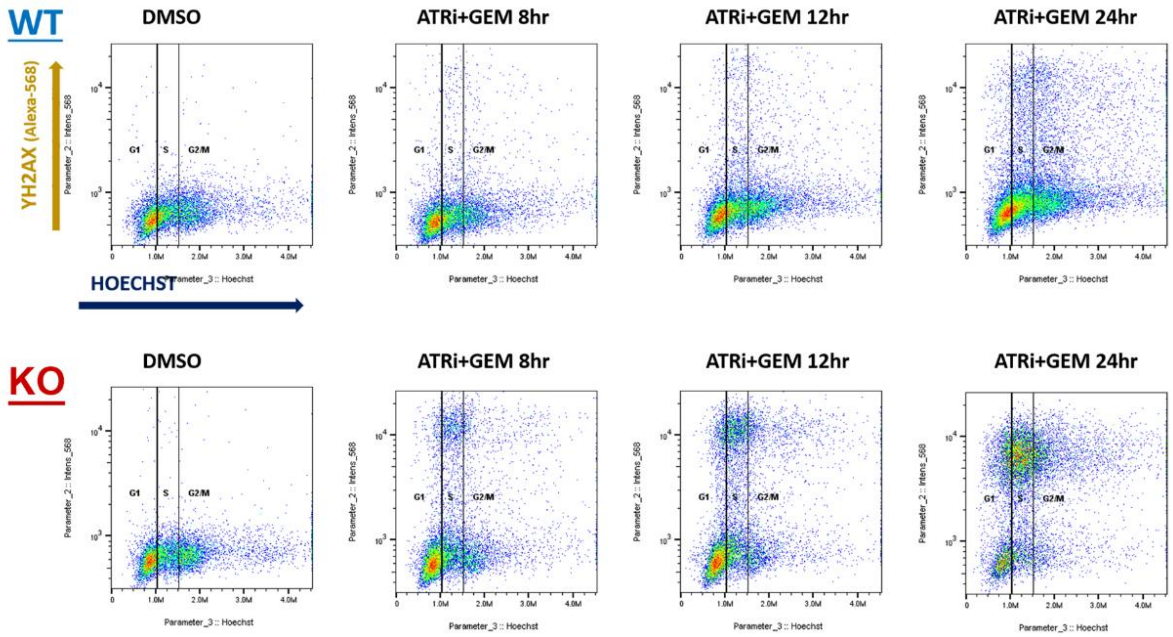

Fig. 4.19 DNA content (Hoechst) of MIA PaCa-2 cells vs γH2AX S139 signal, as determined by quantitative image-based cytometry. Images were acquired using the Operetta CLS, analysis performed using Harmony 4.5 software, with the resulting data imported into FlowJo to generate the pseudo-colour plots shown. ATRi = 500 nM AZD6738, GEM = 10 nM gemcitabine.

4.8. AZD6738 monotherapy causes growth delay in ATM-deficient PDAC xenografts, while combined treatment with gemcitabine induces regression

Next, I assessed the efficacy of AZD6738 monotherapy *in vivo*. NSG mice bearing either MIA PaCa-2 WT or MIA PaCa-2 ATM-KO xenografts were treated with 50 mg/kg AZD6738 (oral gavage, once daily, 5 consecutive days a week) for three weeks. No efficacy was seen in the ATM-proficient model, whereas in the ATM-KO tumours I observed 61% tumour growth inhibition (TGI) after 3 weeks of treatment (**Fig. 4.20A**). Subsequently, I assessed the combination of gemcitabine and AZD6738 using the same *in vivo* models. Previous tolerance studies with ATRi/gem (Yann Wallez, unpublished) had concluded that 25 mg/kg AZD6738, once daily for 5 days per week, plus 100 mg/kg gemcitabine twice per week (the maximum tolerated gemcitabine dose (Bapiro et al., 2014)) was a tolerable schedule. However, rather than drop the AZD6738 to 25 mg/kg, I chose to continue using 50 mg/kg (same as Fig. 4.20A) and assess whether a comparatively lower dose of gemcitabine (50 mg/kg) could be used as a sensitiser to AZD6738, to perhaps improve on the already impressive response seen with ATRi alone in the ATM-KO model.

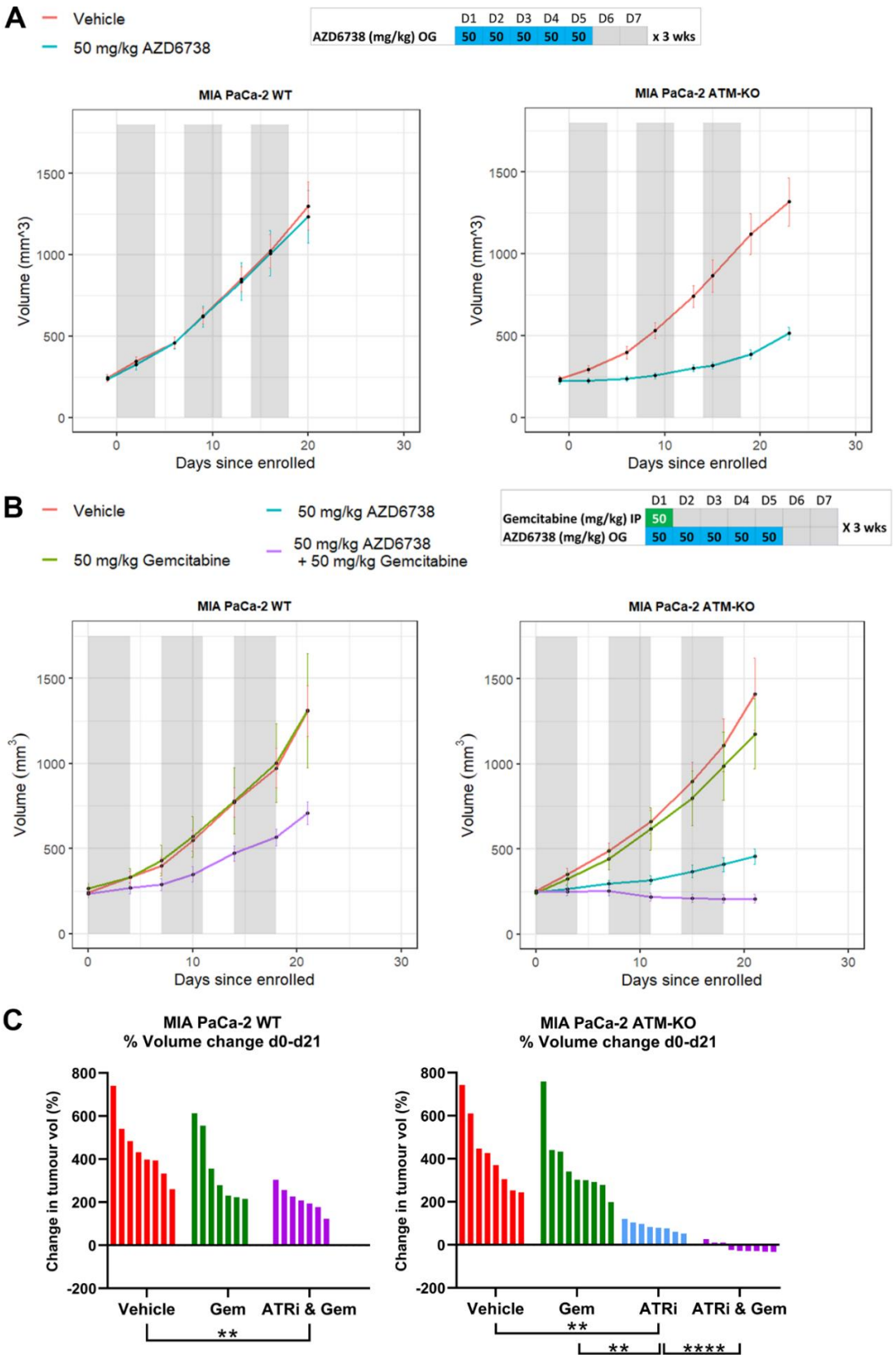

Fig. 4.20 (A) Tumour volumes of MIA PaCa-2 WT and MIA PaCa-2 ATM-KO (clone B7) xenografts in NSG mice, with AZD6738 monotherapy at 50 mg/kg, OG, once daily, 5 days on & 2 days off. Grey bars denote the 5-day dosing cycles. Data, mean ± SEM. WT-Vehicle group, n=10. WT-AZD6738 group, n=9. ATM KO-Vehicle group, n=9. ATM KO-AZD6738 group, n=9. **(B)** AZD6738 and gemcitabine combination. AZD6738 was given at 50 mg/kg, OG, once daily…

…5 days on & 2 days off. Gemcitabine was given at 50 mg/kg, IP, once per week on day 1 of each dosing cycle. Grey bars denote the 5-day dosing cycles. MIA PaCa-2 WT-Vehicle group, n=8. WT-Gemcitabine group, n=7. WT-AZD6738 & Gemcitabine group, n = 7. One mouse from the WT-Gemcitabine group and one from the WT-AZD6738 & Gemcitabine group dropped weight in the first week and their tumour volumes are not included in the mean values shown. MIA PaCa-2 ATM KO-Vehicle group, n=8. ATM KO-Gemcitabine group, n=9. ATM KO-AZD6738 group, n=8. ATM KO-AZD6738 & Gemcitabine group, n=9. **(C)** Changes in individual tumour volume from start to the end of the combination study (day 0 to day 21), as a percentage of starting volume. A one-way ANOVA analysis was performed (with multiple comparisons tests assuming unequal variances), * indicates $p \leq 0.05$, **$p \leq 0.01$, ***$p \leq 0.001$, ****$p \leq 0.0001$.

Regression is rare in MIA PaCa-2 xenograft studies, but adding low dose gemcitabine (50 mg/kg, IP, once per week) to the 50 mg/kg AZD6738 schedule induced regression in the ATM-KO MIA PaCa-2 tumours (mean volume change after 3 weeks = -17.8%, 95% confidence interval -2.7% to -32.8%), and growth delay in the WT tumours (46% TGI) (**Fig. 4.20B-C**). Using a Bliss synergy calculation, I found that the addition of gemcitabine to AZD6738 was supra-additive in the ATM-KO tumours. The mean final volume as a percentage of the vehicle group was 83% for gemcitabine-alone and 32% for AZD6738, giving a Bliss predicted (reference) combination effect (83% x 32%) of 27%; the actual effect seen in the combination group was 15%, giving a synergy score (27% - 15%) of 12%.

The dose-schedules used were well tolerated such that, across the two studies, just two mice experienced notable weight loss, one in ATRi/gem group (1/17) and one in the low dose gemcitabine-alone group (1/17) (**Fig. 4.21A**), even though NSG mice are typically sensitive to DNA damaging agents, due to the $Prkdc^{scid}$ mutation. Endpoint blood cell counts showed no significant difference between the ATRi/gem combination group and gemcitabine single agent (**Fig. 21B).** Though subcutaneous xenografts in immunocompromised mice do have some limitations, such as the lack of intra-tumoural heterogeneity, absence of immune responses and reduced ability to recapitulate the tumour microenvironment, this type of model can offer some advantages over orthotopic models, as previously reported (Dorado et al., 2018), including ease of use, reproducibility and earlier tumour detection. If I had used a syngeneic tumour model in immune competent mice I would have expected the overall result to be the same, with ATM-KO sensitising to ATRi/gem, however it is possible that I would have seen a different toxicity profile, particularly in the white blood cell counts. Additionally, it has been reported that loss of ATM in mouse tissue can prime the type-I interferon response (Härtlova et al., 2015), thus the immune response to syngeneic ATM-KO tumours may differ to that in ATM-WT tumours.

IHC quantification of γH2AX percent positive nuclei in the tumours, in half of each cohort fixed 6 hours after the final dose (day 21), revealed an increase in the ATRi/gem groups compared to vehicle; mean γH2AX positivity increased from 5.7% to 11.4% in WT tumours with ATRi/gem ($p < 0.01$), and from 7.3% to 15.4% in ATM-KO tumours with ATRi/gem compared to vehicle ($p < 0.0001$) (**Fig. 4.21C**). γH2AX positivity was higher in the ATM-KO tumours following ATRi/gem treatment compared to the ATM-WT ($p<0.05$). Analysis of the other half of the cohort, with tumours fixed 24 hours after the final dose, revealed that in both ATM-WT and ATM-KO tumours, the γH2AX positivity persisted for at least 24 hours after dosing (**Fig. 4.21C**). Meanwhile in the small intestine, the high γH2AX induced at 6 hours by gemcitabine or ATRi/gem did not persist at 24 hours (**Fig. 4.21D**), indicative of DNA repair in normal tissue.

In agreement with the *in vitro* findings, these *in vivo* experiments suggest that ATM-loss could be a predictive biomarker of response to ATRi/gem in patients with PDAC.

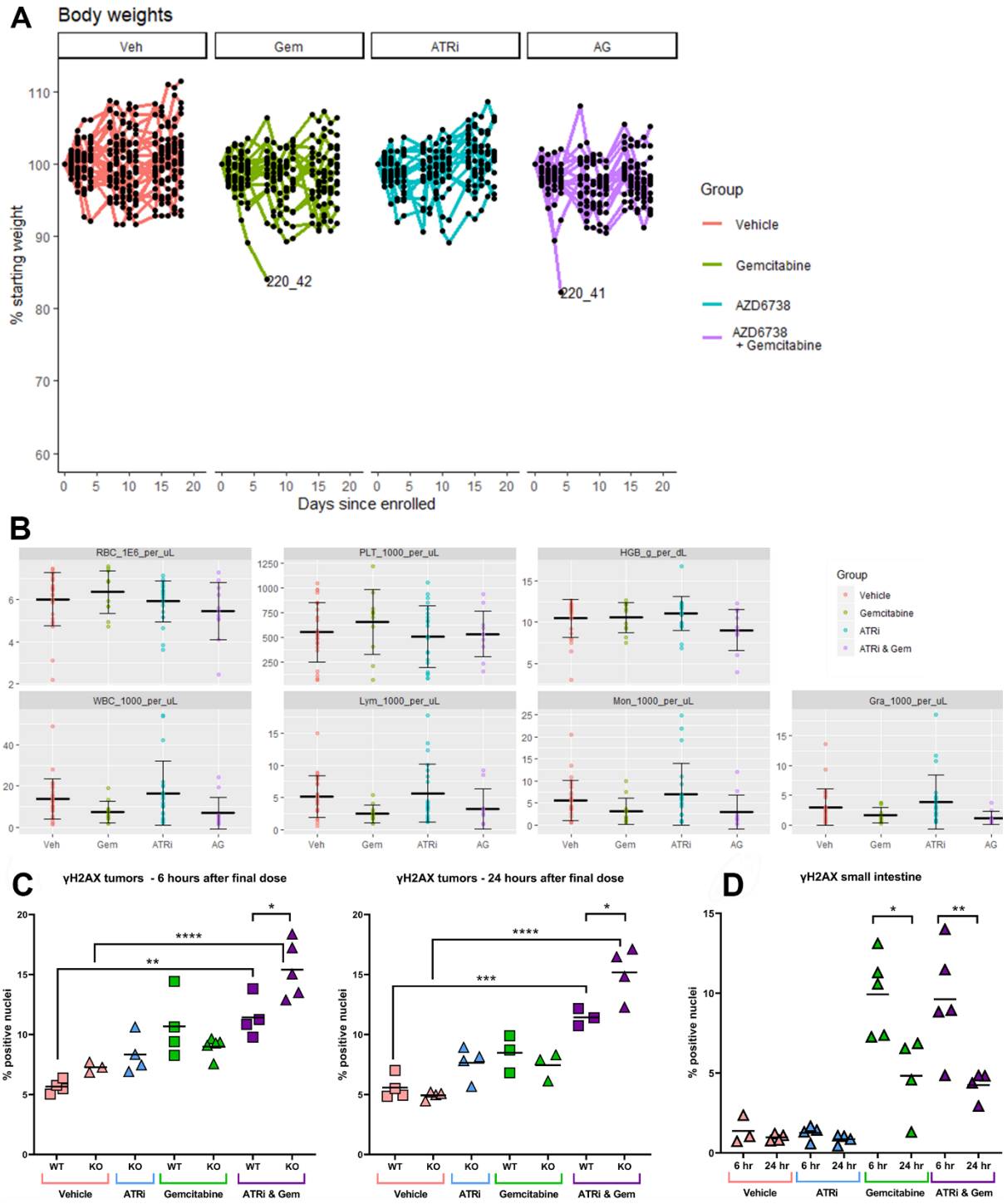

Fig. 4.21 (A) Individual body weights during treatment, as a percentage of the starting weight upon enrolment, for NSG mice bearing MIA PaCa-2 WT or ATM-KO (clone B7) xenografts. Both sets of mice from Figure 6A (monotherapy study) and Figure 6B (subsequent combination study) are plotted. Just two mice showed significant weight loss, Mouse#220_42 (Gemcitabine group) and Mouse#220_42 (ATRi/gem group). **(B)** Blood was taken at endpoint and run on the Mythic 18 Haematology Analyser. The title of each sub-plot denotes the blood component measurement and its units. RBC = red blood cells, PLT = platelets, HGB= haemoglobin; WBC = white blood cells, Lym = lymphocytes, Mon = monocytes, Gra = granulocytes. Each point represents the reading from one mouse. Bars =mean ± SD. **(C & D)** Nuclear γH2AX S139 positivity in the formalin-fixed tumours (B) and the small intestine (C) from the combination study was assessed by IHC and quantified using Halo software. Each point represents data from one histological section from an individual mouse. Horizontal bars…

…denote the mean. A one-way ANOVA analysis was performed with Tukey's multiple comparisons tests, * indicates $p \leq 0.05$, ** $p \leq 0.01$, *** $p \leq 0.001$, **** $p \leq 0.0001$.

4.9. Normal tissue toxicity prevents the use of pharmacodynamically effective dose schedules of ATMi and ATRi *in vivo*

My data so far suggested that ATM-KO PDAC tumours are sensitive to ATRi (**Fig. 4.20A**). Since only a minority of PDAC patients have ATM-deficient tumours, one might assume that only these patients may stand to benefit from any understanding of ATM/ATR synthetic lethality. Having said that, I had also shown earlier that pharmacological inhibition of ATM sensitises (otherwise ATM-proficient) PDAC cell lines to ATRi *in vitro* (**Fig. 4.2)**. With these *in vitro* results in mind, the question remained – could ATMi and ATRi be combined *in vivo* to produce an anti-tumour effect? If so, and if ATMi could perhaps mimic the *in vivo* sensitisation effect seen with ATM-KO, then the synthetic lethality between ATM and ATR could even be exploited in ATM-proficient tumours. I posited that the success of co-targeting both kinases pharmacologically in animal models would likely rest on the toxicity profile of the combination, since ATMi may sensitise all normal tissue to ATRi, and not just the tumour.

For my *in vitro* experiments I had used the ATMi, AZD0156. While AZD0156 is a potent and selective ATM kinase inhibitor, the analogue, AZD1390, is being prioritised for clinical development. Unlike AZD0156, AZD1390 is not a substrate for the efflux transporters P-glycoprotein (ABCB1/MDR1) (Roninson et al., 1986; Thiebaut et al., 1987) and breast cancer resistance protein (ABCG2/BCRP) (Doyle and Ross, 2003), which are multidrug resistance protein (MRP) family members that are expressed by endothelial cells of the blood-brain-barrier. As a result, AZD1390 is more brain-penetrant than AZD0156 and is being assessed clinically as a radiosensitiser in central nervous system malignancies (Durant et al., 2018). MRP efflux pumps have also been found to be overexpressed in numerous cancer types, including in PDAC (König et al., 2005) and have been associated with resistance to chemotherapies such as gemcitabine (Hagmann et al., 2010) and 5-FU (Nambaru et al., 2011).

By mining RNA-seq data from the Cancer Cell Line Encyclopaedia, I found that many commonly used human PDAC cell lines express MRP family members to varying degrees (**Fig. 4.22**). PANC-1, which is highly resistant to AZD6738, gemcitabine, Chk1 inhibition and other agents, showed particularly high expression of MRP1 and BCRP1.

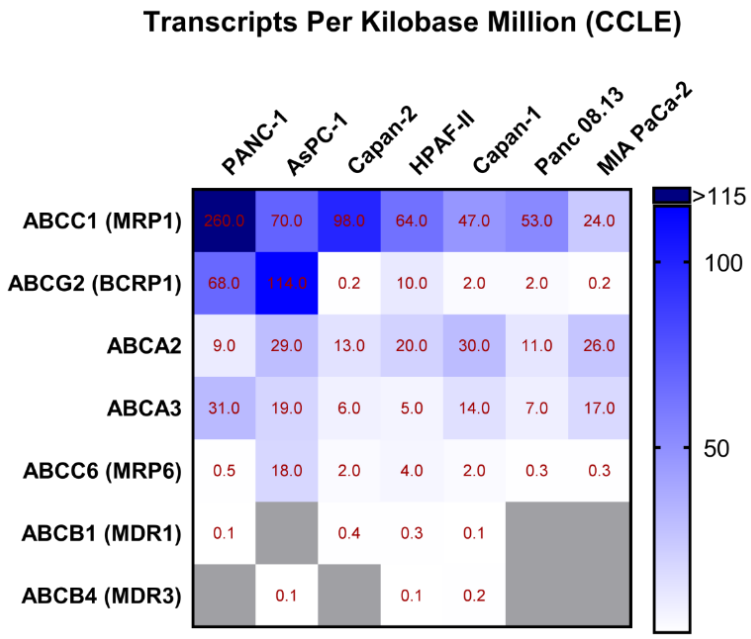

Fig. 4.22. mRNA transcript expression of multidrug resistance protein (MRP) family member genes in commonly used human PDAC cell lines. Source data, Cancer Cell Line Encyclopaedia (CCLE), extracted using EBI Expression Atlas. Numbers denote transcripts per kilobase million.

I hypothesised that AZD1390 would penetrate PDAC tumours more effectively than AZD0156. Therefore, before assessing ATRi and ATMi *in vivo*, I first designed a pharmacokinetic (PK) study to test this theory. At the time that this experiment was devised, I was still carrying out the ATRi/gem combination study shown in Fig. 4.20B, thus Dr Brajesh Kaistha kindly acted as PIL holder for the PK study, liaising with CRUK-CI PGE core facility members who undertook dosing and necropsy duties.

KPC mice with PDAC tumour confirmed by ultrasound scan by the CRUK-CI PGE core were given of single dose of either 10 mg/kg AZD0156 or 10 mg/kg AZD1390, and killed at fixed timepoints after dosing. UPLC-MS/MS was then used to quantify the drug concentrations in flash-frozen plasma and tumour samples. While similar plasma concentrations of AZD0156 and AZD1390 were measured, AZD1390 outperformed AZD0156 in terms of tumour penetrance at every timepoint assessed (**Fig. 4.23**). This confirmed that, for *in vivo* studies using ATMi in PDAC models, AZD1390 should be used in preference to AZD0156.

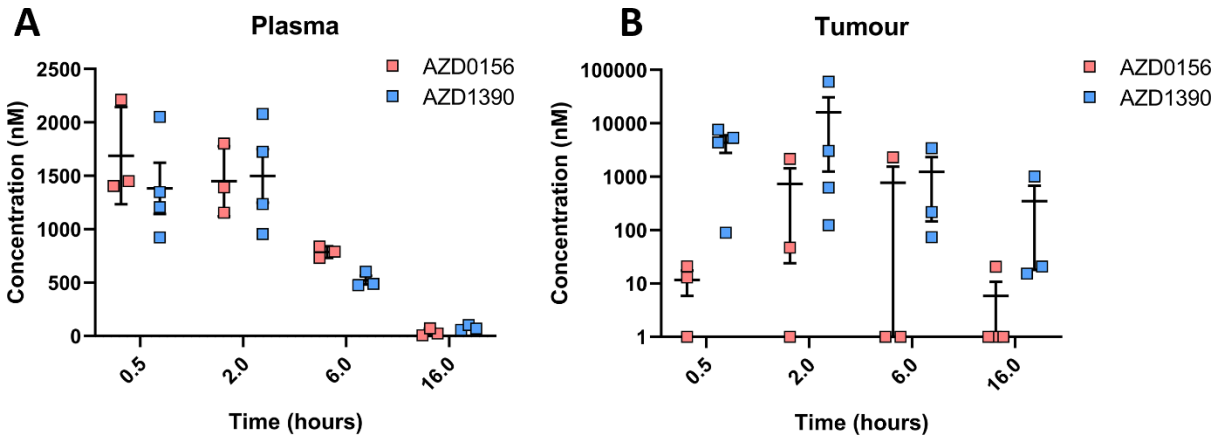

Fig. 4.23 (A) Plasma concentrations from KPC mice dosed with either 10 mg/kg AZD0156 or 10 mg/kg AZD1390. **(B)** Tumour concentrations from KPC mice dosed with either 10 mg/kg AZD0156 or 10 mg/kg AZD1390. Horizontal lines denote mean, ± SEM. In (B), samples below the limit of quantification (<10 nM) were given nominal value of 1 nM for this plot. One mouse in the 2-hour AZD1390 group had ascites that was discovered upon necropsy, and this was the only mouse which had an AZD1390 tumour concentration above 10 µM. Dr Brajesh Kaistha kindly acted as PIL holder for this study, with the CRUK-CI PGE core facility members undertaking dosing and necropsy duties. UPLC-MS/MS was performed by Dr Aaron Smith, AstraZeneca.

Next, I designed an AZD6738 and AZD1390 tolerance study in BALB/c nude mice (NSG mice were avoided since they are mutant for the DNA-PKcs gene, *Prkdc*, and so would almost certainly fail to tolerate combined ATRi and ATMi). Since one of the reasons for assessing this combination was to ascertain if ATMi could mimic ATM-KO in terms of *in vivo* AZD6738 sensitisation (**Fig. 4.20A**), mice were inoculated with MIA PaCa-2 xenografts. 7 different ATRi/ATMi dose-schedules were assessed, with 3 mice per group, while 4 mice were dosed with vehicle-alone (**Fig. 4.24**).

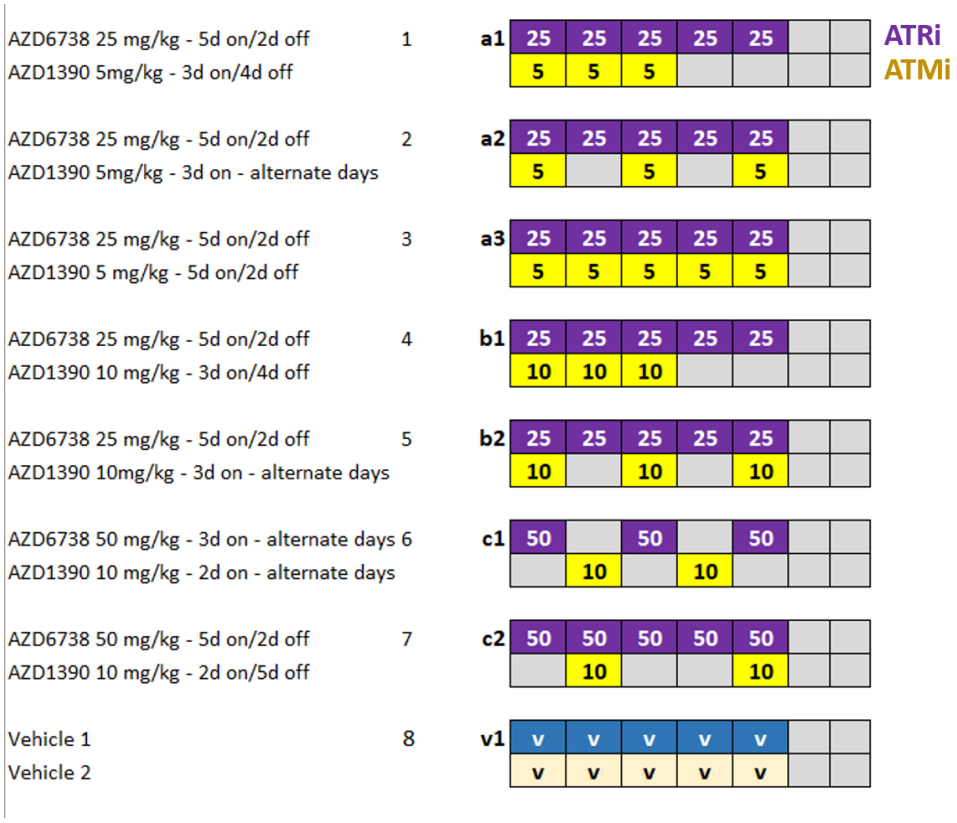

Fig. 4.24. Dose-schedules assessed in AZD6738 and AZD1390 tolerance study. Each square represents one day of a 7-day dosing cycle. Both drugs were administered by oral gavage. On days where both drugs were administered, AZD1390 was given 1 hour after the AZD6738 dose.

Over the course of three 7-day dosing cycles, notable weight loss (that approached or surpassed the limit of 15% of starting weight) was observed in 5 of the 7 combination groups (**Fig. 4.25A**). The only two dose-schedules that did not induce weight loss were schedule B1 (AZD6738 25 mg/kg - 5d on/2d off; AZD1390 10 mg/kg - 3d on/4d off) and schedule C1 (AZD6738 50 mg/kg - 3d on - alternate days; AZD1390 10 mg/kg - 2d on - alternate days). However, these schedules did not induce any notable tumour growth inhibition compared to the vehicle-treated group (**Fig. 4.25B**). The only schedules with potential signs of anti-tumour activity were those that were also toxic to the mice, such as group A3 (AZD6738 25 mg/kg - 5d on/2d off; AZD1390 5 mg/kg - 5d on/2d off), in which 3 out of 3 mice had to be killed, due to weight loss. This suggests that normal tissue toxicity prevents the use of pharmacodynamically effective dose schedules of ATMi and ATRi combination in BALB/c nude mice. The data presented in this chapter therefore indicate that using ATM-loss a predictive biomarker of response for ATRi or ATRi/gem would be a more effective clinical strategy for PDAC than co-targeting ATR and ATM pharmacologically.

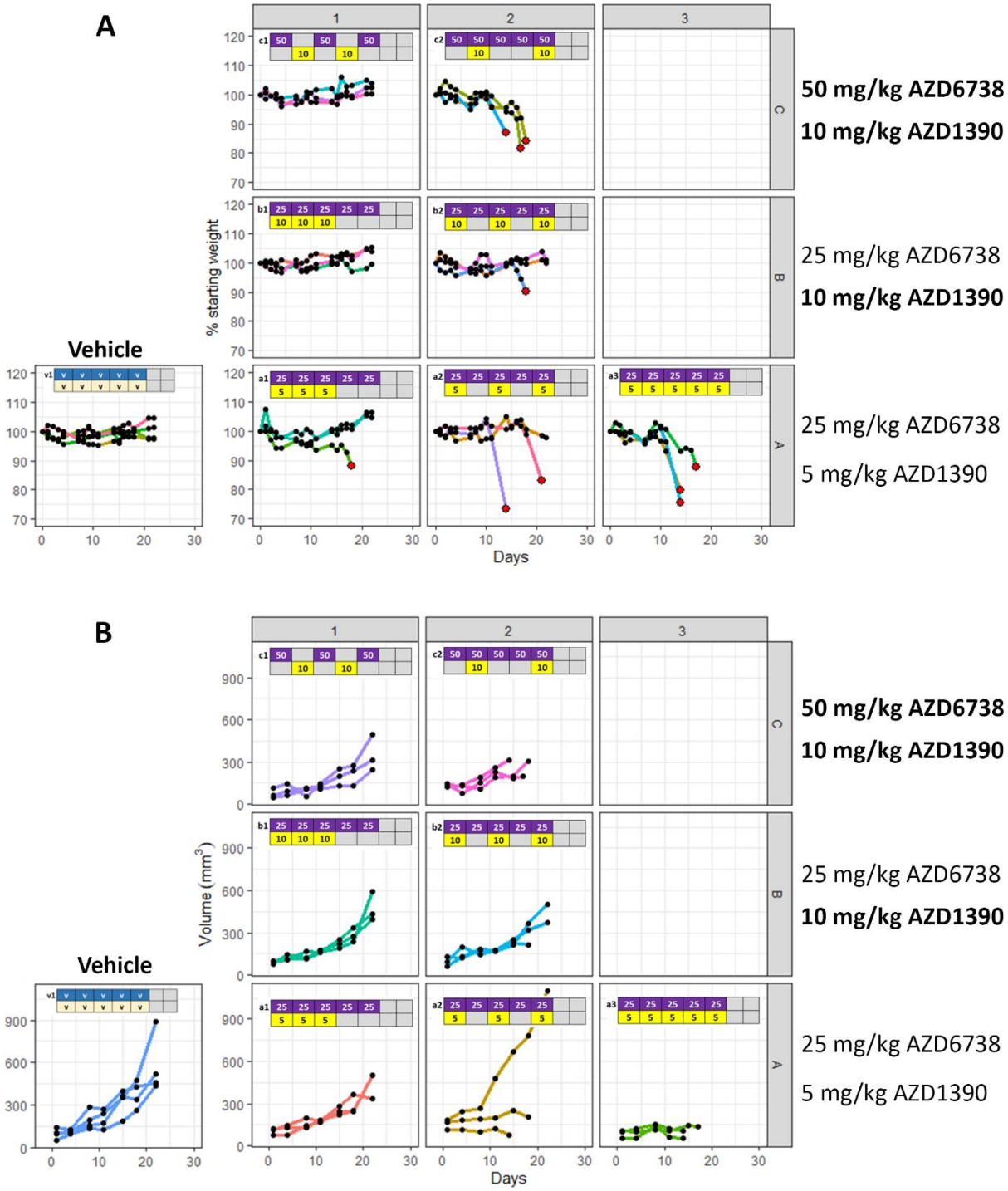

Fig. 4.25 (A) Individual mouse body weights over the course of the AZD6738 and AZD1390 tolerance study in MIA PaCa-2 xenograft-bearing BALB/c nude mice, expressed as a percentage of starting weight. The final weight measurements of mice that had to be killed due to weight loss (approached or surpassed the 85% limit) are marked with a red dot. **(B)** MIA PaCa-2 tumour volumes over the course of the AZD6738 and AZD1390 tolerance study.

4.10. Discussion

The application of precision medicine strategies, where therapies are assigned based on patient-specific tumour vulnerabilities, has the potential to improve outcomes for diseases such as PDAC. Currently, the leading example is the use of BRCA1/2 mutations to select patients whose tumours may be hypersensitive to PARP inhibitor treatment (Bryant et al., 2005; Farmer et al., 2005), which has brought impressive survival rates in ovarian (Moore et al., 2018), breast (Robson et al., 2017) and pancreatic cancer (Golan et al., 2019). With approvals already granted for ovarian and breast cancer, PARP inhibitors are at a later stage of clinical development than ATR inhibitors. AZD6738, M6620 and BAY1895344 are ATR inhibitors currently being assessed in a range of phase I or phase II trials, as monotherapies and in combination with DNA-damaging agents, other molecularly targeted agents or immunotherapeutics.

One of the challenges when combining DDR inhibitors with genotoxic drugs in the clinic has been avoiding increased normal tissue toxicity. For example, in a phase II study that assessed olaparib plus carboplatin and paclitaxel, adverse event such as neutropenia and anaemia were reported more frequently in the olaparib combination arm than with chemotherapy alone (Oza et al., 2015). Furthermore, the large number of possible DDRi/chemotherapy combinations heightens the need to predict which patients would most likely respond to a particular combination. In alignment with the phase I trial set-up to assess the combination of AZD6738 and gemcitabine (ATRiUM, NCT03669601), I sought to investigate the potential utility of ATM-loss as a predictive biomarker of response for ATRi/gem in PDAC. ATM and ATR have been reported to share a synthetic lethal relationship in some cancer types (Kwok et al., 2016; Min et al., 2017; Schmitt et al., 2017; Vendetti et al., 2015). However, it has become increasingly clear that most synthetic lethal interactions depend highly on the genetic background in which they are studied (Ryan et al., 2018). By targeting ATM through multiple methods, I assessed how ATM status affects ATRi/gem sensitivity in PDAC cells.

One of the methods by which I targeted ATM was through CRISPR/Cas9 deletion. I demonstrated that ATM was completely dysfunctional in the CRISPR clones by irradiating the cells and then immunoblotting for phospho-ATM S1981 (**Fig. 4.6A**). Additionally, in later immunoblotting experiments, I probed for downstream markers of DDR activation in ATRi/gem-treated cells, such as for the ATM-specific phospho-RAD50 S635, which was abrogated in ATM-KO cells (**Fig. 4.11**). Another way in which I could have assessed ATM functionality could have been to quantify changes in gene expression following DNA damage

(i.e. similar to the approach taken by Navrkalova et al., discussed in section 1.3.2) for example using RT-qPCR or RNA-Seq. However, all of the cell lines I used were p53-mutant, and since much of ATM's effects on transcriptional programming is often driven via its activation of p53, these data would have to have been interpreted carefully. In hindsight, the irradiation plus phospho-ATM blotting approach that I took to assess ATM functionality in my CRISPR clones could/should have also been applied to my siATM cells. This would have been a positive control to show that the extent of ATM suppression was sufficient to inactivate DDR to the extent that it could elicit a DDR-related synthetic lethality.

As for the other approach I took to target ATM, kinase inhibition with AZD0156, I also demonstrated abrogation of ATM function by blotting for P-ATM S1981 following IR (**Fig. 4.1A**). However, to show that the effect of ATMi on ATRi sensitivity was an on-target effect, I could have carried out further experiments, for example by assessing the ATMi and ATRi combination in ATM-KO cells. In the immunoblotting experiments involving ATMi and ATRi, where I was investigating the DDR signalling pathways activated by ATRi/gem, I initially found that phospho-ATM S1981, phospho-KAP1 S824 and phospho-Chk2 T68 all persisted in the presence of ATMi (**Fig 4.9A)**. I hypothesised that these phosphorylations could be driven by DNA-PKcs, and dissected this using the DNA-PKcs inhibitor, AZD7648. A potential problem with using all of the kinase inhibitors at once (AZD6738, AZD0156, AZD7648) is that they all target kinases belonging to the same PIKK family and so, though designed to be highly selective, they will each partially inhibit these related enzymes to a small degree. For example, in the ATRi/gem-treated MIA PaCa-2 cell in **Fig 4.9A**, the modest abrogation of P-RAD50 S635 caused by 5 μM but not 1 μM DNA-PKi may be due to the DNA-PKi hitting ATM at the higher dose.

One of the findings from this chapter was that complete loss of ATM function is necessary to sensitise PDAC cells to AZD6738 or the AZD6738 and gemcitabine combination. This has important implications, as it brings into question how best to assess ATM status in future clinical trials. A recent example of a trial where ATM status was assessed is Study 39 (NCT01063517). This was a phase II efficacy study assessing the combination of olaparib and paclitaxel in gastric cancer patients, which identified a greater overall survival benefit in patients with "ATM-low" tumours (Bang et al., 2015). Here, "ATM-low" tumours were defined as those with ≤10% ATM tumour cell nuclear staining, quantified by an IHC test using the ATM (Y170) antibody clone. In the follow-up phase III GOLD trial (NCT01924533), a new IHC reporter assay was developed that used the same antibody clone but with different

assay configurations and reagents (Miller et al., 2019). The cut-off for "ATM-low" tumours was redefined as <25% of ATM tumour cell nuclear staining (to account for increased sensitivity of new assay) however this trial failed to meet its primary endpoint and failed to confirm the survival benefit in "ATM-low" patients that had been observed previously (Bang et al., 2017). It remains unclear whether redefining the cut-off to a lower threshold would bring a different result.

In relation to ATRi/gem in PDAC, my data would support the use of complete ATM-loss, as opposed to <10 or 25% staining, since only ATM-null cells appeared to be hypersensitive. This leads to the question of how to define ATM-null in a clinical setting. Such tumour samples have been identified previously, including in the very first phase I dose escalation trial of an ATR inhibitor, which identified a colorectal cancer patient with 100% ATM loss by IHC, who showed a complete response (19+ months) to M660 monotherapy (O'Carrigan et al., 2016; Yap et al., 2015). Evaluating ATM functionality by IHC, using markers such as phospho-RAD50-S635, in conjunction with total ATM could add further depth to ATM status assessments. Tissue microarray analysis of glioblastoma, gastric, triple negative breast and colorectal cancer identified a variability in baseline P-RAD50-S635 levels between patients. Most patients expressed modest but detectable levels of P-RAD50-S635 (Jones et al., 2018). If phospho-RAD50-S635 were to be used to infer or substantiate ATM status, this would likely require patients to be challenged with an DSB-inducing agent prior to biopsy to be most informative. The presence of germline or somatic ATM mutations, combined with a low IHC score, would add confidence that a patient's tumour is indeed ATM negative, thus incorporating next-generation sequencing (NGS) in parallel with IHC could improve clinical biomarker assessments (Sundar et al., 2018). On the whole, if precision medicine techniques are to be implemented successfully, it is becoming increasingly apparent that the field will have to be more precise and detailed in the characterisation of patients and their tumours, and multi-modal assessments of patient samples may facilitate this.

As well as the important distinction between ATM-low and ATM-null, the data I have presented in this chapter also reveal further insight into the mechanism of how AZD6738 and gemcitabine synergise to induce cell death. The increase in nuclear RPA over time upon ATRi/gem exposure, plus the accumulation of S-phase cells pan-nuclear for DNA damage and replication stress markers, suggests that the combination induces replication catastrophe (RC) (**Figs. 4.15-4.19**). One potential limitation of the immunofluorescence experiments assessing RC is that the only concentrations used were 500 nM ATRi and 10 nM gemcitabine. It is

possible that increasing the ATRi to concentrations above 500 nM may have brought about the same or similar RC phenotype as observed by adding 10 nM gemcitabine. Having said that, 2000 nM ATRi was assessed in the flow cytometry cell cycle experiments and this did not induce as significant an S-phase arrest as the ATRi/gem combination (**Fig. 4.15B**) During the catastrophic fork collapse induced by ATRi/gem, Chk1 and Chk2 are phosphorylated by DNA-PKcs, but the lack of clear ATRi/DNA-PKcsi synergy and the inability for DNA-PKcsi to significantly potentiate ATRi/gem (**Fig. 4.14**), suggests that these DNA-PKcs-driven signals may be bystander events during RC. The fact that ATM-deficient cells are hypersensitive to ATRi/gem-induced RC indicates that ATM plays a critical role in protecting against this widespread fork collapse. A recent study found that topotecan- or olaparib-induced breakage of replication forks is lethal in ATM-deficient models due to the induction of toxic NHEJ (Balmus et al., 2019). Their data suggested that the toxic NHEJ was mediated by XRCC4 and ligase IV, but not DNA-PKcs. Here, I found that DNA-PKcsi did not significantly potentiate nor attenuate the effect of ATRi/gem in WT or ATM-KO cells. Given more time, it would be interesting to interrogate whether the hypersensitivity of ATM-null PDAC cells to ATRi/gem is also due to toxic NHEJ.

As already alluded to, minimising toxicity is a major challenge when combining DDRi and chemotherapy in the clinic. Most phase I trials of this type are designed such that the DNA-damaging cytotoxic is administered at its standard-of-care dose – i.e. at the expected maximum tolerated dose – and the DDRi is titrated in at increasing levels. As a result, any increase in toxicity will immediately become dose limiting and the true potential of these combinations may not be fully explored. The ATRiUM trial design is unique, in that it is using a model-based approach to guide dose escalation, starting each drug at dosages that are <100% of the predicted or actual single agent dose. In essence, the aim is to use the gemcitabine as a sensitiser to the AZD6738, rather than simply administering the cytotoxic at its typical maximum dosage. In this chapter, I demonstrated that this strategy can indeed be effective, particularly in an ATM-deficient setting. I first found that 50 mg/kg AZD6738 monotherapy, once daily for 5 consecutive days a week, induced significant growth delay in the ATM-null tumours. Rather than introduce gemcitabine at its typical pre-clinical single agent dose of 100 mg/kg twice per week (Bapiro et al., 2014), I used a comparatively low gemcitabine dose of 50 mg/kg, once per week, to allow pharmacodynamically effective dose schedules of AZD6738. This regimen induced growth delay in the ATM-WT and tumour regression in the ATM-KO tumours (**Fig.**

4.20), thus demonstrating proof-of-principle that low dose gemcitabine can be used as a sensitiser to AZD6738 *in vivo*.

As well as assessing the safety, tolerability and preliminary anti-tumour activity of ATRi/gem in a novel model-based approach, the ATRiUM trial is incorporating IHC assessment of baseline ATM, NGS of patient DNA and on-treatment biopsies. This will enable some of the conclusions that I have made in this chapter to be scrutinised clinically. This could steer the design of future precision-medicine based trials that will examine the promise that ATM shows as a predictive biomarker of response for AZD6738 and gemcitabine combination therapy in PDAC.

CHAPTER FIVE: Combined PARP inhibition and ATR inhibition as a therapeutic strategy in PDAC

5.1. Background

My investigations into ATM-loss and ATRi/gem from Chapter 4 had initially stemmed from a set of experiments performed by myself and others in the Jodrell lab, where AZD6738 had been combined with a range of cytotoxic drugs and DDR-targeted agents in a panel of PDAC cell lines (Chapter 3). Gemcitabine was not the only drug that had demonstrated synergy with AZD6738, in fact, the PARP inhibitor olaparib was one of the agents that also synergised with ATRi. As summarised in Chapter 1, PARP inhibition leads to the trapping of PARP on DNA, which poses a physical obstacle to the replisome during S-phase, leading to the stalling of replication forks. This could explain why PARPi and ATRi synergise to induce cell death, since olaparib-induced stalled forks would go unresolved in the absence of ATR activity, resulting in fork collapse and the induction of DSBs. Though olaparib monotherapy has primarily been explored in BRCA-mutant populations, the combination of ATRi and PARPI had demonstrated *in vitro* synergy in BRCA-proficient PDAC cell lines (**Fig. 3.6**). Two-thirds of PDAC patients harbour no somatic mutations in any DDR genes, thus an effective therapy for these patients would fulfil a serious unmet need. Combined AZD6738 and olaparib is currently being assessed in patients with gastric cancer and triple negative breast cancer (NCT02264678) (Krebs et al., 2018). The combination has also been proposed for future PDAC trials, as part of the PRECISION-Panc initiative (Dreyer et al., 2020).

Dr Yann Wallez carried out an initial efficacy study (code Pr149) to assess the olaparib and AZD6738 combination in BALB/c nude mice with MIA PaCa-2 xenografts, using a dose-schedule recommended by AstraZeneca. No efficacy was observed in either single agent arms, nor in the combination arm (**Fig. 5.1A**). Pharmacokinetic data indicated that the olaparib and AZD6738 concentrations measured in the tumours were marginally below the doses required for maximal synergy and growth inhibition *in vitro* (**Fig 5.1B-C**). This raised the possibility that an altered dose-schedule may increase the chances of observing an anti-tumour effect using this combination in PDAC models.

I took on this project, with the aim to further investigate the olaparib and AZD6738 combination in BRCA-proficient PDAC models.

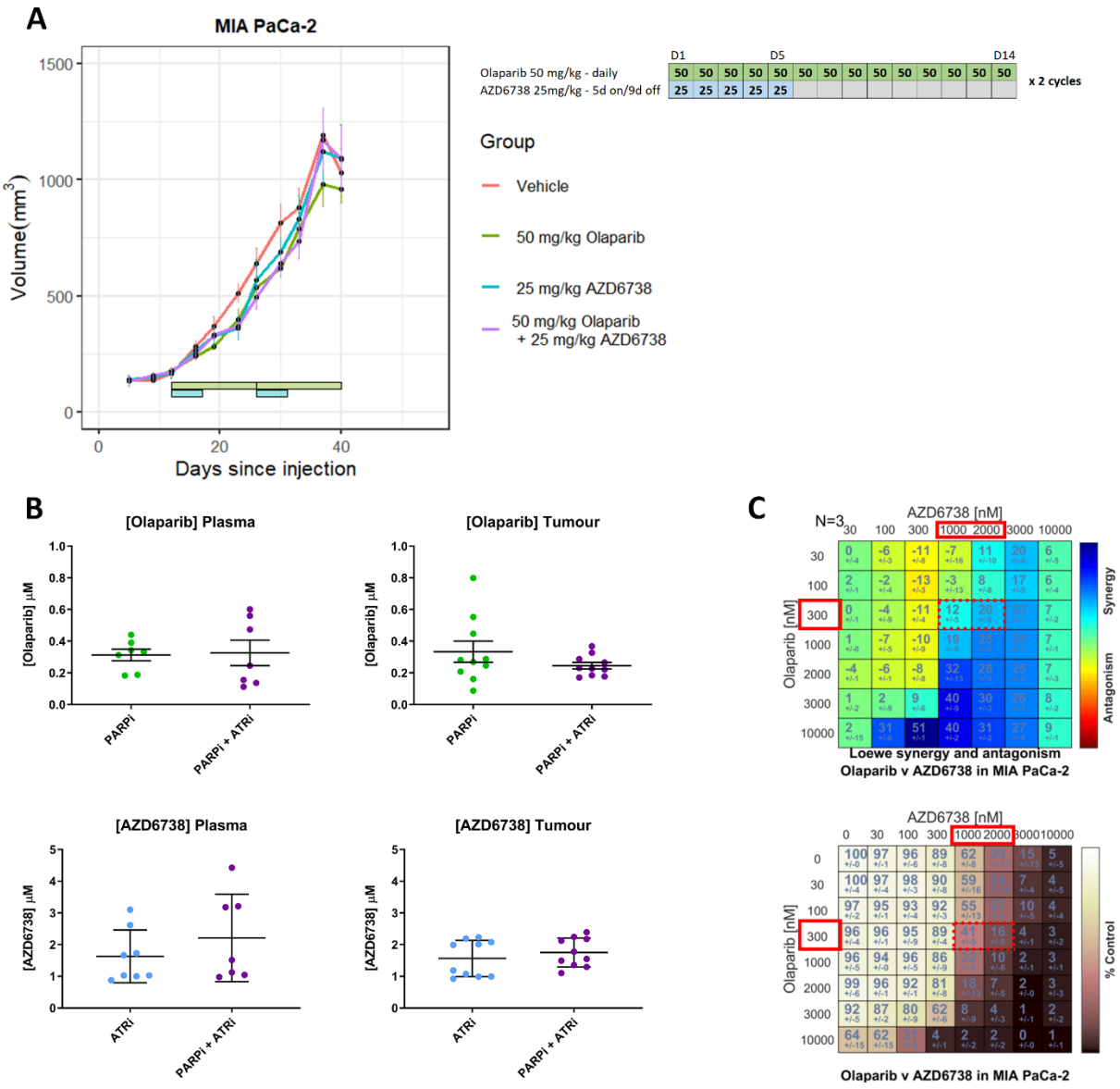

Fig. 5.1 (A) Tumour volumes of MIA PaCa-2 xenografts in BALB/c Nude mice, from the initial olaparib and AZD6738 combination study carried out by Dr Yann Wallez (Pr149). Data, mean ± SEM. 10 mice per group. Olaparib was given at 50 mg/kg, OG, once daily, for the full 28-day dosing period. AZD6738 was given at 25 mg/kg, OG, once daily, (one hour after the olaparib dose in the combination arm), 5 days on & 9 days off, for 2 cycles. The horizontal bars below the curves denote the dosing period for olaparib (green) and AZD6738 (blue). **(B)** UPLC-MS/MS was performed by Astra Zeneca (Aaron Smith) to quantify the drug concentrations in flash-frozen plasma and tumour samples from the combination study, 3 hours after the final AZD6738 dose (4 hours after olaparib). Horizontal bars denote mean ± SEM. **(C)** Olaparib and AZD6738 combination in MIA PaC-2, *in vitro*, with the tumour drug concentrations measured in study Pr149 highlighted in red boxes. MIA PaCa-2 were treated with increasing concentrations of olaparib and AZD6738 for 120 hours, and cell number at endpoint was determined by measuring total protein content using the SRB assay. Top = Combenefit synergy score (Loewe). Bottom = growth as % of solvent control. Data, mean ± SD, n=3.

5.2. Supra-micromolar olaparib concentrations induce activation of the intra-S checkpoint in PDAC cell lines

First, to gain more mechanistic insight into the *in vitro* synergy observed with olaparib and AZD6738 in PDAC cell lines, I treated K8484 and MIA PaCa-2 cells with increasing concentrations of olaparib, and immunoblotted for markers of ATR activation. 48-hour olaparib treatment induced a dose-dependent upregulation of phospho-Chk1 S345 and phospho-CDK1 Y15, along with a downregulation of the mitotic marker phospho-Histone H3 S10, indicating activation of the intra-S checkpoint (**Fig. 5.2A**).

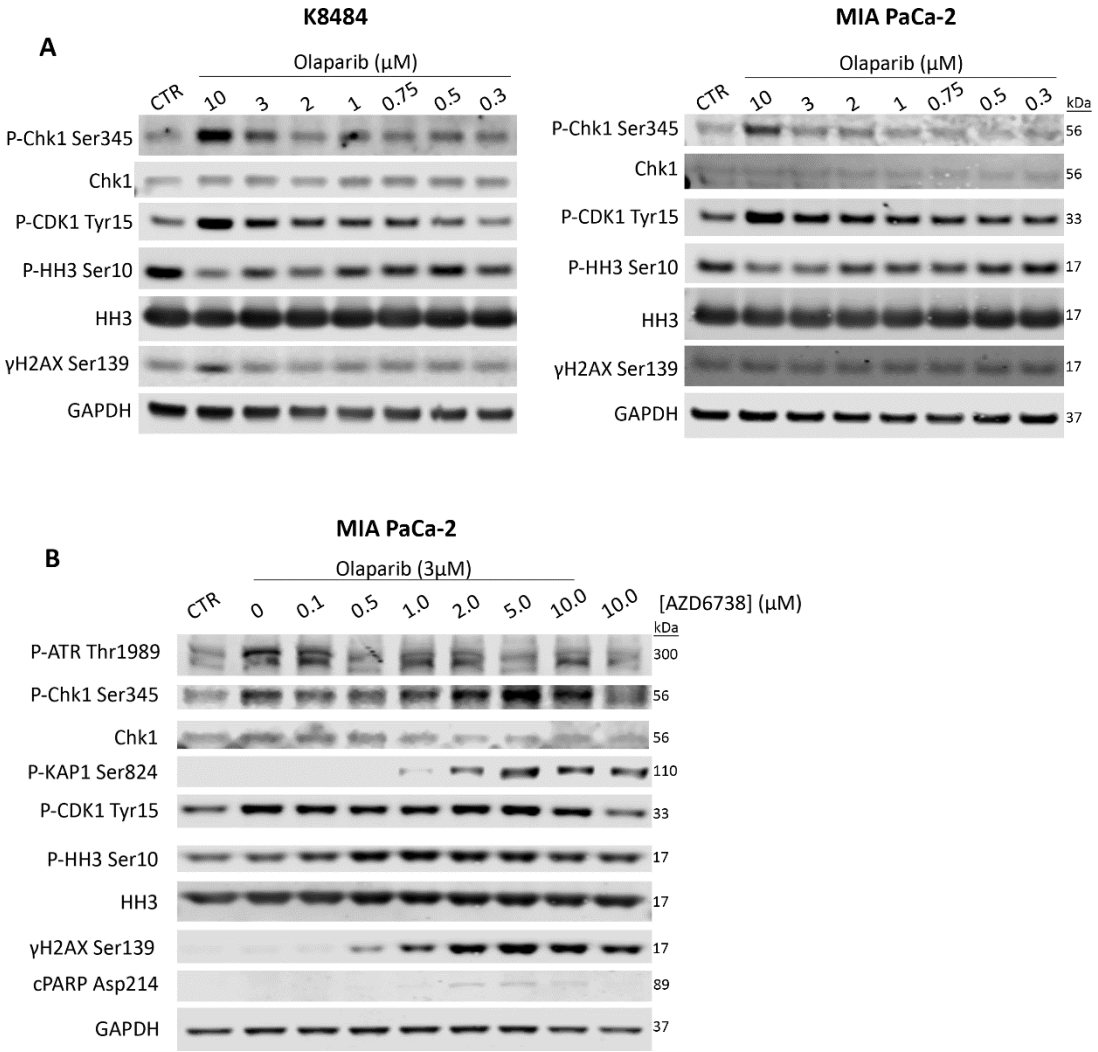

Fig. 5.2 (A) Immunoblot analysis of K8484 (mouse) and MIA PaCa-2 (human). Cells were harvested after 48 hours of drug exposure. **(B)** Immunoblot analysis of MIA PaCa-2. Cells were harvested after 48 hours of drug exposure.

Previously, double-digit nM concentrations of olaparib have been shown to elicit *in vitro* synthetic lethality in BRCA-mutant cell lines (Bryant et al., 2005; Farmer et al., 2005), suggesting that even low olaparib concentrations can induce toxic PARP-trapping. However, in my experimental setup (BRCA-WT PDAC cell lines, 48-hour treatment), low olaparib concentrations such as 0.3 µM did not induce markers of ATR activation. The concentration of olaparib measured in the MIA PaCa-2 tumours from the previous *in vivo* study (Pr149) averaged around 0.3 µM, thus I posited that the use of higher olaparib doses in subsequent mouse studies may increase the likelihood of observing *in vivo* efficacy with PARPi and ATRi.

Combining 3 µM olaparib with increasing concentrations of AZD6738 induced upregulation of DSB markers, phospho-KAP1 S824 and γH2AX S139, as well as the apoptosis marker, cleaved-PARP (Asp214) (**Fig. 5.2B**). These markers of DNA damage and cell death underly the grow inhibition induced by the combination at synergistic doses (**Fig. 5.1C**).

5.3. Assessment of olaparib and AZD6738 tolerability using a range of *in vivo* dose-schedules

I hypothesised that the previous *in vivo* assessment of olaparib and AZD6738 in PDAC may have shown no efficacy due to either; a) the use of olaparib or AZD6738 doses that were too low, b) insufficient coverage of AZD6738, which was given on only the first 5 days of the 14-day dosing cycle, or c) a combination of both (other factors that may have affected the result, including the type of mouse model used, are explained in section 5.4 and in the Discussion, section 5.5). I therefore designed a pilot study to assess the tolerability of alternative dose-schedules in BALB/c nude mice bearing MIA PaCa-2 xenografts (study code, Pr169). 8 different dose-schedules were tested, with two mice assigned per group, and one vehicle arm (**Fig. 5.3**).

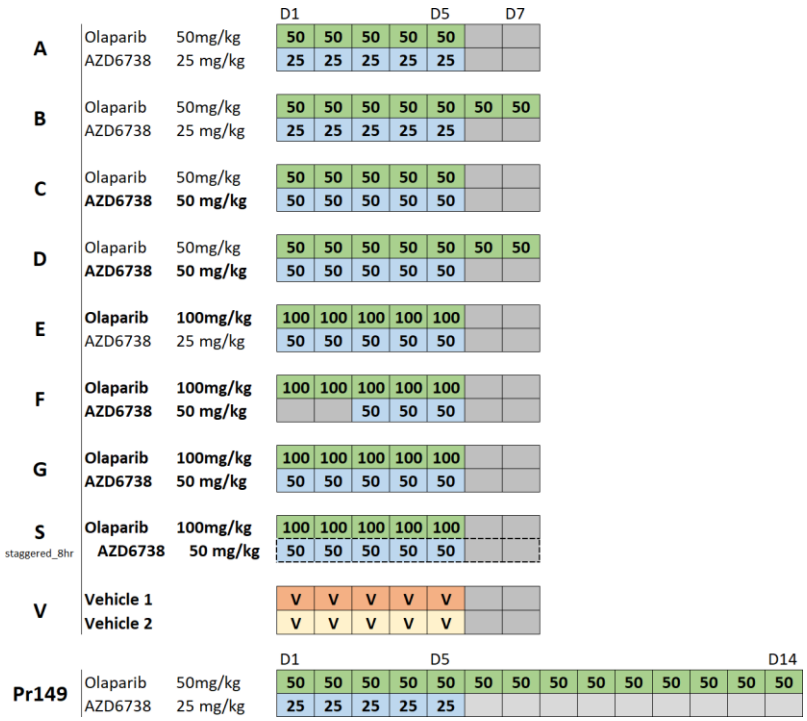

Fig. 5.3. Dose-schedules assessed in olaparib and AZD6738 tolerance study. Each square represents one day of a 7-day dosing cycle. Both drugs were administered by oral gavage. On days where both drugs were administered, AZD6738 was given 1 hour after the olaparib dose, except for in schedule S where it was given 8 hours after. The dose-schedule used in the previous efficacy study, Pr149, is also shown for comparison.

During the course of the pilot study, 7 of the 8 schedules appeared tolerable, with no considerable weight loss observed in these groups (**Fig. 5.4A**). Group S, in which 50 mg/kg AZD6738 was dosed 8 hours after a 100 mg/kg olaparib dose, was the only schedule that induced notable weight loss in both mice (**Fig. 5.4A**).

In all other groups, AZD6738 was given 1 hour after the olaparib dose. Since both drugs were given orally, it is difficult to know whether the weight loss in the staggered 8-hour group was due to a pharmacodynamic effect or simply because of prolonged inappetence – receiving a dose in both the morning and the evening may have impacted the food intake of these mice differently to those mice receiving both doses in the morning. In any case, the fact that 7 schedules appeared tolerable was promising and meant a decision had to be made on which to take forward.

Since there were two mice per group, this pilot study was not powered to differentiate tumour growth rates between the groups, but did prove useful for PK analysis. One mouse in group B had a tumour which seemingly regressed to become undetectable, however the growth curve

suggested that this could have due to an inability of the xenograft to take and not necessarily a drug-induced effect (**Fig. 5.4B**). All mice were killed 3 hours after the final AZD6738 dose (4 hours after olaparib) and tumour samples were flash-frozen, to allow pharmacokinetic analysis.

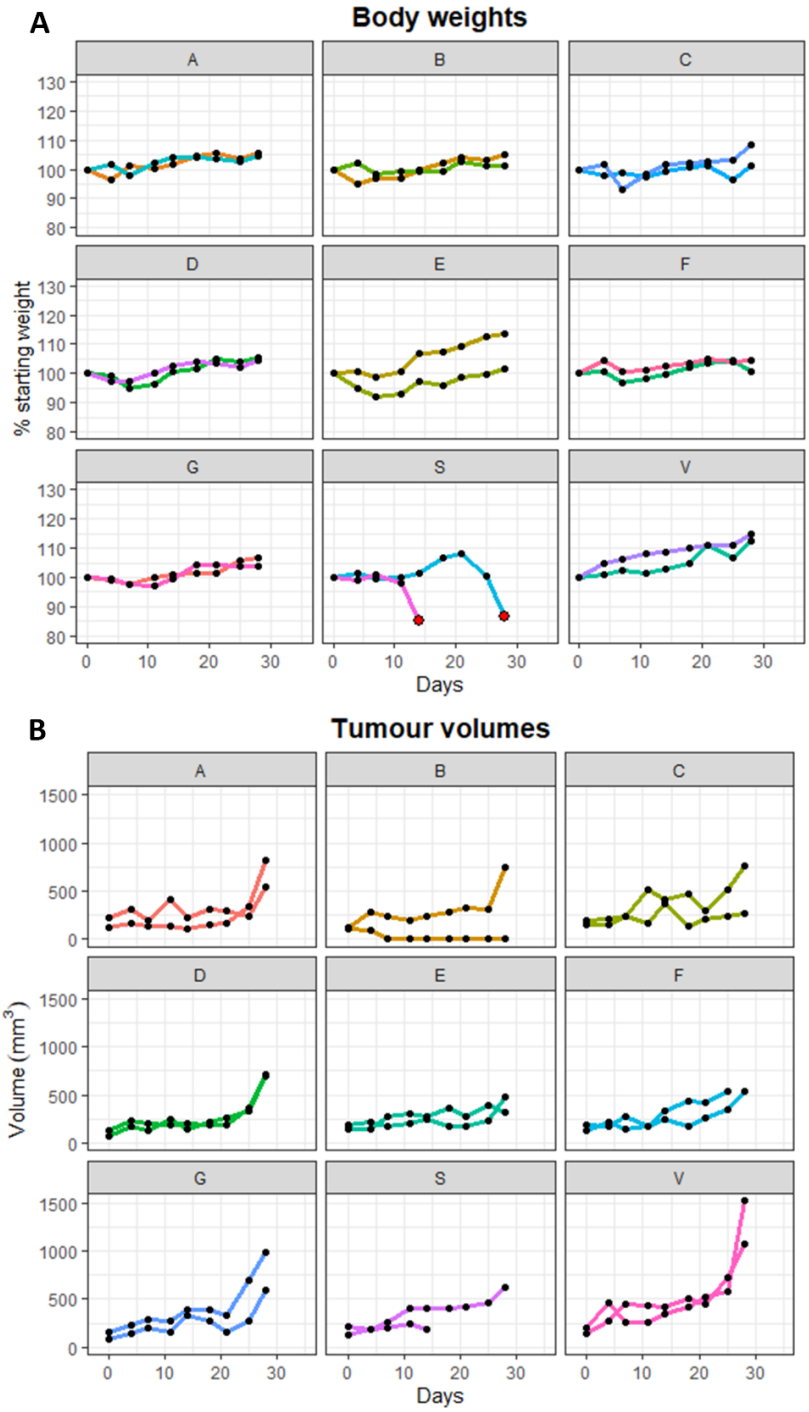

Fig. 5.4 (A) Individual mouse body weights over the course of the olaparib and AZD6738 tolerance study (Pr169), expressed as a percentage of starting weight. The final weight measurements of mice that had to be killed due to weight loss (approached or surpassed the 85% limit) are marked with a red dot. **(B)** MIA PaCa-2 tumour volumes over the course of the olaparib and AZD6738 tolerance study.

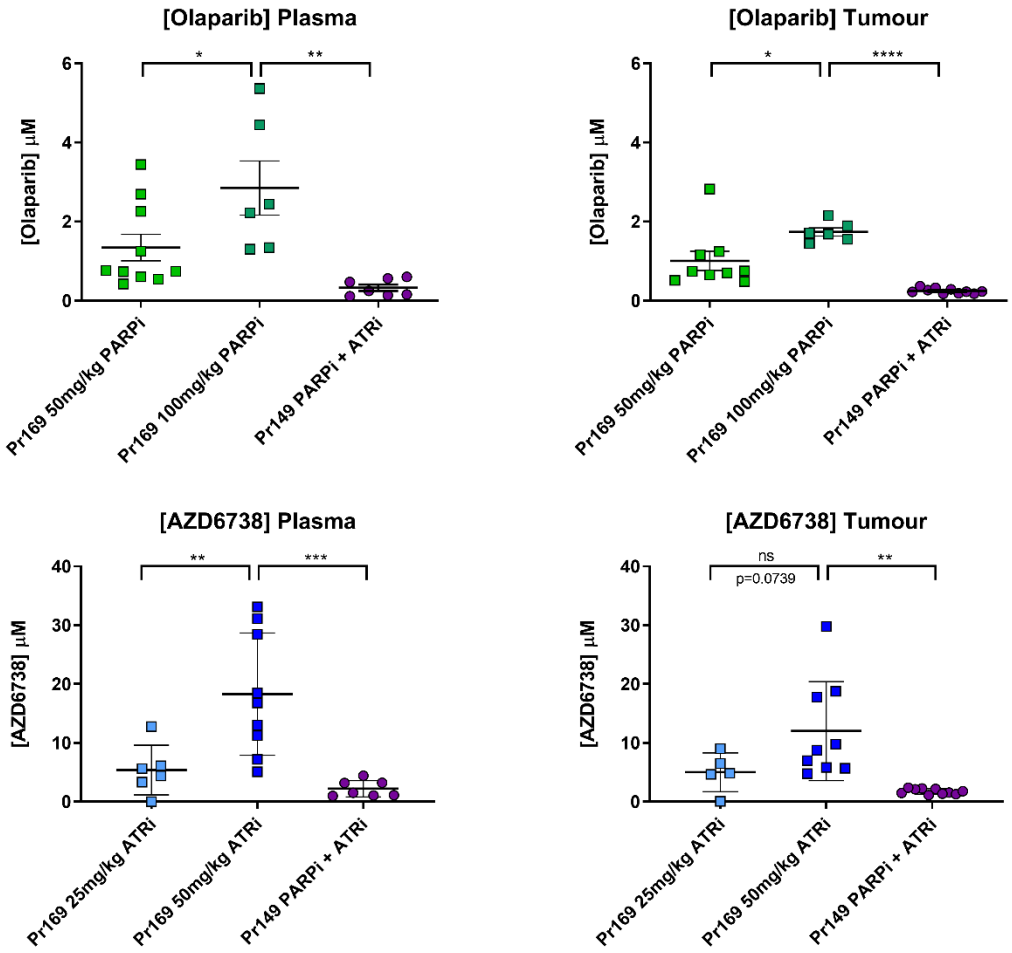

Fig. 5.5. UPLC-MS/MS was used to quantify the drug concentrations in flash-frozen plasma and tumour samples from the tolerance study, Pr169. Also shown for comparison are the PK data from the previous efficacy study, Pr149. Horizontal bars denote mean ± SEM. A one-way ANOVA analysis was performed with Tukey's multiple comparisons tests, * indicates $p \leq 0.05$, ** $p \leq 0.01$, *** $p \leq 0.001$, **** $p \leq 0.0001$

Tumour samples from mice which received 50 mg/kg olaparib had a mean olaparib concentration of 0.8 µM, while those that received 100 mg/kg olaparib had a mean of 1.7 µM (**Fig. 5.5**). These were higher concentrations than had been observed in the previous efficacy study that used 50 mg/kg olaparib (mean = 0.3 µM). Though unclear as to why 50 mg/kg dosing in Pr169 resulted in higher intra-tumour olaparib concentrations than previously, the fact that dosing at 100 mg/kg was resulting in olaparib concentrations above 1 µM was promising. Mean tumour AZD6738 concentrations from the mice that received 25 mg/kg and 50 mg/kg AZD6738 were 5.0 µM and 12.0 µM respectively, once again higher than in the previous study (mean = 1.8 µM) (**Fig. 5.5**).

To assess PARP target engagement by olaparib, the remaining half of the tumour samples from this study were processed into lysates for PAR ELISA analysis (as part of a collaboration, samples were run by Anna Staniszewska, AstraZeneca). 50 mg/kg and 100 mg/kg olaparib administration reduced PAR to concentrations below the limit of detection in most samples (PAR was undetectable in 6/8 of 50 mg/kg samples and 10/10 of 100 mg/kg samples tested), demonstrating that PARP activity was effectively inhibited (**Fig. 5.6**).

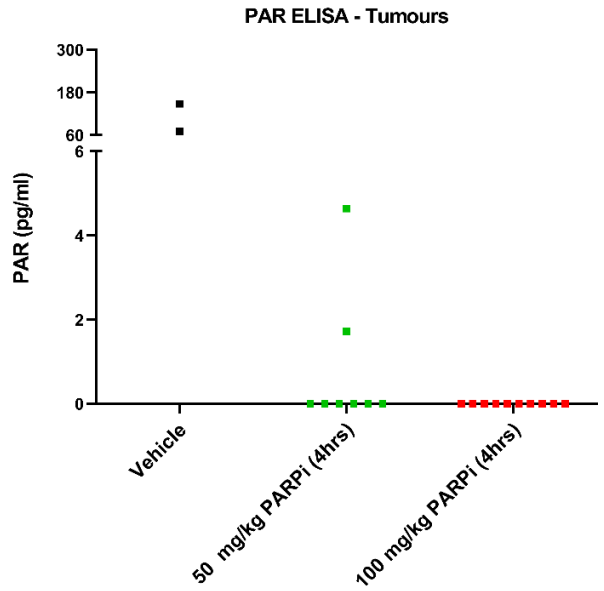

Fig. 5.6 Protein lysates from frozen tumour samples were analysed using the *PARP In Vivo Pharmacodynamic Assay II* ELISA kit (Trevigen). Samples were run by Anna Staniszewska, AstraZeneca.

I decided to take forward into an efficacy study the two strongest schedules in terms of dose level and/or dose regularity. These were schedule G (olaparib 100 mg/kg, OG, once daily, 5 days on & 2 days off; AZD6738 50 mg/kg, OG, once daily, 5 days on & 2 days off) and schedule D (olaparib 50 mg/kg, OG, 7 days per week; AZD6738 50 mg/kg, OG, once daily, 5 days on & 2 days off). Both share the same backbone of AZD6738, at a dose and regularity higher than the Pr149 study, but differ in their olaparib schedule - 100 mg/kg with a 2-day 'drug holiday' vs 50 mg/kg uninterrupted.

5.4. Olaparib and AZD6738 efficacy studies

Since I planned to assess two different combinatorial dose-schedules, including each individual single agent arm as well as the combination arms would have required a lot of mice. In keeping with the principle of the 3Rs in animal research, I decided to first to compare tumour growth in the combination groups to a vehicle-treated group. If growth inhibition were observed compared to vehicle, I would later enrol mice into the single-agent arms.

Following three weeks of treatment, neither of the combinatorial regimens demonstrated anti-tumour effect in BALB/c nude mice with MIA-PaCa-2 xenografts (**Fig. 5.7A**). Furthermore, despite appearing tolerable in the pilot study, weight loss was observed in both drug combination groups (3/12 mice in the 50 mg/kg olaparib group and 4/12 mice in the 100 mg/kg olaparib group) (**Fig. 5.7B**).

This highlights one of the major challenges in cancer research, which is that a drug-induced anti-cancer effect observed *in vitro* does not always translate *in vivo.* Though MIA PaCa-2 cells cultured as a mono-layer in 96 well plates were effectively growth inhibited by olaparib and AZD6738 (Fig. 5.1C), when the same cells were used as subcutaneous xenografts, oral dosing of the same drugs failed to inhibit tumour growth. This discrepancy between *in vitro* and *in vivo* results is discussed in more detail in section 5.5 (Discussion).

Up to this point, all of the *in vivo* assessments of the AZ6738 and olaparib combination had been using human MIA PaCa-2 xenografts in immunocompromised mice. Though easy to use, relatively inexpensive and often reproducible, xenograft models have a number of disadvantages such as the lack of intra-tumoural heterogeneity, the absence of immune responses and the inability to recapitulate the tumour microenvironment (TME) (Richmond and Su, 2008). Alternatively, genetically engineered mouse models (GEMM), such as the KPC mouse, do successfully model these features of cancer (Gopinathan et al., 2015). The TME significantly modulates responses to anticancer agents (McMillin et al., 2013). Though tumour-stroma interactions are typically associated with drug resistance, their compounding effects on the TME can in some instances confer drug sensitivity. For example, a hypoxic TME can increase the sensitivity of solid tumours to PARP inhibition (referred to as microenvironment-mediated “contextual synthetic lethality”) (Chan et al., 2010).

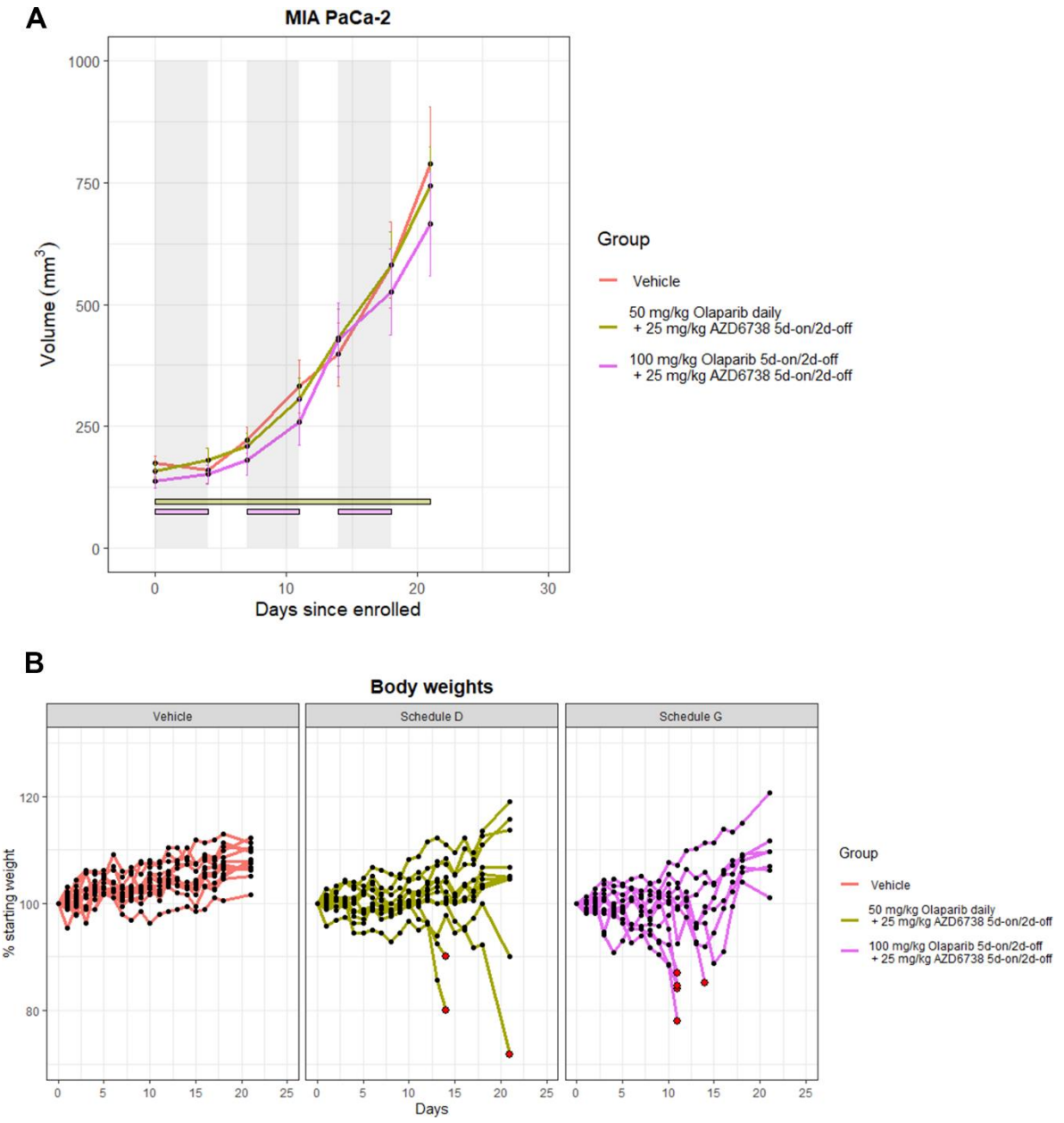

Fig. 5.7 (A) Tumour volumes of MIA PaCa-2 xenografts in BALB/c Nude mice, over the course of the olaparib and AZD6738 combination study. Data, mean ± SEM. 12 mice per group. The horizontal bars below the curves denote the olaparib dosing period for combination schedule D (gold - olaparib 50 mg/kg, OG, 7 days per week) and combination schedule G (pink - olaparib 100 mg/kg, OG, once daily, 5 days on & 2 days off). Both combination schedules shared the same AZD6738 dosing (AZD6738 50 mg/kg, OG, once daily, 1 hour after olaparib dose, 5 days on & 2 days off), as denoted by grey bars. **(B)** Individual mouse body weights over the course of the AZD6738 and olaparib efficacy study, expressed as a percentage of starting weight. The final weight measurements of mice that had to be killed due to weight loss (approached or surpassed the 85% limit) are marked with a red dot.

In addition, the presence of functioning immune cells in the TME will impact drug responses. This is not only relevant for immunotherapies, rather, the response of some preclinical tumour models to certain DDR-targeting therapies can be dependent on a functioning immune system. The Bakkenist group demonstrated that AZD6738 potentiated radiation in syngeneic colorectal CT26 tumours in BALB/c mice. The response was diminished upon cytotoxic T cell depletion using an anti-CD8 antibody, and also when the experiments were repeated in athymic nudes, suggesting that CD8+ T cells are required for maximal efficacy of AZD6738 plus radiation in CT26 tumours (Vendetti et al., 2018). As for the AZD6738 and olaparib combination in PDAC models, it remained unclear whether assessment in an immune-proficient GEMM that recapitulates the TME, such as the KPC mouse, would give a different result than the MIA PaCa-2 xenograft experiments.

The next steps were coordinated with the Jen Morton group at the Beatson Institute in Glasgow, who are collaborators through the PRECISION-Panc consortium. They had plans to assess the AZD6738 and olaparib combination in KPC-ATM-flox mice. They had generated this model by crossing KPC mice with ATM flox mice, the ATM-flox under the PDX1 Cre promotor such that ATM is specifically deleted in the pancreas during development. It was agreed that the standard KPC colony in Cambridge could be used to contribute ATM-proficient mice. I was PIL holder for this time-to-clinical-endpoint (survival) study, with the aim to assess the efficacy of 50 mg/kg olaparib (dosed 5 days per week, 2 days rest, repeated each week until clinical endpoint reached) and 25 mg/kg AZD6738 (dosed 1 hour after olaparib, 5 days per week, 2 days rest) in KPC mice (**Fig. 5.8A**).

In the ATM-proficient KPC model, though the median survival in the combination arm was greater than the vehicle or single agent arms, there was no significant separation in the survival curves (**Fig. 5.8B**). Primary tumour diameters were measured by ultrasound one day prior to enrolment and on day 12 (for those mice that survived to day 12). In accordance with RECIST criteria, a change in long tumour diameter between -30% and +20% was defined as stable disease, while a change greater than +20% was classified as progressive disease. Stable disease was observed in 0/6 vehicle-treated mice, 0/8 olaparib-treated mice, 4/9 AZD6738-treated mice and 3/8 combination-treated mice (**Fig. 5.8C**). This suggests that ATR inhibition-alone may have induced modest tumour growth control, but this was not enhanced by combined AZD6783 and olaparib treatment.

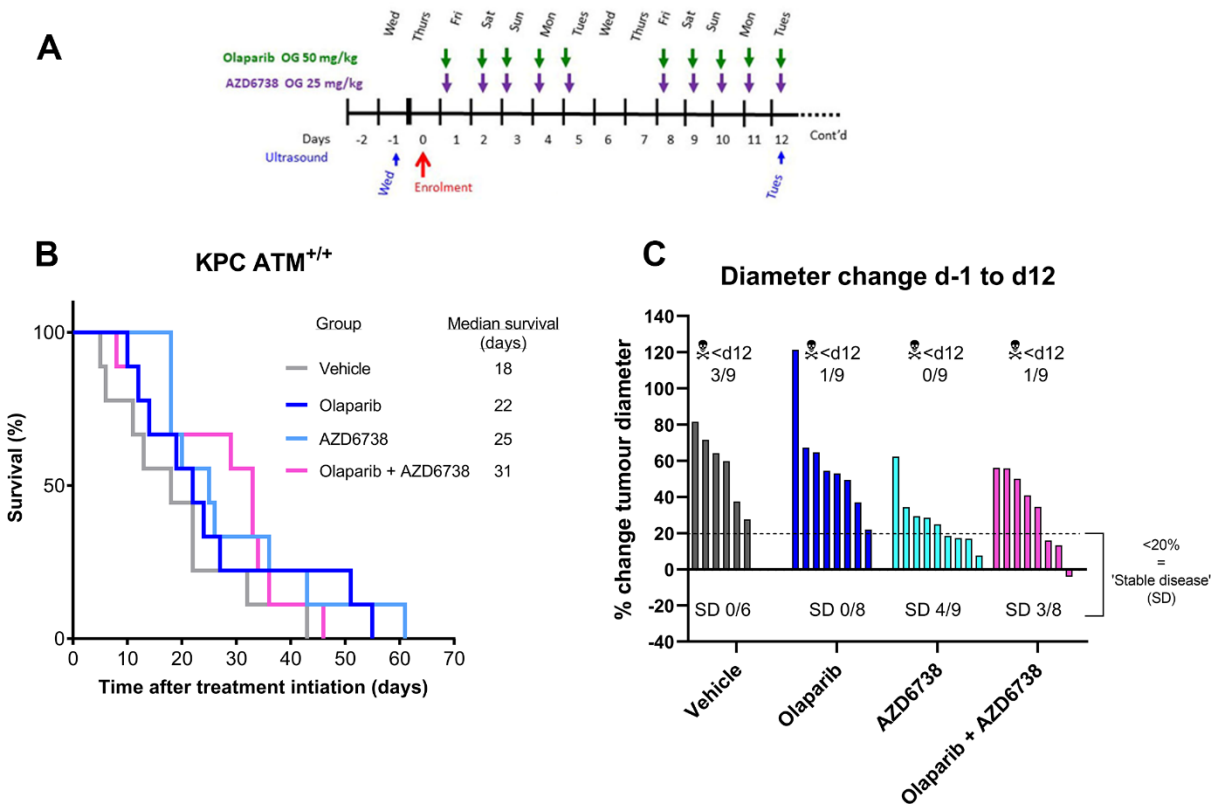

Fig. 5.8 (A) Dosing schedule for time-to-clinical-endpoint (survival) study in KPC mice (ATM-proficient), assessing efficacy of AZD6738 and olaparib. Mice were enrolled when tumour diameter of 3-6mm was confirmed by ultrasound (provided health suitable for minimum 12-day study). 50 mg/kg olaparib was dosed 5 days per week, 2 days rest, repeated each week until clinical endpoint reached. 25 mg/kg AZD6738 was dosed 1 hour after olaparib, 5 days per week, 2 days rest. 9 mice per group. Dosing was carried out by members of the CRUK-CI PGE core **(B)** Kaplan-Meier curve for KPC mice enrolled onto AZD6738 and olaparib survival study. Clinical endpoint was determined by body condition score and other clinical signs, as assessed by the CRUK-CI PGE core. **(C)** Change in primary tumour long dimeter from day -1 to day 12, as assessed by ultrasound. The number of mice in each group that reached clinical endpoint before day 12 (and so could not have diameters plotted) is displayed above each group. In accordance with RECIST criteria, a change in long tumour diameter between -30% and +20% was defined as stable disease (SD), while a change greater than 20% was classified as progressive disease. The number of mice in each group that had SD at day 12 is displayed beneath the x axis.

In the KPC ATM-flox mice that were assessed in Glasgow (which, when untreated, show poorer survival than their KPC ATM$^{+/+}$ counterparts (**Fig. 5.9A**)), the combination of olaparib and AZD6738 did extend survival compared to vehicle or olaparib-alone (**Fig. 5.9B**) and showed evidence of tumour growth inhibition (**Fig. 5.9C**).

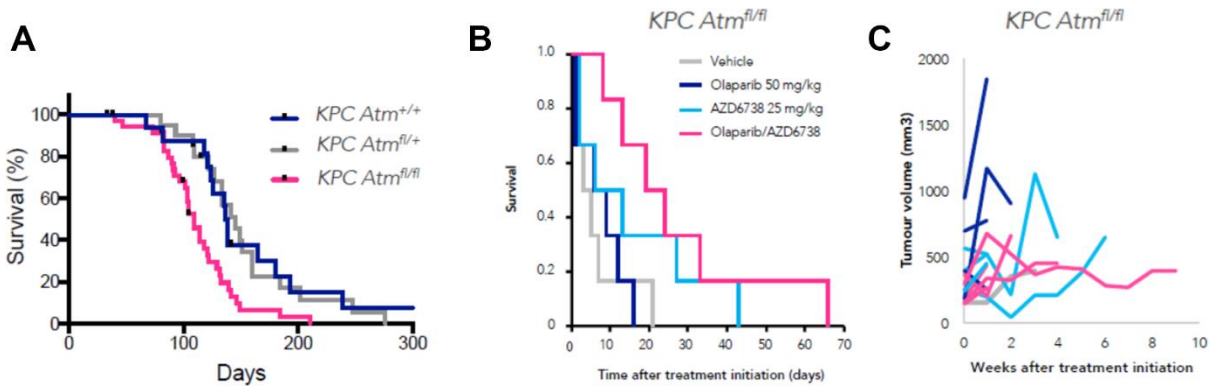

Fig. 5.9 (A) Survival comparison of untreated KPC ATM$^{+/+}$, KPC ATM$^{fl/+}$ and KPC ATM$^{fl/fl}$ mice. **(B&C)** The same treatment conditions assessed in Fig 5.8 were tested in KPC ATM$^{fl/fl}$ mice. Data courtesy of the Jen Morton group, Beatson Institute, Glasgow.

In support of this, I found that ATM-knockout sensitised MIA PaCa-2 to the AZD6738 and olaparib combination *in vitro* (**Fig. 5.10**). In WT MIA PaCa-2 cells dosed for 72-hours, the olaparib GI_{50} was > 10 µM, while in ATM-KO cells the mean GI_{50} was calculated as 2 µM (**Fig. 5.10A**). Synergy with olaparib and AZD6738 in WT cells could only be achieved at high olaparib doses (3 to 10 µM - note that these were 3-day assays, rather than 5-day as presented in **Fig. 5.1**), whereas in KO cells the surface of synergy was broader, such that even sub-micromolar doses of olaparib and AZD6738 showed synergy (**Fig. 5.10B**). This suggests that ATM might be a predictive biomarker of response for the AZD6738 and olaparib combination in PDAC.

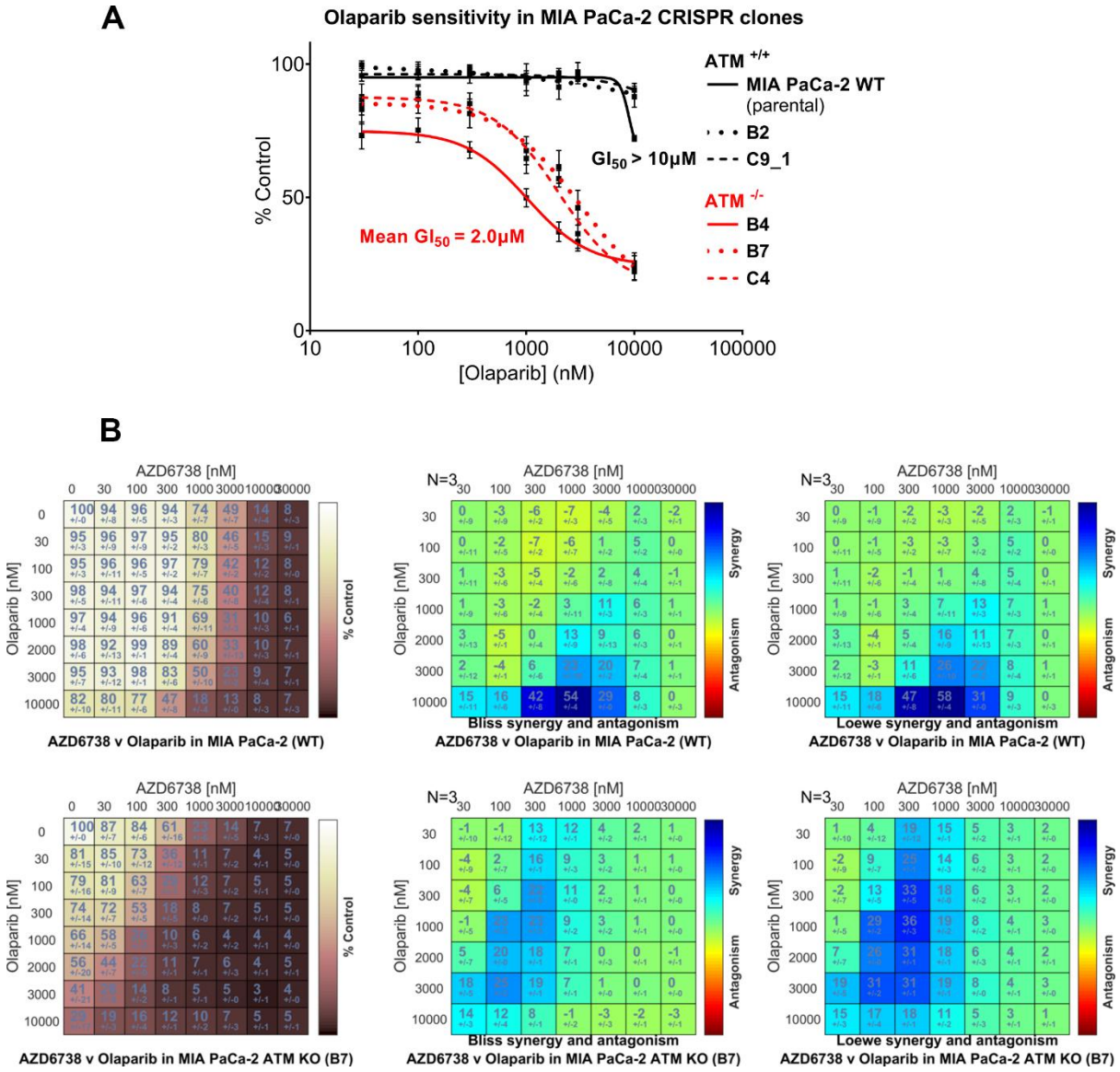

Fig. 5.10 (A) Olaparib dose-response curves of MIA PaCa-2 CRISPR clones. Assay duration was 72-hours. Each point represents the mean of three independent experiments ± SEM. **(B)** AZD6738 and olaparib combination in MIA PaCa-2 WT (top) and MIA PaCa-2 ATM-KO (clone B7, bottom). Assay duration was 72-hours. Left = growth as % of solvent control, mean ± SD, n=3 independent experiments. Right = Combenefit synergy score (Bliss and Loewe).

5.5. Discussion

In 2016, there were just two clinical trials assessing combined AZD6738 and olaparib therapy. At the time of writing, in Spring 2020, there are at least 15, thus demonstrating the significant interest in this combination. There is good rationale for dual targeting of ATR and PARP as previously explained. While olaparib monotherapy has primarily been explored in HR-deficient populations, mechanistically one might predict the combination of AZD6738 and olaparib to even show benefit in HR-proficient tumour types. Two-thirds of PDAC patients harbour no somatic mutations in any DDR genes, thus an effective therapy for these patients would fulfil a serious unmet need. This formed the basis of my *in vivo* investigations of the combination, since the Jodrell group already had evidence that AZD6738 and olaparib synergistically inhibited cell growth in HR-proficient PDAC lines *in vitro*. Unfortunately, none of my assessments of AZD6738 and olaparib in HR-proficient tumour models demonstrated efficacy. The current preclinical data in PDAC, including those generated by fellow members of the PRECISION-Panc consortium, indicate that AZD6738 and olaparib will most likely benefit patients DDR-deficiencies such as ATM-loss or BRCA mutations (Jen Morton, personal communication).

With hindsight, one of the strategic faults of this particular section was perhaps expecting the *in vitro* data of the AZD6738 and olaparib combination in MIA PaCa-2 to translate into *in vivo* efficacy with MIA PaCa-2 xenografts. The original AZD6738 and olaparib SRB assays presented in Figure 5.1C were performed before my arrival, using 5-days of continuous drug exposure. The majority of other SRB experiments presented in this thesis are 3-day assays – historically, olaparib combinations were performed differently because, in most PDAC cell lines, olaparib monotherapy has minimal effect on cell growth when treated for just 3 days, thus making it impossible to generate a dose response curve. The exposure of cancer cells growing as a monolayer in a 96-well plate to drug for 5-days continuously, cannot be mimicked in a mouse. Nor, indeed, can continuous exposure for 3-days, however one could argue that the longer the treatment the less physiologically relevant the results, since drugs such as AZD6738 and olaparib are rapidly metabolised and excreted when administered *in vivo*. A prolonged exposure to olaparib would give more time for PARP trapping and in turn more chance for replication fork stalling, enabling the pronounced synergy with ATR inhibition that is seen in Figure 5.1C. When 3-day SRB assays were performed, synergy with olaparib and AZD6738 could only be achieved at high olaparib doses (**Fig. 5.10B**), concentrations that were above the levels I detected in MIA PaCa-2 tumours from olaparib-dosed mice (**Fig. 5.5**). Though I had

evidence that dosing BALB/c nude mice with 50 mg/kg or 100 mg/kg olaparib could lead to inhibition of PARP activity in MIA PaCa-2 tumours (PAR ELISA in **Fig. 5.6**), I should have confirmed that this was actually leading to activation of the ATR/Chk1 pathway. Administering single agent olaparib at different dose levels and frequencies and then assessing P-Chk1-S345 by IHC at various timepoints after dosing, would have given me more insight into the extent of olaparib dosing that is required before ATR/Chk1 pathway activation occurs *in vivo*, if at all.

As previously mentioned, one of the limitations of using immunocompromised mice for combination studies is that the response of some preclinical tumour models to certain DDR-targeting therapies can be dependent on a functioning immune system. In 2019, the Byers group showed that PARPi induced activation of innate immune pathways in small cell lung cancer models, specifically activation of the DNA sensor cyclic guanosine monophosphate (GMP)–adenosine monophosphate (AMP) synthase (cGAS) (Sen et al., 2019). The second messenger of cGAS, cyclic GMP–AMP (cGAMP), binds and activates the adaptor protein STING, leading to TBK1-dependent phosphorylation of IRF3, which then translocates to the nucleus to trigger transcription of inflammatory genes such as interferons (Burdette et al., 2011; Sun et al., 2013). Byers and colleagues found that PARPi augmented anti–PD-L1–induced antitumor immunity in a cGAS-STING-dependent manner (Sen et al., 2019). Other groups have also demonstrated the ability for PARPi to induce interferon-mediated anti-tumour immune responses (Reisländer et al., 2019; Shen et al., 2019). Though cGAS-STING is an innate immune pathway, and so may be functional in immunocompromised mice, the potential downstream effects of STING activation on *adaptive* anticancer immunity would be absent in the Balb/C nude mice studies presented here in this chapter. As for the immune-competent KPC mouse studies, it would perhaps be interesting to repeat the experiments in Figures 5.8 & 5.9 but with an immune-checkpoint blockade such as anti-PDL1 added, to see if olaparib, AZD6738 or the PARPi/ATRi combination augments anti–PD-L1–induced antitumor immunity in PDAC models, and whether this is cGAS-STING-dependent. Combining DDR-targeted therapy with immunotherapy does come with challenges, however, since agents such as olaparib and can induce leucopoenia and neutropoenia (Thomas et al., 2019; Zhou et al., 2017).

My experiments using ATM-KO cells, in addition to the KPC-ATM-flox data from Glasgow, suggest that AZD6738 and olaparib may be efficacious in ATM-deficient PDAC. Given more time, I would perhaps have liked to have studied the effect of ATM-loss on the response of human PDAC cells to AZD6738 and olaparib in as much detail as I did with the ATRi/gem

combination (Chapter 4), for example asking whether replication catastrophe can be detected and if it is augmented in ATM-null cells. However, numerous trials for AZD6738 and olaparib are already either underway or in preparation (unlike ATRi/gem) and many will be assessing potential predictive biomarkers such as ATM-loss. Thus, ultimately, these clinical experiments will steer which biomarkers are prioritised for the AZD6738 and olaparib combination.

CHAPTER SIX: Summary and Future Outlook

In this dissertation, I have presented investigations into the therapeutic potential of combining the ATR inhibitor, AZD6738, with DNA-damaging drugs and DDR-targeted agents in preclinical models of PDAC. The data presented in Chapter 4 represent the most productive and informative section of the thesis, since the conclusions I made have immediately impacted the strategy of an ongoing clinical trial. By targeting ATM through multiple methods, my data in Chapter 4 indicated that complete loss of ATM function is necessary to sensitise PDAC cells to AZD6738 or the AZD6738 and gemcitabine combination. This has brought into question how best to assess ATM status clinically, including in the ATRiUM trial.

As described previously, there have been past examples of trials failing to meet their primary endpoint when simply using "low" ATM expression as predictive biomarker. The potential importance of distinguishing ATM-null from ATM-low highlights the need for precise characterisation of cancer patient samples in the precision medicine era. Accordingly, ATRiUM is incorporating IHC assessment of baseline ATM as well as targeted sequencing of tumour DNA, with ATM included in the gene panel. In addition to a baseline biopsy during the screening period before treatment, patients enrolled into ATRiUM undergo a second biopsy on day 10, 2±1 hour after the second, weekly gemcitabine administration. Through techniques such as multiplex immunofluorescence or imaging-mass-cytometry, it may be possible to assess how certain DDR markers alter post-treatment and compare this to the gemcitabine and AZD6738 drug concentrations that will be measured by Mass-Spec Imaging. My immunoblotting experiments in Chapter 4 demonstrated that many of the post-translational modifications typically attributed to ATM activity, such as P-ATM-S1981, P-Chk2-T68 and P-KAP1-S824, may actually be DNA-PK-driven in the specific context of ATRi/gem-induced damage. These modifications should therefore be ruled out as reliable indicators of ATM activity or ATM status. However, my experiments suggested that ATRi/gem-induced P-RAD50-S635 is more ATM-specific. Thus, one might predict that any fold-increase in this marker following ATRi/gem treatment may be dependent on the ATM status of that patient's tumour. Thus, it will be interesting to correlate any changes in P-RAD50 expression with the IHC and NGS assessments of ATM that are to be made during the ATRiUM trial.

As for AZD6738 and olaparib, the utility of ATM as a predictive biomarker in PDAC populations will be assessed in the planned PRECISION-Panc PRIMUS-004 trial (ISRCTN16004234). This multi-centre study, targeting patients with advanced pancreatic

cancer who have previously been treated with chemotherapy, is an umbrella trial that will offer a range of second-line treatment arms with extensive molecular profiling and evaluation of multiple candidate selection biomarkers. In alignment with the multi-modal approach to biomarker assessment, PRIMUS-004 will not only be assessing the mutation status of HR genes such as ATM, BRCA1, BRCA2 and PALB2, but will also incorporate transcriptomic profiling to evaluate signatures of HR-deficiency (Davies et al., 2017) and replication stress (Dreyer et al., 2018), as well as stratification on the basis of previous platinum response.

In some ways, a PhD project is akin to a journey. Hypotheses can be formed at the beginnings of a project that may be partly answered by other groups later on in the PhD. A notable paper that was published during the middle of my project came from Perkhofer and colleagues in 2017 (Perkhofer et al., 2017). Using a genetically engineered mouse model of PDAC with ATM deletion, they showed that ATM-deficiency sensitised *in vitro* PDAC cell lines to the ATR inhibitor, VE-822, and also to olaparib. In addition, using a subcutaneous transplantation model, they found that ATM-loss sensitised PDAC tumours to VE-822 and to the combination of VE-822 plus gemcitabine (Perkhofer et al., 2017). Differences from my work include: (1) the PDAC models they assessed were all p53 wild-type, whereas mine were all p53 mutant, (2) they were not using AZD6738 but VE-822 (also known as VX-970, M6620 or berzosertib), which, along with having different molecular properties to AZD6738, is typically administered to patients by intravenous injection rather than orally, (3) they did not study ATM-loss in any human PDAC models, only in mouse backgrounds, and (4) they did not assess replication catastrophe. On the whole our conclusions agreed, in that ATM-loss did sensitise to ATRi/gem in our models and in theirs. My work was sufficiently different to theirs and interesting enough that it was accepted for publication in the British Journal of Cancer in 2020 (Dunlop et al., 2020).

Towards the end of my PhD, another notable observation made externally came from the lab of Kent Mouw. Their work suggested that ATM-loss confers greater sensitivity to ATR inhibition than PARP inhibition in prostate cancer models (Rafiei et al., 2020). Like myself, they used CRISPR/Cas9 to delete ATM and generate ATM-null human cancer cell line clones. In agreement with my studies, ATM-KO did sensitise to ATRi (VX-970) in the clones. However, results from their prostate cancer cell lines appeared to differ in two key ways to my results in PDAC. Firstly, they found that siRNA depletion of ATM *did* sensitise the human prostate line DU145 to ATRi (Rafiei et al., 2020), whereas I had found siATM to be ineffective at sensitising in MIA PaCa-2, PANC-1 or HPAF-II (**Fig. 4.4**). Secondly, in the Mouw lab,

ATM-KO did *not* significantly sensitise prostate cancer cells to olaparib (as expected, BRCA2-deficiency did), whereas I had observed sensitisation effect with ATM-KO in MIA PaCa-2 (**Fig. 5.10A**). This again highlights that synthetic lethalities are not always maintained across different genetic backgrounds. The suggestion that ATM-loss does not sensitise to PARPi in prostate models, but BRCA1/2-deficiency does, has interesting clinical implications, since the recent phase III *PROfound* trial assessing PARPi in prostate cancer patients had in fact compiled men with ATM mutations and men with BRCA1/2mutations together as one analysis cohort (de Bono et al., 2020). Progression-free survival was significantly longer in the olaparib group than in the control group among the cohort of patients with a BRCA1, BRCA2, or ATM mutation, however it remains to be seen if most of this signal was due to the selection of BRCA1/2-mutant patients and whether selecting for ATM-mutant patients actually added anything. The preclinical data from the Mouw lab, at least, suggests that an ATM-mutant prostate cancer patient may benefit more from ATRi therapy than from PARPi treatment. The notion that PARPi may not be the best option in an ATM-mutant prostate setting is indeed supported by preliminary results from the phase II TRITON2 trial investigating rucaparib in prostate cancer patients, which showed an overall response rate of 44% among men with BRCA1/2 loss or mutation versus a response rate of 0% for men with ATM loss or mutation (Abida et al., 2018).

Another clinical study, which was published during the write-up period of this thesis and is particularly pertinent to my PhD project, is the trial NCT02595892. This was a phase II assessment of berzosertib (VX-970/M6620) plus gemcitabine in platinum-resistant high-grade serous ovarian cancer (HGSOC) (Konstantinopoulos et al., 2020). Patients were randomly assigned (1:1) to receive intravenous gemcitabine (1000 mg/m^2) on day 1 and day 8, or gemcitabine plus intravenous berzosertib (210 mg/m^2) on day 2 and day 9 of a 21-day cycle until disease progression or intolerable toxicity. The combination was tolerated and demonstrated benefit compared to gemcitabine monotherapy, with median progression-free survival of 22.9 weeks (17.9–72.0) in the gemcitabine plus berzosertib group (34 patients) and 14.7 weeks (90% CI 9.7–36.7) in the gemcitabine-alone group (36 patients) (hazard ratio 0.57, 90% CI 0.33–0.98; one-sided log-rank test p=0.044). This is the first randomised study of an ATRi therapy in any tumour type to be completed and the first suggesting a benefit of adding an ATR inhibitor to standard chemotherapy. Interestingly, their analysis indicated that there was a benefit of adding ATRi to gemcitabine in more heavily pre-treated patients (i.e. $\geq$ 2 previous lines of therapy), suggesting that heavy pre-treatment with chemotherapy may

promote resistance mechanisms that render tumours more susceptible to ATR inhibition. These results in HGSOC are promising for other ATRi trials, including ATRiUM, which will assess the oral drug AZD6738 in solid tumours (with a PDAC expansion arm) and explore various dose-schedules.

As for the combination of ATRi and PARPi, literature exploring this regimen has continued to emerge during my PhD, including very recently. In May 2020, colleagues at AstraZeneca published preclinical data showing that combined AZD6738 and olaparib potentiates genome instability and cell death in ATM-deficient cancer cells (Lloyd et al., 2020). Unlike myself, they did not investigate PDAC, but focused on models of hypopharyngeal carcinoma and lung adenocarcinoma. They showed that AZD6738 abrogated the olaparib-induced DNA damage G2-M checkpoint, independent of ATM status, but detected greater and earlier formation of micronuclei in ATM-null cells treated with the combination, plus earlier commitment to apoptosis in the absence of ATM. Their demonstration, in head & neck as well as lung cancer models, that ATM-loss sensitises to ATRi/PARPi supports my finding in ATM-KO PDAC cells, in addition to the KPC-ATM-flox data from Glasgow (**Figs 5.9 & 5.10**).

Though myself and others have demonstrated that, across various cancer models, ATM-loss can sensitise to ATRi, further mechanistic investigation is still required to pin-down exactly how and why this sensitisation occurs. While I have shown augmented replication catastrophe in ATM-null cells treated with ATRi (with and without gemcitabine), the precise events that lead to this phenotype in the absence of ATM still need to be elucidated. We know that ATRi in cancer cells can lead to unscheduled firing of replication origins and breakage of stalled forks (Toledo et al., 2013), but the exact role of ATM in responding to these replication-associated chromosomal aberrations remains to be fully explored. It seems logical that the DSBs that arise from these aberrations would be resolved by HR and this form of repair would be compromised in ATM-nulls cells. However, the Mouw lab found that ATM-loss, unlike BRCA2-loss, did not directly abolish HR function in prostate cancer cells (Rafiei et al., 2020). Furthermore, tumours with ATM alterations have been reported to lack the mutational signature of HR deficiency that is present in those with BRCA1/2 alterations (Quigley et al., 2018), thus HR-defects may not explain the hypersensitivity of ATM-null cancer cells to ATRi. ATR and ATM do share many targets (as my investigations into the DDR signalling of PDAC cells treated with ATRi and ATMi (**Fig4.9**) further demonstrated), therefore pathway inter-dependency may partly underly the synthetic lethality between ATR and ATM. Another consideration is the aforementioned ‘toxic end-joining’ which has been shown to be important

in the hypersensitivity of ATM-null cells to replication-associated damage induced by olaparib (Balmus et al., 2019), but whether this is true for ATRi-induced damage remains to be seen. Going forward, biochemical methods that directly assess events occurring at the replication fork in ATRi-treated cells may improve our mechanistic understanding of how ATM-loss impacts the cellular response to ATRi. For example, the Cortez group have combined a method that purifies replication-associated proteins (iPOND - isolation of proteins on nascent DNA) with mass spectrometry to analyse the replisome at stalled forks in cells treated with hydroxyurea and ATRi (Dungrawala et al., 2015). They found that ATM and HR repair factors are the first recruited components to collapsed forks, whereas DNA-PK is instead recruited later to the damaged forks generated by new origin firing. This type of technique could perhaps be applied to ATM-WT versus ATM-KO cancer cells treated to with ATRi (or ATRi and gemcitabine) to further our understanding of how ATM-loss sensitises to ATRi.

To sum up, though the regulatory approvals of PARP inhibitors in BRCA-mutant populations have been transformative in the way we think about DDR-targeting cancer therapies, no other synthetic lethal relationship has yet been exploited as successfully in the clinic. Whether the use of ATM as a predictive biomarker for ATR inhibitor-based therapies such as ATRi/gem succeeds as a clinical strategy, will depend upon well-designed trials that collect as much information as possible from every patient. Preclinical investigations, such as those presented here, are prerequisites for early phase trials like ATRiUM and PRIMUS-004, which will guide the next phase of cancer treatments for the precision medicine era.

REFERENCES

Abida, W., Bryce, A.H., Vogelzang, N.J., Amato, R.J., Percent, I., Shapiro, J.D., McDermott, R., Hussain, A., Patnaik, A., Petrylak, D., et al. (2018). Preliminary results from TRITON2: A phase II study of rucaparib in patients (pts) with metastatic castration-resistant prostate cancer (mCRPC) associated with homologous recombination repair (HRR) gene alterations. Ann. Oncol. *29*, viii272.

Aguirre, A.J., Nowak, J.A., Camarda, N.D., Moffitt, R.A., Ghazani, A.A., Hazar-Rethinam, M., Raghavan, S., Kim, J., Brais, L.K., Ragon, D., et al. (2018). Real-time Genomic Characterization of Advanced Pancreatic Cancer to Enable Precision Medicine. Cancer Discov. *8*, 1096–1111.

Ai, L., Vo, Q.N., Zuo, C., Li, L., Ling, W., Suen, J.Y., Hanna, E., Brown, K.D., and Fan, C.-Y. (2004). Ataxia-Telangiectasia-Mutated (ATM) Gene in Head and Neck Squamous Cell Carcinoma: Promoter Hypermethylation with Clinical Correlation in 100 Cases. Cancer Epidemiol. Prev. Biomark. *13*, 150–156.

Álvarez-Quilón, A., Serrano-Benítez, A., Ariel Lieberman, J., Quintero, C., Sánchez-Gutiérrez, D., Escudero, L.M., and Cortés-Ledesma, F. (2014). ATM specifically mediates repair of double-strand breaks with blocked DNA ends. Nat. Commun. *5*, 1–10.

Arlander, S.J.H., Greene, B.T., Innes, C.L., and Paules, R.S. (2008). DNA-PK-Dependent G2 Checkpoint Revealed Following Knockdown of ATM in Human Mammary Epithelial Cells. Cancer Res. *68*, 89–97.

Armstrong, S.A., Schultz, C.W., Azimi-Sadjadi, A., Brody, J.R., and Pishvaian, M.J. (2019). ATM Dysfunction in Pancreatic Adenocarcinoma and Associated Therapeutic Implications. Mol. Cancer Ther. *18*, 1899–1908.

Ayars, M., Eshleman, J., and Goggins, M. (2017). Susceptibility of ATM-deficient pancreatic cancer cells to radiation. Cell Cycle *16*, 991–998.

Bailey, P., Chang, D.K., Nones, K., Johns, A.L., Patch, A.-M., Gingras, M.-C., Miller, D.K., Christ, A.N., Bruxner, T.J.C., Quinn, M.C., et al. (2016). Genomic analyses identify molecular subtypes of pancreatic cancer. Nature *531*, 47–52.

Bakkenist, C.J., and Kastan, M.B. (2003). DNA damage activates ATM through intermolecular autophosphorylation and dimer dissociation. Nature *421*, 499–506.

Bakr, A., Oing, C., Köcher, S., Borgmann, K., Dornreiter, I., Petersen, C., Dikomey, E., and Mansour, W.Y. (2015). Involvement of ATM in homologous recombination after end resection and RAD51 nucleofilament formation. Nucleic Acids Res. *43*, 3154–3166.

Balmus, G., Pilger, D., Coates, J., Demir, M., Sczaniecka-Clift, M., Barros, A.C., Woods, M., Fu, B., Yang, F., Chen, E., et al. (2019). ATM orchestrates the DNA-damage response to counter toxic non-homologous end-joining at broken replication forks. Nat. Commun. *10*, 87.

Bang, Y.-J., Im, S.-A., Lee, K.-W., Cho, J.Y., Song, E.-K., Lee, K.H., Kim, Y.H., Park, J.O., Chun, H.G., Zang, D.Y., et al. (2015). Randomized, Double-Blind Phase II Trial With Prospective Classification by ATM Protein Level to Evaluate the Efficacy and Tolerability of Olaparib Plus Paclitaxel in Patients With Recurrent or Metastatic Gastric Cancer. J. Clin. Oncol. Off. J. Am. Soc. Clin. Oncol. *33*, 3858–3865.

Bang, Y.-J., Xu, R.-H., Chin, K., Lee, K.-W., Park, S.H., Rha, S.Y., Shen, L., Qin, S., Xu, N., Im, S.-A., et al. (2017). Olaparib in combination with paclitaxel in patients with advanced gastric cancer who

have progressed following first-line therapy (GOLD): a double-blind, randomised, placebo-controlled, phase 3 trial. Lancet Oncol. *18*, 1637–1651.

Banin, S., Moyal, L., Shieh, S.-Y., Taya, Y., Anderson, C.W., Chessa, L., Smorodinsky, N.I., Prives, C., Reiss, Y., Shiloh, Y., et al. (1998). Enhanced Phosphorylation of p53 by ATM in Response to DNA Damage. Science *281*, 1674–1677.

Bapiro, T.E., Frese, K.K., Courtin, A., Bramhall, J.L., Madhu, B., Cook, N., Neesse, A., Griffiths, J.R., Tuveson, D.A., Jodrell, D.I., et al. (2014). Gemcitabine diphosphate choline is a major metabolite linked to the Kennedy pathway in pancreatic cancer models in vivo. Br. J. Cancer *111*, 318–325.

Baretić, D., Pollard, H.K., Fisher, D.I., Johnson, C.M., Santhanam, B., Truman, C.M., Kouba, T., Fersht, A.R., Phillips, C., and Williams, R.L. (2017). Structures of closed and open conformations of dimeric human ATM. Sci. Adv. *3*, e1700933.

Barlaam, B., and Pike, K. (2016). Identifying high quality, potent and selective inhibitors of ATM kinase: Discovery of AZD0156. Eur. J. Cancer *61*, S118–S118.

Bartek, J., Falck, J., and Lukas, J. (2001). Chk2 kinase — a busy messenger. Nat. Rev. Mol. Cell Biol. *2*, 877–886.

Bartkova, J., Hořejší, Z., Koed, K., Krämer, A., Tort, F., Zieger, K., Guldberg, P., Sehested, M., Nesland, J.M., Lukas, C., et al. (2005). DNA damage response as a candidate anti-cancer barrier in early human tumorigenesis. Nature *434*, 864–870.

Bennett, C.B., Lewis, A.L., Baldwin, K.K., and Resnick, M.A. (1993). Lethality induced by a single site-specific double-strand break in a dispensable yeast plasmid. Proc. Natl. Acad. Sci. *90*, 5613–5617.

Beucher, A., Birraux, J., Tchouandong, L., Barton, O., Shibata, A., Conrad, S., Goodarzi, A.A., Krempler, A., Jeggo, P.A., and Löbrich, M. (2009). ATM and Artemis promote homologous recombination of radiation-induced DNA double-strand breaks in G2. EMBO J. *28*, 3413–3427.

Biankin, A.V., Waddell, N., Kassahn, K.S., Gingras, M.-C., Muthuswamy, L.B., Johns, A.L., Miller, D.K., Wilson, P.J., Patch, A.-M., Wu, J., et al. (2012). Pancreatic cancer genomes reveal aberrations in axon guidance pathway genes. Nature *491*, 399–405.

Blier, P.R., Griffith, A.J., Craft, J., and Hardin, J.A. (1993). Binding of Ku protein to DNA. Measurement of affinity for ends and demonstration of binding to nicks. J. Biol. Chem. *268*, 7594–7601.

de Bono, J., Mateo, J., Fizazi, K., Saad, F., Shore, N., Sandhu, S., Chi, K.N., Sartor, O., Agarwal, N., Olmos, D., et al. (2020). Olaparib for Metastatic Castration-Resistant Prostate Cancer. N. Engl. J. Med. *382*, 2091–2102.

Boshuizen, J., and Peeper, D.S. (2020). Rational Cancer Treatment Combinations: An Urgent Clinical Need. Mol. Cell *78*, 1002–1018.

Bowman, K.J., Newell, D.R., Calvert, A.H., and Curtin, N.J. (2001). Differential effects of the poly (ADP-ribose) polymerase (PARP) inhibitor NU1025 on topoisomerase I and II inhibitor cytotoxicity in L1210 cells in vitro. Br. J. Cancer *84*, 106–112.

Bradbury, A., Hall, S., Curtin, N., and Drew, Y. (2019). Targeting ATR as Cancer Therapy: A new era for synthetic lethality and synergistic combinations? Pharmacol. Ther. 107450.

Brand, R., Borazanci, E., Speare, V., Dudley, B., Karloski, E., Peters, M.L.B., Stobie, L., Bahary, N., Zeh, H., Zureikat, A., et al. (2018). Prospective study of germline genetic testing in incident cases of pancreatic adenocarcinoma. Cancer *124*, 3520–3527.

Brown, E.J., and Baltimore, D. (2000). ATR disruption leads to chromosomal fragmentation and early embryonic lethality. Genes Dev. *14*, 397–402.

Bryant, H.E., Schultz, N., Thomas, H.D., Parker, K.M., Flower, D., Lopez, E., Kyle, S., Meuth, M., Curtin, N.J., and Helleday, T. (2005). Specific killing of BRCA2-deficient tumours with inhibitors of poly(ADP-ribose) polymerase. Nature *434*, 913–917.

Buisson, R., Boisvert, J.L., Benes, C.H., and Zou, L. (2015). Distinct but Concerted Roles of ATR, DNA-PK, and Chk1 in Countering Replication Stress during S Phase. Mol. Cell *59*, 1011–1024.

Bukhari, A.B., Lewis, C.W., Pearce, J.J., Luong, D., Chan, G.K., and Gamper, A.M. (2019). Inhibiting Wee1 and ATR kinases produces tumor-selective synthetic lethality and suppresses metastasis. J. Clin. Invest. *129*, 1329–1344.

Burdette, D.L., Monroe, K.M., Sotelo-Troha, K., Iwig, J.S., Eckert, B., Hyodo, M., Hayakawa, Y., and Vance, R.E. (2011). STING is a direct innate immune sensor of cyclic di-GMP. Nature *478*, 515–518.

Burris, H.A., Moore, M.J., Andersen, J., Green, M.R., Rothenberg, M.L., Modiano, M.R., Cripps, M.C., Portenoy, R.K., Storniolo, A.M., Tarassoff, P., et al. (1997). Improvements in survival and clinical benefit with gemcitabine as first-line therapy for patients with advanced pancreas cancer: a randomized trial. J. Clin. Oncol. *15*, 2403–2413.

Byun, T.S., Pacek, M., Yee, M., Walter, J.C., and Cimprich, K.A. (2005). Functional uncoupling of MCM helicase and DNA polymerase activities activates the ATR-dependent checkpoint. Genes Dev. *19*, 1040–1052.

Canman, C.E., Lim, D.-S., Cimprich, K.A., Taya, Y., Tamai, K., Sakaguchi, K., Appella, E., Kastan, M.B., and Siliciano, J.D. (1998). Activation of the ATM Kinase by Ionizing Radiation and Phosphorylation of p53. Science *281*, 1677–1679.

Cao, D., Ashfaq, R., Goggins, M.G., Hruban, R.H., Kern, S.E., and Iacobuzio-Donahue, C.A. (2008). Differential expression of multiple genes in association with MADH4/DPC4/SMAD4 inactivation in pancreatic cancer. Int. J. Clin. Exp. Pathol. *1*, 510–517.

Cerami, E., Gao, J., Dogrusoz, U., Gross, B.E., Sumer, S.O., Aksoy, B.A., Jacobsen, A., Byrne, C.J., Heuer, M.L., Larsson, E., et al. (2012). The cBio cancer genomics portal: an open platform for exploring multidimensional cancer genomics data. Cancer Discov. *2*, 401–404.

Chan, N., Pires, I.M., Bencokova, Z., Coackley, C., Luoto, K.R., Bhogal, N., Lakshman, M., Gottipati, P., Oliver, F.J., Helleday, T., et al. (2010). Contextual Synthetic Lethality of Cancer Cell Kill Based on the Tumor Microenvironment. Cancer Res. *70*, 8045–8054.

Charrier, J.-D., Durrant, S.J., Golec, J.M.C., Kay, D.P., Knegtel, R.M.A., MacCormick, S., Mortimore, M., O'Donnell, M.E., Pinder, J.L., Reaper, P.M., et al. (2011). Discovery of potent and selective inhibitors of ataxia telangiectasia mutated and Rad3 related (ATR) protein kinase as potential anticancer agents. J. Med. Chem. *54*, 2320–2330.

Choi, M., Kipps, T., and Kurzrock, R. (2016). ATM Mutations in Cancer: Therapeutic Implications. Mol. Cancer Ther. *15*, 1781–1791.

Chou, T.-C. (2010). Drug combination studies and their synergy quantification using the Chou-Talalay method. Cancer Res. *70*, 440–446.

Ciszewski, W.M., Tavecchio, M., Dastych, J., and Curtin, N.J. (2014). DNA-PK inhibition by NU7441 sensitizes breast cancer cells to ionizing radiation and doxorubicin. Breast Cancer Res. Treat. *143*, 47–55.

Conroy, T., Desseigne, F., Ychou, M., Bouché, O., Guimbaud, R., Bécouarn, Y., Adenis, A., Raoul, J.-L., Gourgou-Bourgade, S., de la Fouchardière, C., et al. (2011). FOLFIRINOX versus gemcitabine for metastatic pancreatic cancer. N. Engl. J. Med. *364*, 1817–1825.

Couch, F.B., Bansbach, C.E., Driscoll, R., Luzwick, J.W., Glick, G.G., Bétous, R., Carroll, C.M., Jung, S.Y., Qin, J., Cimprich, K.A., et al. (2013). ATR phosphorylates SMARCAL1 to prevent replication fork collapse. Genes Dev. *27*, 1610–1623.

Coussy, F., El-Botty, R., Château-Joubert, S., Dahmani, A., Montaudon, E., Leboucher, S., Morisset, L., Painsec, P., Sourd, L., Huguet, L., et al. (2020). BRCAness, SLFN11, and RB1 loss predict response to topoisomerase I inhibitors in triple-negative breast cancers. Sci. Transl. Med. *12*.

Cuadrado, M., Martinez-Pastor, B., Murga, M., Toledo, L.I., Gutierrez-Martinez, P., Lopez, E., and Fernandez-Capetillo, O. (2006). ATM regulates ATR chromatin loading in response to DNA double-strand breaks. J. Exp. Med. *203*, 297–303.

Dai, J.L., Turnacioglu, K.K., Schutte, M., Sugar, A.Y., and Kern, S.E. (1998). Dpc4 transcriptional activation and dysfunction in cancer cells. Cancer Res. *58*, 4592–4597.

Damstrup, L., Zimmerman, A., Sirrenberg, C., Zenke, F., and Vassilev, L. (2016). M3814, a DNA-dependent Protein Kinase Inhibitor (DNA-PKi), Potentiates the Effect of Ionizing Radiation (IR) in Xenotransplanted Tumors in Nude Mice. Int. J. Radiat. Oncol. *94*, 940–941.

Davies, H., Glodzik, D., Morganella, S., Yates, L.R., Staaf, J., Zou, X., Ramakrishna, M., Martin, S., Boyault, S., Sieuwerts, A.M., et al. (2017). HRDetect is a predictor of BRCA1 and BRCA2 deficiency based on mutational signatures. Nat. Med. *23*, 517–525.

Davies, S.L., North, P.S., and Hickson, I.D. (2007). Role for BLM in replication-fork restart and suppression of origin firing after replicative stress. Nat. Struct. Mol. Biol. *14*, 677–679.

Denko, N.C., Giaccia, A.J., Stringer, J.R., and Stambrook, P.J. (1994). The human Ha-ras oncogene induces genomic instability in murine fibroblasts within one cell cycle. Proc. Natl. Acad. Sci. *91*, 5124–5128.

Derenzini, E., Agostinelli, C., Imbrogno, E., Iacobucci, I., Casadei, B., Brighenti, E., Righi, S., Fuligni, F., Ghelli Luserna Di Rorà, A., Ferrari, A., et al. (2015). Constitutive activation of the DNA damage response pathway as a novel therapeutic target in diffuse large B-cell lymphoma. Oncotarget *6*, 6553–6569.

Dhoonmoon, A., Schleicher, E.M., Clements, K.E., Nicolae, C.M., and Moldovan, G.-L. (2020). Genome-wide CRISPR synthetic lethality screen identifies a role for the ADP-ribosyltransferase PARP14 in DNA replication dynamics controlled by ATR. Nucleic Acids Res. *48*, 7252–7264.

Di Micco, R., Fumagalli, M., Cicalese, A., Piccinin, S., Gasparini, P., Luise, C., Schurra, C., Garre', M., Giovanni Nuciforo, P., Bensimon, A., et al. (2006). Oncogene-induced senescence is a DNA damage response triggered by DNA hyper-replication. Nature *444*, 638–642.

Di Veroli, G.Y., Fornari, C., Wang, D., Mollard, S., Bramhall, J.L., Richards, F.M., and Jodrell, D.I. (2016). Combenefit: an interactive platform for the analysis and visualization of drug combinations. Bioinforma. Oxf. Engl. *32*, 2866–2868.

Di Virgilio, M., Ying, C.Y., and Gautier, J. (2009). PIKK-dependent phosphorylation of Mre11 induces MRN complex inactivation by disassembly from chromatin. DNA Repair *8*, 1311–1320.

Ditch, S., and Paull, T.T. (2012). The ATM protein kinase and cellular redox signaling: beyond the DNA damage response. Trends Biochem. Sci. *37*, 15–22.

Dorado, M.R.-M., Gómez, L.M.M., Sánchez, D.A., Arenas, S.P., Praena-Fernández, J.M., Martín, J.J.B., López, F.F., Bravo, M.Á.G., Relat, J.M., and Ruiz, J.P. (2018). Translational pancreatic cancer research: A comparative study on patient-derived xenograft models. World J. Gastroenterol. *24*, 794–809.

Doyle, L.A., and Ross, D.D. (2003). Multidrug resistance mediated by the breast cancer resistance protein BCRP (ABCG2). Oncogene *22*, 7340–7358.

Dréan, A., Lord, C.J., and Ashworth, A. (2016). PARP inhibitor combination therapy. Crit. Rev. Oncol. Hematol. *108*, 73–85.

Dreyer, S.B., Paulus-Hock, V., Lampraki, E., Upstill-Goddard, R., Caligiuri, G., Brunton, H., Serrels, B., Cunningham, R., Jamieson, N.B., McKay, C.J., et al. (2018). AB001. S001. Defining DDR deficiency and replication stress in pancreatic cancer. Ann. Pancreat. Cancer *1*.

Dreyer, S.B., Jamieson, N.B., Cooke, S.L., Valle, J.W., McKay, C.J., Biankin, A.V., and Chang, D.K. (2020). PRECISION-Panc: the Next Generation Therapeutic Development Platform for Pancreatic Cancer. Clin. Oncol. *32*, 1–4.

Dungrawala, H., Rose, K.L., Bhat, K.P., Mohni, K.N., Glick, G.G., Couch, F.B., and Cortez, D. (2015). The replication checkpoint prevents two types of fork collapse without regulating replisome stability. Mol. Cell *59*, 998–1010.

Dunlop, C.R., Wallez, Y., Johnson, T.I., Bernaldo de Quirós Fernández, S., Durant, S.T., Cadogan, E.B., Lau, A., Richards, F.M., and Jodrell, D.I. (2020). Complete loss of ATM function augments replication catastrophe induced by ATR inhibition and gemcitabine in pancreatic cancer models. Br. J. Cancer 1–13.

Durant, S.T., Zheng, L., Wang, Y., Chen, K., Zhang, L., Zhang, T., Yang, Z., Riches, L., Trinidad, A.G., Fok, J.H.L., et al. (2018). The brain-penetrant clinical ATM inhibitor AZD1390 radiosensitizes and improves survival of preclinical brain tumor models. Sci. Adv. *4*, eaat1719.

Durkacz, B.W., Omidiji, O., Gray, D.A., and Shall, S. (1980). (ADP-ribose) n participates in DNA excision repair. Nature *283*, 593–596.

Dylgjeri, E., McNair, C., Goodwin, J.F., Raymon, H.K., McCue, P.A., Shafi, A.A., Leiby, B.E., Leeuw, R. de, Kothari, V., McCann, J.J., et al. (2019). Pleiotropic Impact of DNA-PK in Cancer and Implications for Therapeutic Strategies. Clin. Cancer Res.

El-Khamisy, S.F., Masutani, M., Suzuki, H., and Caldecott, K.W. (2003). A requirement for PARP-1 for the assembly or stability of XRCC1 nuclear foci at sites of oxidative DNA damage. Nucleic Acids Res. *31*, 5526–5533.

Elliott, S.L., Crawford, C., Mulligan, E., Summerfield, G., Newton, P., Wallis, J., Mainou-Fowler, T., Evans, P., Bedwell, C., Durkacz, B.W., et al. (2011). Mitoxantrone in combination with an inhibitor

of DNA-dependent protein kinase: a potential therapy for high risk B-cell chronic lymphocytic leukaemia. Br. J. Haematol. *152*, 61–71.

Erber, J., Steiner, J.D., Isensee, J., Lobbes, L.A., Toschka, A., Beleggia, F., Schmitt, A., Kaiser, R.W.J., Siedek, F., Persigehl, T., et al. (2019). Dual inhibition of GLUT1 and the ATR/CHK1 kinase axis displays synergistic cytotoxicity in KRAS-mutant cancer cells. Cancer Res.

Evert, M., Frau, M., Tomasi, M.L., Latte, G., Simile, M.M., Seddaiu, M.A., Zimmermann, A., Ladu, S., Staniscia, T., Brozzetti, S., et al. (2013). Deregulation of DNA-dependent protein kinase catalytic subunit contributes to human hepatocarcinogenesis development and has a putative prognostic value. Br. J. Cancer *109*, 2654–2664.

Falck, J., Coates, J., and Jackson, S.P. (2005). Conserved modes of recruitment of ATM, ATR and DNA-PKcs to sites of DNA damage. Nature *434*, 605–611.

Farmer, H., McCabe, N., Lord, C.J., Tutt, A.N.J., Johnson, D.A., Richardson, T.B., Santarosa, M., Dillon, K.J., Hickson, I., Knights, C., et al. (2005). Targeting the DNA repair defect in BRCA mutant cells as a therapeutic strategy. Nature *434*, 917–921.

Fedier, A., Schlamminger, M., Schwarz, V.A., Haller, U., Howell, S.B., and Fink, D. (2003). Loss of atm sensitises p53-deficient cells to topoisomerase poisons and antimetabolites. Ann. Oncol. *14*, 938–945.

Feig, C., Jones, J.O., Kraman, M., Wells, R.J.B., Deonarine, A., Chan, D.S., Connell, C.M., Roberts, E.W., Zhao, Q., Caballero, O.L., et al. (2013). Targeting CXCL12 from FAP-expressing carcinoma-associated fibroblasts synergizes with anti–PD-L1 immunotherapy in pancreatic cancer. Proc. Natl. Acad. Sci. *110*, 20212–20217.

Fisher, A.E.O., Hochegger, H., Takeda, S., and Caldecott, K.W. (2007). Poly(ADP-Ribose) Polymerase 1 Accelerates Single-Strand Break Repair in Concert with Poly(ADP-Ribose) Glycohydrolase. Mol. Cell. Biol. *27*, 5597–5605.

Flint, T.R., Janowitz, T., Connell, C.M., Roberts, E.W., Denton, A.E., Coll, A.P., Jodrell, D.I., and Fearon, D.T. (2016). Tumor-Induced IL-6 Reprograms Host Metabolism to Suppress Anti-tumor Immunity. Cell Metab. *24*, 672–684.

Fok, J.H.L., Ramos-Montoya, A., Vazquez-Chantada, M., Wijnhoven, P.W.G., Follia, V., James, N., Farrington, P.M., Karmokar, A., Willis, S.E., Cairns, J., et al. (2019). AZD7648 is a potent and selective DNA-PK inhibitor that enhances radiation, chemotherapy and olaparib activity. Nat. Commun. *10*, 1–15.

Fokas, E., Prevo, R., Pollard, J.R., Reaper, P.M., Charlton, P.A., Cornelissen, B., Vallis, K.A., Hammond, E.M., Olcina, M.M., Gillies McKenna, W., et al. (2012). Targeting ATR in vivo using the novel inhibitor VE-822 results in selective sensitization of pancreatic tumors to radiation. Cell Death Dis. *3*, e441.

Foote, K.M., Blades, K., Cronin, A., Fillery, S., Guichard, S.S., Hassall, L., Hickson, I., Jacq, X., Jewsbury, P.J., McGuire, T.M., et al. (2013). Discovery of 4-{4-[(3R)-3-Methylmorpholin-4-yl]-6-[1-(methylsulfonyl)cyclopropyl]pyrimidin-2-yl}-1H-indole (AZ20): a potent and selective inhibitor of ATR protein kinase with monotherapy in vivo antitumor activity. J. Med. Chem. *56*, 2125–2138.

Foote, K.M., Nissink, J.W.M., McGuire, T., Turner, P., Guichard, S., Yates, J.W.T., Lau, A., Blades, K., Heathcote, D., Odedra, R., et al. (2018). Discovery and Characterization of AZD6738, a Potent Inhibitor of Ataxia Telangiectasia Mutated and Rad3 Related (ATR) Kinase with Application as an Anticancer Agent. J. Med. Chem. *61*, 9889–9907.

Forbes, S.A., Beare, D., Boutselakis, H., Bamford, S., Bindal, N., Tate, J., Cole, C.G., Ward, S., Dawson, E., Ponting, L., et al. (2017). COSMIC: somatic cancer genetics at high-resolution. Nucleic Acids Res. *45*, D777–D783.

Frese, K.K., Neesse, A., Cook, N., Bapiro, T.E., Lolkema, M.P., Jodrell, D.I., and Tuveson, D.A. (2012). nab-Paclitaxel potentiates gemcitabine activity by reducing cytidine deaminase levels in a mouse model of pancreatic cancer. Cancer Discov. *2*, 260–269.

Gatei, M., Jakob, B., Chen, P., Kijas, A.W., Becherel, O.J., Gueven, N., Birrell, G., Lee, J.-H., Paull, T.T., Lerenthal, Y., et al. (2011). ATM protein-dependent phosphorylation of Rad50 protein regulates DNA repair and cell cycle control. J. Biol. Chem. *286*, 31542–31556.

Gibson, B.A., and Kraus, W.L. (2012). New insights into the molecular and cellular functions of poly(ADP-ribose) and PARPs. Nat. Rev. Mol. Cell Biol. *13*, 411–424.

Gilad, O., Nabet, B.Y., Ragland, R.L., Schoppy, D.W., Smith, K.D., Durham, A.C., and Brown, E.J. (2010). Combining ATR suppression with oncogenic Ras synergistically increases genomic instability, causing synthetic lethality or tumorigenesis in a dosage-dependent manner. Cancer Res. *70*, 9693–9702.

Golan, T., Hammel, P., Reni, M., Van Cutsem, E., Macarulla, T., Hall, M.J., Park, J.-O., Hochhauser, D., Arnold, D., Oh, D.-Y., et al. (2019). Maintenance Olaparib for Germline BRCA-Mutated Metastatic Pancreatic Cancer. N. Engl. J. Med. *381*, 317–327.

Goldberg, F.W., Finlay, M.R.V., Ting, A.K.T., Beattie, D., Lamont, G.M., Fallan, C., Wrigley, G.L., Schimpl, M., Howard, M.R., Williamson, B., et al. (2019). The Discovery of 7-Methyl-2-[(7-methyl[1,2,4]triazolo[1,5-a]pyridin-6-yl)amino]-9-(tetrahydro-2H-pyran-4-yl)-7,9-dihydro-8H-purin-8-one (AZD7648), a Potent and Selective DNA-Dependent Protein Kinase (DNA-PK) Inhibitor. J. Med. Chem.

Goodarzi, A.A., Noon, A.T., Deckbar, D., Ziv, Y., Shiloh, Y., Löbrich, M., and Jeggo, P.A. (2008). ATM signaling facilitates repair of DNA double-strand breaks associated with heterochromatin. Mol. Cell *31*, 167–177.

Gopinathan, A., Morton, J.P., Jodrell, D.I., and Sansom, O.J. (2015). GEMMs as preclinical models for testing pancreatic cancer therapies. Dis. Model. Mech. *8*, 1185–1200.

Gorgoulis, V.G., Vassiliou, L.-V.F., Karakaidos, P., Zacharatos, P., Kotsinas, A., Liloglou, T., Venere, M., DiTullio, R.A., Kastrinakis, N.G., Levy, B., et al. (2005). Activation of the DNA damage checkpoint and genomic instability in human precancerous lesions. Nature *434*, 907–913.

Graham, J., Muhsin, M., and Kirkpatrick, P. (2004). Oxaliplatin. Nat. Rev. Drug Discov. *3*, 11–12.

Griffin, J.F., Poruk, K.E., and Wolfgang, C.L. (2015). Pancreatic cancer surgery: past, present, and future. Chin. J. Cancer Res. Chung-Kuo Yen Cheng Yen Chiu *27*, 332–348.

Griffin, R.J., Pemberton, L.C., Rhodes, D., Bleasdale, C., Bowman, K., Calvert, A.H., Curtin, N.J., Durkacz, B.W., Newell, D.R., and Porteous, J.K. (1995). Novel potent inhibitors of the DNA repair enzyme poly(ADP-ribose)polymerase (PARP). Anticancer. Drug Des. *10*, 507–514.

Grignani, G., Merlini, A., Sangiolo, D., D'Ambrosio, L., and Pignochino, Y. (2020). Delving into PARP inhibition from bench to bedside and back. Pharmacol. Ther. *206*, 107446.

Gullo, L., Tomassetti, P., Migliori, M., Casadei, R., and Marrano, D. (2001). Do early symptoms of pancreatic cancer exist that can allow an earlier diagnosis? Pancreas *22*, 210–213.

Guo, Z., Kumagai, A., Wang, S.X., and Dunphy, W.G. (2000). Requirement for Atr in phosphorylation of Chk1 and cell cycle regulation in response to DNA replication blocks and UV-damaged DNA in Xenopus egg extracts. Genes Dev. *14*, 2745–2756.

Hagmann, W., Jesnowski, R., and Löhr, J.M. (2010). Interdependence of gemcitabine treatment, transporter expression, and resistance in human pancreatic carcinoma cells. Neoplasia N. Y. N *12*, 740–747.

Hanahan, D., and Weinberg, R.A. (2011). Hallmarks of Cancer: The Next Generation. Cell *144*, 646–674.

Härtlova, A., Erttmann, S.F., Raffi, F.A., Schmalz, A.M., Resch, U., Anugula, S., Lienenklaus, S., Nilsson, L.M., Kröger, A., Nilsson, J.A., et al. (2015). DNA damage primes the type I interferon system via the cytosolic DNA sensor STING to promote anti-microbial innate immunity. Immunity *42*, 332–343.

Helleday, T. (2011). The underlying mechanism for the PARP and BRCA synthetic lethality: Clearing up the misunderstandings. Mol. Oncol. *5*, 387–393.

Herrero, A.B., San Miguel, J., and Gutierrez, N.C. (2015). Deregulation of DNA double-strand break repair in multiple myeloma: implications for genome stability. PloS One *10*, e0121581.

Hickson, I., Pike, K.G., and Durant, S.T. (2018). Targeting ATM for Cancer Therapy: Prospects for Drugging ATM. In Targeting the DNA Damage Response for Anti-Cancer Therapy, J. Pollard, and N. Curtin, eds. (Cham: Springer International Publishing), pp. 185–208.

Hingorani, S.R., Wang, L., Multani, A.S., Combs, C., Deramaudt, T.B., Hruban, R.H., Rustgi, A.K., Chang, S., and Tuveson, D.A. (2005). Trp53R172H and KrasG12D cooperate to promote chromosomal instability and widely metastatic pancreatic ductal adenocarcinoma in mice. Cancer Cell *7*, 469–483.

Hocke, S., Guo, Y., Job, A., Orth, M., Ziesch, A., Lauber, K., De Toni, E.N., Gress, T.M., Herbst, A., Göke, B., et al. (2016). A synthetic lethal screen identifies ATR-inhibition as a novel therapeutic approach for POLD1-deficient cancers. Oncotarget *7*, 7080–7095.

Hollstein, M., Sidransky, D., Vogelstein, B., and Harris, C.C. (1991). p53 mutations in human cancers. Science *253*, 49–53.

Hosoi, Y., Watanabe, T., Nakagawa, K., Matsumoto, Y., Enomoto, A., Morita, A., Nagawa, H., and Suzuki, N. (2004). Up-regulation of DNA-dependent protein kinase activity and Sp1 in colorectal cancer. Int. J. Oncol. *25*, 461–468.

Hruban, R.H., Goggins, M., Parsons, J., and Kern, S.E. (2000). Progression Model for Pancreatic Cancer. Clin. Cancer Res. *6*, 2969–2972.

Huang, P., Chubb, S., Hertel, L.W., Grindey, G.B., and Plunkett, W. (1991). Action of 2',2'-difluorodeoxycytidine on DNA synthesis. Cancer Res. *51*, 6110–6117.

Huehls, A.M., Wagner, J.M., Huntoon, C.J., and Karnitz, L.M. (2012). Identification of DNA repair pathways that affect the survival of ovarian cancer cells treated with a poly(ADP-ribose) polymerase inhibitor in a novel drug combination. Mol. Pharmacol. *82*, 767–776.

Huntoon, C.J., Flatten, K.S., Wahner Hendrickson, A.E., Huehls, A.M., Sutor, S.L., Kaufmann, S.H., and Karnitz, L.M. (2013). ATR inhibition broadly sensitizes ovarian cancer cells to chemotherapy independent of BRCA status. Cancer Res. *73*, 3683–3691.

Hustedt, N., Álvarez-Quilón, A., McEwan, A., Yuan, J.Y., Cho, T., Koob, L., Hart, T., and Durocher, D. (2019). A consensus set of genetic vulnerabilities to ATR inhibition. Open Biol. *9*, 190156.

Jackson, S.P., and Bartek, J. (2009). The DNA-damage response in human biology and disease. Nature *461*, 1071–1078.

Jacobetz, M.A., Chan, D.S., Neesse, A., Bapiro, T.E., Cook, N., Frese, K.K., Feig, C., Nakagawa, T., Caldwell, M.E., Zecchini, H.I., et al. (2013). Hyaluronan impairs vascular function and drug delivery in a mouse model of pancreatic cancer. Gut *62*, 112–120.

Jazayeri, A., Falck, J., Lukas, C., Bartek, J., Smith, G.C.M., Lukas, J., and Jackson, S.P. (2006). ATM- and cell cycle-dependent regulation of ATR in response to DNA double-strand breaks. Nat. Cell Biol. *8*, 37–45.

Jeggo, P.A., and Downs, J.A. (2014). Roles of chromatin remodellers in DNA double strand break repair. Exp. Cell Res. *329*, 69–77.

Jiang, H., Reinhardt, H.C., Bartkova, J., Tommiska, J., Blomqvist, C., Nevanlinna, H., Bartek, J., Yaffe, M.B., and Hemann, M.T. (2009). The combined status of ATM and p53 link tumor development with therapeutic response. Genes Dev. *23*, 1895–1909.

Jin, J., Fang, H., Yang, F., Ji, W., Guan, N., Sun, Z., Shi, Y., Zhou, G., and Guan, X. (2018). Combined Inhibition of ATR and WEE1 as a Novel Therapeutic Strategy in Triple-Negative Breast Cancer. Neoplasia N. Y. N *20*, 478–488.

Job, A., Schmitt, L.-M., von Wenserski, L., Lankat-Buttgereit, B., Gress, T.M., Buchholz, M., and Gallmeier, E. (2018). Inactivation of PRIM1 Function Sensitizes Cancer Cells to ATR and CHK1 Inhibitors. Neoplasia N. Y. N *20*, 1135–1143.

Jones, G.N., Rooney, C., Griffin, N., Roudier, M., Young, L.A., Garcia-Trinidad, A., Hughes, G.D., Whiteaker, J.R., Wilson, Z., Odedra, R., et al. (2018). pRAD50: a novel and clinically applicable pharmacodynamic biomarker of both ATM and ATR inhibition identified using mass spectrometry and immunohistochemistry. Br. J. Cancer 1.

Jossé, R., Martin, S.E., Guha, R., Ormanoglu, P., Pfister, T.D., Reaper, P.M., Barnes, C.S., Jones, J., Charlton, P., Pollard, J.R., et al. (2014). ATR inhibitors VE-821 and VX-970 sensitize cancer cells to topoisomerase i inhibitors by disabling DNA replication initiation and fork elongation responses. Cancer Res. *74*, 6968–6979.

Kalser, M.H., Barkin, J., and Macintyre, J.M. (1985). Pancreatic cancer. Assessment of prognosis by clinical presentation. Cancer *56*, 397–402.

Kamphues, C., Bova, R., Bahra, M., Klauschen, F., Muckenhuber, A., Sinn, B.V., Warth, A., Goeppert, B., Endris, V., Neuhaus, P., et al. (2015). Ataxia-telangiectasia-mutated protein kinase levels stratify patients with pancreatic adenocarcinoma into prognostic subgroups with loss being a strong indicator of poor survival. Pancreas *44*, 296–301.

Kanda, M., Matthaei, H., Wu, J., Hong, S.-M., Yu, J., Borges, M., Hruban, R.H., Maitra, A., Kinzler, K., Vogelstein, B., et al. (2012). Presence of somatic mutations in most early-stage pancreatic intraepithelial neoplasia. Gastroenterology *142*, 730-733.e9.

Karamitopoulou, E. (2019). Tumour microenvironment of pancreatic cancer: immune landscape is dictated by molecular and histopathological features. Br. J. Cancer *121*, 5–14.

Kastan, M.B., Zhan, Q., el-Deiry, W.S., Carrier, F., Jacks, T., Walsh, W.V., Plunkett, B.S., Vogelstein, B., and Fornace, A.J. (1992). A mammalian cell cycle checkpoint pathway utilizing p53 and GADD45 is defective in ataxia-telangiectasia. Cell *71*, 587–597.

Kern, S.E., Pietenpol, J.A., Thiagalingam, S., Seymour, A., Kinzler, K.W., and Vogelstein, B. (1992). Oncogenic forms of p53 inhibit p53-regulated gene expression. Science *256*, 827–830.

Kim, H., Saka, B., Knight, S., Borges, M., Childs, E., Klein, A., Wolfgang, C., Herman, J., Adsay, V.N., Hruban, R.H., et al. (2014). Having pancreatic cancer with tumoral loss of ATM and normal TP53 protein expression is associated with a poorer prognosis. Clin. Cancer Res. Off. J. Am. Assoc. Cancer Res. *20*, 1865–1872.

Kirshner, M., Rathavs, M., Nizan, A., Essers, J., Kanaar, R., Shiloh, Y., and Barzilai, A. (2009). Analysis of the relationships between ATM and the Rad54 paralogs involved in homologous recombination repair. DNA Repair *8*, 253–261.

Köcher, S., Rieckmann, T., Rohaly, G., Mansour, W.Y., Dikomey, E., Dornreiter, I., and Dahm-Daphi, J. (2012). Radiation-induced double-strand breaks require ATM but not Artemis for homologous recombination during S-phase. Nucleic Acids Res. *40*, 8336–8347.

König, J., Hartel, M., Nies, A.T., Martignoni, M.E., Guo, J., Büchler, M.W., Friess, H., and Keppler, D. (2005). Expression and localization of human multidrug resistance protein (ABCC) family members in pancreatic carcinoma. Int. J. Cancer *115*, 359–367.

Konstantinopoulos, P.A., Cheng, S.-C., Wahner Hendrickson, A.E., Penson, R.T., Schumer, S.T., Doyle, L.A., Lee, E.K., Kohn, E.C., Duska, L.R., Crispens, M.A., et al. (2020). Berzosertib plus gemcitabine versus gemcitabine alone in platinum-resistant high-grade serous ovarian cancer: a multicentre, open-label, randomised, phase 2 trial. Lancet Oncol.

Koorstra, J.-B.M., Hong, S.-M., Shi, C., Meeker, A.K., Ryu, J.K., Offerhaus, G.J.A., Goggins, M.G., Hruban, R.H., and Maitra, A. (2009). Widespread activation of the DNA damage response in human pancreatic intraepithelial neoplasia. Mod. Pathol. Off. J. U. S. Can. Acad. Pathol. Inc *22*, 1439–1445.

Krajewska, M., Fehrmann, R.S.N., Schoonen, P.M., Labib, S., de Vries, E.G.E., Franke, L., and van Vugt, M.A.T.M. (2015). ATR inhibition preferentially targets homologous recombination-deficient tumor cells. Oncogene *34*, 3474–3481.

Krebs, M.G., Lopez, J., El-Khoueiry, A., Bang, Y.-J., Postel-Vinay, S., Abida, W., Carter, L., Xu, W., Im, S.-A., Pierce, A., et al. (2018). Abstract CT026: Phase I study of AZD6738, an inhibitor of ataxia telangiectasia Rad3-related (ATR), in combination with olaparib or durvalumab in patients (pts) with advanced solid cancers. Cancer Res. *78*, CT026–CT026.

Krejci, L., Altmannova, V., Spirek, M., and Zhao, X. (2012). Homologous recombination and its regulation. Nucleic Acids Res. *40*, 5795–5818.

Kumagai, A., Lee, J., Yoo, H.Y., and Dunphy, W.G. (2006). TopBP1 activates the ATR-ATRIP complex. Cell *124*, 943–955.

Kurimasa, A., Kumano, S., Boubnov, N.V., Story, M.D., Tung, C.S., Peterson, S.R., and Chen, D.J. (1999). Requirement for the kinase activity of human DNA-dependent protein kinase catalytic subunit in DNA strand break rejoining. Mol. Cell. Biol. *19*, 3877–3884.

Kwok, M., Davies, N., Agathanggelou, A., Smith, E., Oldreive, C., Petermann, E., Stewart, G., Brown, J., Lau, A., Pratt, G., et al. (2016). ATR inhibition induces synthetic lethality and overcomes

chemoresistance in TP53- or ATM-defective chronic lymphocytic leukemia cells. Blood *127*, 582–595.

Lavin, M.F., and Shiloh, Y. (1996). Ataxia-telangiectasia: a multifaceted genetic disorder associated with defective signal transduction. Curr. Opin. Immunol. *8*, 459–464.

Ledermann, J., Harter, P., Gourley, C., Friedlander, M., Vergote, I., Rustin, G., Scott, C.L., Meier, W., Shapira-Frommer, R., Safra, T., et al. (2014). Olaparib maintenance therapy in patients with platinum-sensitive relapsed serous ovarian cancer: a preplanned retrospective analysis of outcomes by BRCA status in a randomised phase 2 trial. Lancet Oncol. *15*, 852–861.

Lee, J.-H., and Paull, T.T. (2005). ATM activation by DNA double-strand breaks through the Mre11-Rad50-Nbs1 complex. Science *308*, 551–554.

Lee, H.S., Yang, H.-K., Kim, W.H., and Choe, G. (2005). Loss of DNA-dependent protein kinase catalytic subunit (DNA-PKcs) expression in gastric cancers. Cancer Res. Treat. Off. J. Korean Cancer Assoc. *37*, 98–102.

Li, J., and Stern, D.F. (2005). Regulation of CHK2 by DNA-dependent Protein Kinase. J. Biol. Chem. *280*, 12041–12050.

Lim, D.S., Kim, S.T., Xu, B., Maser, R.S., Lin, J., Petrini, J.H., and Kastan, M.B. (2000). ATM phosphorylates p95/nbs1 in an S-phase checkpoint pathway. Nature *404*, 613–617.

Lin, Y.-F., Shih, H.-Y., Shang, Z., Matsunaga, S., and Chen, B.P. (2014). DNA-PKcs is required to maintain stability of Chk1 and Claspin for optimal replication stress response. Nucleic Acids Res. *42*, 4463–4473.

Liu, J., Wang, X., Ren, Y., Li, X., Zhang, X., and Zhou, B. (2014). Effect of single nucleotide polymorphism Rs189037 in ATM gene on risk of lung cancer in Chinese: a case-control study. PloS One *9*, e115845.

Liu, J., Lichtenberg, T., Hoadley, K.A., Poisson, L.M., Lazar, A.J., Cherniack, A.D., Kovatich, A.J., Benz, C.C., Levine, D.A., Lee, A.V., et al. (2018). An Integrated TCGA Pan-Cancer Clinical Data Resource to Drive High-Quality Survival Outcome Analytics. Cell *173*, 400-416.e11.

Liu, Q., Guntuku, S., Cui, X.S., Matsuoka, S., Cortez, D., Tamai, K., Luo, G., Carattini-Rivera, S., DeMayo, F., Bradley, A., et al. (2000). Chk1 is an essential kinase that is regulated by Atr and required for the G(2)/M DNA damage checkpoint. Genes Dev. *14*, 1448–1459.

Lloyd, R.L., Wijnhoven, P.W.G., Ramos-Montoya, A., Wilson, Z., Illuzzi, G., Falenta, K., Jones, G.N., James, N., Chabbert, C.D., Stott, J., et al. (2020). Combined PARP and ATR inhibition potentiates genome instability and cell death in ATM-deficient cancer cells. Oncogene 1–15.

Longley, D.B., Harkin, D.P., and Johnston, P.G. (2003). 5-Fluorouracil: mechanisms of action and clinical strategies. Nat. Rev. Cancer *3*, 330–338.

López-Contreras, A.J., Gutierrez-Martinez, P., Specks, J., Rodrigo-Perez, S., and Fernandez-Capetillo, O. (2012). An extra allele of Chk1 limits oncogene-induced replicative stress and promotes transformation. J. Exp. Med. *209*, 455–461.

Maitra, A., Adsay, N.V., Argani, P., Iacobuzio-Donahue, C., De Marzo, A., Cameron, J.L., Yeo, C.J., and Hruban, R.H. (2003). Multicomponent analysis of the pancreatic adenocarcinoma progression model using a pancreatic intraepithelial neoplasia tissue microarray. Mod. Pathol. Off. J. U. S. Can. Acad. Pathol. Inc *16*, 902–912.

Majka, J., Binz, S.K., Wold, M.S., and Burgers, P.M.J. (2006). Replication Protein A Directs Loading of the DNA Damage Checkpoint Clamp to 5′-DNA Junctions. J. Biol. Chem. *281*, 27855–27861.

Malyuchenko, N.V., Kotova, E.Yu., Kulaeva, O.I., Kirpichnikov, M.P., and Studitskiy, V.M. (2015). PARP1 Inhibitors: antitumor drug design. Acta Naturae *7*, 27–37.

Marais, R., Light, Y., Paterson, H.F., and Marshall, C.J. (1995). Ras recruits Raf-1 to the plasma membrane for activation by tyrosine phosphorylation. EMBO J. *14*, 3136–3145.

McGuigan, A., Kelly, P., Turkington, R.C., Jones, C., Coleman, H.G., and McCain, R.S. (2018). Pancreatic cancer: A review of clinical diagnosis, epidemiology, treatment and outcomes. World J. Gastroenterol. *24*, 4846–4861.

McMillin, D.W., Negri, J.M., and Mitsiades, C.S. (2013). The role of tumour–stromal interactions in modifying drug response: challenges and opportunities. Nat. Rev. Drug Discov. *12*, 217–228.

Mego, M., Cierna, Z., Svetlovska, D., Macak, D., Machalekova, K., Miskovska, V., Chovanec, M., Usakova, V., Obertova, J., Babal, P., et al. (2013). PARP expression in germ cell tumours. J. Clin. Pathol. *66*, 607–612.

Mehdipour, P., Karami, F., Javan, F., and Mehrazin, M. (2015). Linking ATM Promoter Methylation to Cell Cycle Protein Expression in Brain Tumor Patients: Cellular Molecular Triangle Correlation in ATM Territory. Mol. Neurobiol. *52*, 293–302.

Miller, R.M., Nworu, C., McKee, L., Balcerzak, D., Pham, L., Pugh, J., Liu, Y.-Z., Gustafson, H., Marwah, E., Lamb, T., et al. (2019). Development of an Immunohistochemical Assay to Detect the Ataxia-Telangiectasia Mutated (ATM) Protein in Gastric Carcinoma. Appl. Immunohistochem. Mol. Morphol. AIMM.

Min, A., Im, S.-A., Jang, H., Kim, S., Lee, M., Kim, D.K., Yang, Y., Kim, H.-J., Lee, K.-H., Kim, J.W., et al. (2017). AZD6738, A Novel Oral Inhibitor of ATR, Induces Synthetic Lethality with ATM Deficiency in Gastric Cancer Cells. Mol. Cancer Ther. *16*, 566–577.

Mini, E., Nobili, S., Caciagli, B., Landini, I., and Mazzei, T. (2006). Cellular pharmacology of gemcitabine. Ann. Oncol. Off. J. Eur. Soc. Med. Oncol. ESMO *17 Suppl 5*, v7-12.

Mohni, K.N., Kavanaugh, G.M., and Cortez, D. (2014). ATR pathway inhibition is synthetically lethal in cancer cells with ERCC1 deficiency. Cancer Res. *74*, 2835–2845.

Mohni, K.N., Thompson, P.S., Luzwick, J.W., Glick, G.G., Pendleton, C.S., Lehmann, B.D., Pietenpol, J.A., and Cortez, D. (2015). A Synthetic Lethal Screen Identifies DNA Repair Pathways that Sensitize Cancer Cells to Combined ATR Inhibition and Cisplatin Treatments. PLOS ONE *10*, e0125482.

Mokrani-Benhelli, H., Gaillard, L., Biasutto, P., Le Guen, T., Touzot, F., Vasquez, N., Komatsu, J., Conseiller, E., Pïcard, C., Gluckman, E., et al. (2013). Primary microcephaly, impaired DNA replication, and genomic instability caused by compound heterozygous ATR mutations. Hum. Mutat. *34*, 374–384.

Mondal, G., Stevers, M., Goode, B., Ashworth, A., and Solomon, D.A. (2019). A requirement for STAG2 in replication fork progression creates a targetable synthetic lethality in cohesin-mutant cancers. Nat. Commun. *10*, 1686.

Montano, R., Khan, N., Hou, H., Seigne, J., Ernstoff, M.S., Lewis, L.D., and Eastman, A. (2017). Cell cycle perturbation induced by gemcitabine in human tumor cells in cell culture, xenografts and

bladder cancer patients: implications for clinical trial designs combining gemcitabine with a Chk1 inhibitor. Oncotarget *8*, 67754–67768.

Moore, K., Colombo, N., Scambia, G., Kim, B.-G., Oaknin, A., Friedlander, M., Lisyanskaya, A., Floquet, A., Leary, A., Sonke, G.S., et al. (2018). Maintenance Olaparib in Patients with Newly Diagnosed Advanced Ovarian Cancer. N. Engl. J. Med. *379*, 2495–2505.

Mordes, D.A., Glick, G.G., Zhao, R., and Cortez, D. (2008). TopBP1 activates ATR through ATRIP and a PIKK regulatory domain. Genes Dev. *22*, 1478–1489.

Morrell, D., Cromartie, E., and Swift, M. (1986). Mortality and Cancer Incidence in 263 Patients with Ataxia-Telangiectasia. J. Natl. Cancer Inst. *77*, 89–92.

Murai, J., and Pommier, Y. (2015). Classification of PARP Inhibitors Based on PARP Trapping and Catalytic Inhibition, and Rationale for Combinations with Topoisomerase I Inhibitors and Alkylating Agents. In PARP Inhibitors for Cancer Therapy, N.J. Curtin, and R.A. Sharma, eds. (Cham: Springer International Publishing), pp. 261–274.

Murai, J., Huang, S.N., Das, B.B., Renaud, A., Zhang, Y., Doroshow, J.H., Ji, J., Takeda, S., and Pommier, Y. (2012). Trapping of PARP1 and PARP2 by Clinical PARP Inhibitors. Cancer Res. *72*, 5588–5599.

Murai, J., Feng, Y., Yu, G.K., Ru, Y., Tang, S.-W., Shen, Y., and Pommier, Y. (2016). Resistance to PARP inhibitors by SLFN11 inactivation can be overcome by ATR inhibition. Oncotarget *7*, 76534–76550.

de Murcia, J.M., Niedergang, C., Trucco, C., Ricoul, M., Dutrillaux, B., Mark, M., Oliver, F.J., Masson, M., Dierich, A., LeMeur, M., et al. (1997). Requirement of poly(ADP-ribose) polymerase in recovery from DNA damage in mice and in cells. Proc. Natl. Acad. Sci. U. S. A. *94*, 7303–7307.

Murga, M., Campaner, S., Lopez-Contreras, A.J., Toledo, L.I., Soria, R., Montaña, M.F., Artista, L.D., Schleker, T., Guerra, C., Garcia, E., et al. (2011). Exploiting oncogene-induced replicative stress for the selective killing of Myc-driven tumors. Nat. Struct. Mol. Biol. *18*, 1331–1335.

Mutreja, K., Krietsch, J., Hess, J., Ursich, S., Berti, M., Roessler, F.K., Zellweger, R., Patra, M., Gasser, G., and Lopes, M. (2018). ATR-Mediated Global Fork Slowing and Reversal Assist Fork Traverse and Prevent Chromosomal Breakage at DNA Interstrand Cross-Links. Cell Rep. *24*, 2629-2642.e5.

Nambaru, P.K., Hübner, T., Köck, K., Mews, S., Grube, M., Payen, L., Guitton, J., Sendler, M., Jedlitschky, G., Rimmbach, C., et al. (2011). Drug efflux transporter multidrug resistance-associated protein 5 affects sensitivity of pancreatic cancer cell lines to the nucleoside anticancer drug 5-fluorouracil. Drug Metab. Dispos. Biol. Fate Chem. *39*, 132–139.

Navrkalova, V., Sebejova, L., Zemanova, J., Kminkova, J., Kubesova, B., Malcikova, J., Mraz, M., Smardova, J., Pavlova, S., Doubek, M., et al. (2013). ATM mutations uniformly lead to ATM dysfunction in chronic lymphocytic leukemia: application of functional test using doxorubicin. Haematologica *98*, 1124–1131.

Neal, J.A., and Meek, K. (2011). Choosing the right path: does DNA-PK help make the decision? Mutat. Res. *711*, 73–86.

Negrini, S., Gorgoulis, V.G., and Halazonetis, T.D. (2010). Genomic instability--an evolving hallmark of cancer. Nat. Rev. Mol. Cell Biol. *11*, 220–228.

Nishida, H., Tatewaki, N., Nakajima, Y., Magara, T., Ko, K.M., Hamamori, Y., and Konishi, T. (2009). Inhibition of ATR protein kinase activity by schisandrin B in DNA damage response. Nucleic Acids Res. *37*, 5678–5689.

Nosho, K., Yamamoto, H., Mikami, M., Taniguchi, H., Takahashi, T., Adachi, Y., Imamura, A., Imai, K., and Shinomura, Y. (2006). Overexpression of poly(ADP-ribose) polymerase-1 (PARP-1) in the early stage of colorectal carcinogenesis. Eur. J. Cancer Oxf. Engl. 1990 *42*, 2374–2381.

O'Carrigan, B., de Miguel Luken, M.J., Papadatos-Pastos, D., Brown, J., Tunariu, N., Perez Lopez, R., Ganegoda, M., Riisnaes, R., Figueiredo, I., Carreira, S., et al. (2016). Phase I trial of a first-in-class ATR inhibitor VX-970 as monotherapy (mono) or in combination (combo) with carboplatin (CP) incorporating pharmacodynamics (PD) studies. J. Clin. Oncol. *34*, 2504–2504.

O'Driscoll, M., and Jeggo, P.A. (2003). Clinical impact of ATR checkpoint signalling failure in humans. Cell Cycle Georget. Tex *2*, 194–195.

Olive, K.P., Jacobetz, M.A., Davidson, C.J., Gopinathan, A., McIntyre, D., Honess, D., Madhu, B., Goldgraben, M.A., Caldwell, M.E., Allard, D., et al. (2009). Inhibition of Hedgehog Signaling Enhances Delivery of Chemotherapy in a Mouse Model of Pancreatic Cancer. Science *324*, 1457–1461.

Osterman, M., Kathawa, D., Liu, D., Guo, H., Zhang, C., Li, M., Yu, X., and Li, F. (2014). Elevated DNA damage response in pancreatic cancer. Histochem. Cell Biol. *142*, 713–720.

Oza, A.M., Cibula, D., Benzaquen, A.O., Poole, C., Mathijssen, R.H.J., Sonke, G.S., Colombo, N., Špaček, J., Vuylsteke, P., Hirte, H., et al. (2015). Olaparib combined with chemotherapy for recurrent platinum-sensitive ovarian cancer: a randomised phase 2 trial. Lancet Oncol. *16*, 87–97.

Pabla, N., Huang, S., Mi, Q.-S., Daniel, R., and Dong, Z. (2008). ATR-Chk2 signaling in p53 activation and DNA damage response during cisplatin-induced apoptosis. J. Biol. Chem. *283*, 6572–6583.

Pacek, M., and Walter, J.C. (2004). A requirement for MCM7 and Cdc45 in chromosome unwinding during eukaryotic DNA replication. EMBO J. *23*, 3667–3676.

Parrilla-Castellar, E.R., Arlander, S.J.H., and Karnitz, L. (2004). Dial 9-1-1 for DNA damage: the Rad9-Hus1-Rad1 (9-1-1) clamp complex. DNA Repair *3*, 1009–1014.

Peasland, A., Wang, L.-Z., Rowling, E., Kyle, S., Chen, T., Hopkins, A., Cliby, W.A., Sarkaria, J., Beale, G., Edmondson, R.J., et al. (2011). Identification and evaluation of a potent novel ATR inhibitor, NU6027, in breast and ovarian cancer cell lines. Br. J. Cancer *105*, 372–381.

Perkhofer, L., Schmitt, A., Romero Carrasco, M.C., Ihle, M., Hampp, S., Ruess, D.A., Hessmann, E., Russell, R., Lechel, A., Azoitei, N., et al. (2017). ATM Deficiency Generating Genomic Instability Sensitizes Pancreatic Ductal Adenocarcinoma Cells to Therapy-Induced DNA Damage. Cancer Res. *77*, 5576–5590.

Petermann, E., Maya-Mendoza, A., Zachos, G., Gillespie, D.A.F., Jackson, D.A., and Caldecott, K.W. (2006). Chk1 requirement for high global rates of replication fork progression during normal vertebrate S phase. Mol. Cell. Biol. *26*, 3319–3326.

Petermann, E., Woodcock, M., and Helleday, T. (2010). Chk1 promotes replication fork progression by controlling replication initiation. Proc. Natl. Acad. Sci. U. S. A. *107*, 16090–16095.

Pettitt, S.J., Krastev, D.B., Brandsma, I., Dréan, A., Song, F., Aleksandrov, R., Harrell, M.I., Menon, M., Brough, R., Campbell, J., et al. (2018). Genome-wide and high-density CRISPR-Cas9 screens identify point mutations in PARP1 causing PARP inhibitor resistance. Nat. Commun. *9*, 1–14.

Pichierri, P., Rosselli, F., and Franchitto, A. (2003). Werner's syndrome protein is phosphorylated in an ATR/ATM-dependent manner following replication arrest and DNA damage induced during the S phase of the cell cycle. Oncogene *22*, 1491–1500.

Pike, K.G., Barlaam, B., Cadogan, E., Campbell, A., Chen, Y., Colclough, N., Davies, N.L., de-Almeida, C., Degorce, S.L., Didelot, M., et al. (2018). The Identification of Potent, Selective, and Orally Available Inhibitors of Ataxia Telangiectasia Mutated (ATM) Kinase: The Discovery of AZD0156 (8-{6-[3-(Dimethylamino)propoxy]pyridin-3-yl}-3-methyl-1-(tetrahydro-2H- pyran-4-yl)-1,3-dihydro-2H-imidazo[4,5-c]quinolin-2-one). J. Med. Chem. *61*, 3823–3841.

Plunkett, W., Huang, P., Xu, Y.Z., Heinemann, V., Grunewald, R., and Gandhi, V. (1995). Gemcitabine: metabolism, mechanisms of action, and self-potentiation. Semin. Oncol. *22*, 3–10.

Pommier, Y., Leo, E., Zhang, H., and Marchand, C. (2010). DNA Topoisomerases and Their Poisoning by Anticancer and Antibacterial Drugs. Chem. Biol. *17*, 421–433.

Purnell, M.R., and Whish, W.J. (1980). Novel inhibitors of poly(ADP-ribose) synthetase. Biochem. J. *185*, 775–777.

Quigley, D.A., Dang, H.X., Zhao, S.G., Lloyd, P., Aggarwal, R., Alumkal, J.J., Foye, A., Kothari, V., Perry, M.D., Bailey, A.M., et al. (2018). Genomic Hallmarks and Structural Variation in Metastatic Prostate Cancer. Cell *174*, 758-769.e9.

Rafiei, S., Fitzpatrick, K., Liu, D., Cai, M.-Y., Elmarakeby, H.A., Park, J., Ricker, C., Kochupurakkal, B.S., Choudhury, A.D., Hahn, W.C., et al. (2020). ATM Loss Confers Greater Sensitivity to ATR Inhibition than PARP Inhibition in Prostate Cancer. Cancer Res.

Rahib, L., Smith, B.D., Aizenberg, R., Rosenzweig, A.B., Fleshman, J.M., and Matrisian, L.M. (2014). Projecting cancer incidence and deaths to 2030: the unexpected burden of thyroid, liver, and pancreas cancers in the United States. Cancer Res. *74*, 2913–2921.

Reaper, P.M., Griffiths, M.R., Long, J.M., Charrier, J.-D., Maccormick, S., Charlton, P.A., Golec, J.M.C., and Pollard, J.R. (2011). Selective killing of ATM- or p53-deficient cancer cells through inhibition of ATR. Nat. Chem. Biol. *7*, 428–430.

Reisländer, T., Lombardi, E.P., Groelly, F.J., Miar, A., Porru, M., Di Vito, S., Wright, B., Lockstone, H., Biroccio, A., Harris, A., et al. (2019). BRCA2 abrogation triggers innate immune responses potentiated by treatment with PARP inhibitors. Nat. Commun. *10*, 3143.

Riballo, E., Kühne, M., Rief, N., Doherty, A., Smith, G.C.M., Recio, M.-J., Reis, C., Dahm, K., Fricke, A., Krempler, A., et al. (2004). A Pathway of Double-Strand Break Rejoining Dependent upon ATM, Artemis, and Proteins Locating to γ-H2AX Foci. Mol. Cell *16*, 715–724.

Riches, L.C., Trinidad, A.G., Hughes, G., Jones, G.N., Hughes, A.M., Thomason, A.G., Gavine, P., Cui, A., Ling, S., Stott, J., et al. (2019). Pharmacology of the ATM inhibitor AZD0156: potentiation of irradiation and olaparib responses pre-clinically. Mol. Cancer Ther. molcanther.1394.2018.

Richmond, A., and Su, Y. (2008). Mouse xenograft models vs GEM models for human cancer therapeutics. Dis. Model. Mech. *1*, 78–82.

Riesenberg, S., Chintalapati, M., Macak, D., Kanis, P., Maricic, T., and Pääbo, S. (2019). Simultaneous precise editing of multiple genes in human cells. Nucleic Acids Res. *47*, e116.

Roberts, C.W.M., and Orkin, S.H. (2004). The SWI/SNF complex--chromatin and cancer. Nat. Rev. Cancer *4*, 133–142.

Roberts, N.J., Jiao, Y., Yu, J., Kopelovich, L., Petersen, G.M., Bondy, M.L., Gallinger, S., Schwartz, A.G., Syngal, S., Cote, M.L., et al. (2012). ATM mutations in patients with hereditary pancreatic cancer. Cancer Discov. *2*, 41–46.

Robson, M., Im, S.-A., Senkus, E., Xu, B., Domchek, S.M., Masuda, N., Delaloge, S., Li, W., Tung, N., Armstrong, A., et al. (2017). Olaparib for Metastatic Breast Cancer in Patients with a Germline BRCA Mutation. N. Engl. J. Med. *377*, 523–533.

Rojo, F., García-Parra, J., Zazo, S., Tusquets, I., Ferrer-Lozano, J., Menendez, S., Eroles, P., Chamizo, C., Servitja, S., Ramírez-Merino, N., et al. (2012). Nuclear PARP-1 protein overexpression is associated with poor overall survival in early breast cancer. Ann. Oncol. Off. J. Eur. Soc. Med. Oncol. *23*, 1156–1164.

Roninson, I.B., Chin, J.E., Choi, K.G., Gros, P., Housman, D.E., Fojo, A., Shen, D.W., Gottesman, M.M., and Pastan, I. (1986). Isolation of human mdr DNA sequences amplified in multidrug-resistant KB carcinoma cells. Proc. Natl. Acad. Sci. *83*, 4538–4542.

Ruiz, S., Lopez-Contreras, A.J., Gabut, M., Marion, R.M., Gutierrez-Martinez, P., Bua, S., Ramirez, O., Olalde, I., Rodrigo-Perez, S., Li, H., et al. (2015). Limiting replication stress during somatic cell reprogramming reduces genomic instability in induced pluripotent stem cells. Nat. Commun. *6*, 8036.

Ruiz, S., Mayor-Ruiz, C., Lafarga, V., Murga, M., Vega-Sendino, M., Ortega, S., and Fernandez-Capetillo, O. (2016). A genomewide CRISPR screen identifies CDC25A as a determinant of sensitivity to ATR inhibitors. Mol. Cell *62*, 307–313.

Rundle, S., Bradbury, A., Drew, Y., and Curtin, N.J. (2017). Targeting the ATR-CHK1 Axis in Cancer Therapy. Cancers *9*, 41.

Ryan, C.J., Bajrami, I., and Lord, C.J. (2018). Synthetic Lethality and Cancer - Penetrance as the Major Barrier. Trends Cancer *4*, 671–683.

Saeki, H., Siaud, N., Christ, N., Wiegant, W.W., van Buul, P.P.W., Han, M., Zdzienicka, M.Z., Stark, J.M., and Jasin, M. (2006). Suppression of the DNA repair defects of BRCA2-deficient cells with heterologous protein fusions. Proc. Natl. Acad. Sci. U. S. A. *103*, 8768–8773.

Sanchez, Y., Wong, C., Thoma, R.S., Richman, R., Wu, Z., Piwnica-Worms, H., and Elledge, S.J. (1997). Conservation of the Chk1 Checkpoint Pathway in Mammals: Linkage of DNA Damage to Cdk Regulation Through Cdc25. Science *277*, 1497–1501.

Sanjiv, K., Hagenkort, A., Calderón-Montaño, J.M., Koolmeister, T., Reaper, P.M., Mortusewicz, O., Jacques, S.A., Kuiper, R.V., Schultz, N., Scobie, M., et al. (2015). Cancer-Specific Synthetic Lethality between ATR and CHK1 Kinase Activities. Cell Rep. *14*, 298–309.

Sarkaria, J.N., Busby, E.C., Tibbetts, R.S., Roos, P., Taya, Y., Karnitz, L.M., and Abraham, R.T. (1999). Inhibition of ATM and ATR kinase activities by the radiosensitizing agent, caffeine. Cancer Res. *59*, 4375–4382.

Sarmento, L.M., Póvoa, V., Nascimento, R., Real, G., Antunes, I., Martins, L.R., Moita, C., Alves, P.M., Abecasis, M., Moita, L.F., et al. (2015). CHK1 overexpression in T-cell acute lymphoblastic

leukemia is essential for proliferation and survival by preventing excessive replication stress. Oncogene *34*, 2978–2990.

Sartori, A.A., Lukas, C., Coates, J., Mistrik, M., Fu, S., Bartek, J., Baer, R., Lukas, J., and Jackson, S.P. (2007). Human CtIP promotes DNA end resection. Nature *450*, 509–514.

Satoh, M.S., and Lindahl, T. (1992). Role of poly(ADP-ribose) formation in DNA repair. Nature *356*, 356–358.

Schmitt, A., Knittel, G., Welcker, D., Yang, T.-P., George, J., Nowak, M., Leeser, U., Buettner, R., Perner, S., Peifer, M., et al. (2017). ATM Deficiency Is Associated with Sensitivity to PARP1-and ATR Inhibitors in Lung Adenocarcinoma. Cancer Res. *77*, 3040–3056.

Schoppy, D.W., Ragland, R.L., Gilad, O., Shastri, N., Peters, A.A., Murga, M., Fernandez-Capetillo, O., Diehl, J.A., and Brown, E.J. (2012). Oncogenic stress sensitizes murine cancers to hypomorphic suppression of ATR. J. Clin. Invest. *122*, 241–252.

Schutte, M., Hruban, R.H., Geradts, J., Maynard, R., Hilgers, W., Rabindran, S.K., Moskaluk, C.A., Hahn, S.A., Schwarte-Waldhoff, I., Schmiegel, W., et al. (1997). Abrogation of the Rb/p16 tumor-suppressive pathway in virtually all pancreatic carcinomas. Cancer Res. *57*, 3126–3130.

Sen, T., Rodriguez, B.L., Chen, L., Corte, C.D., Morikawa, N., Fujimoto, J., Cristea, S., Nguyen, T., Diao, L., Li, L., et al. (2019). Targeting DNA damage response promotes anti-tumor immunity through STING-mediated T-cell activation in small cell lung cancer. Cancer Discov. CD-18-1020.

Serrano, M.A., Li, Z., Dangeti, M., Musich, P.R., Patrick, S., Roginskaya, M., Cartwright, B., and Zou, Y. (2013). DNA-PK, ATM and ATR collaboratively regulate p53-RPA interaction to facilitate homologous recombination DNA repair. Oncogene *32*, 2452–2462.

Shechter, D., Costanzo, V., and Gautier, J. (2004). ATR and ATM regulate the timing of DNA replication origin firing. Nat. Cell Biol. *6*, 648–655.

Shen, J., Zhao, W., Ju, Z., Wang, L., Peng, Y., Labrie, M., Yap, T.A., Mills, G.B., and Peng, G. (2019). PARPi Triggers the STING-Dependent Immune Response and Enhances the Therapeutic Efficacy of Immune Checkpoint Blockade Independent of BRCAness. Cancer Res. *79*, 311–319.

Shen, L., Yin, Z.-H., Wan, Y., Zhang, Y., Li, K., and Zhou, B.-S. (2012). Association between ATM polymorphisms and cancer risk: a meta-analysis. Mol. Biol. Rep. *39*, 5719–5725.

Singhi, A.D., George, B., Greenbowe, J.R., Chung, J., Suh, J., Maitra, A., Klempner, S.J., Hendifar, A., Milind, J.M., Golan, T., et al. (2019). Real-Time Targeted Genome Profile Analysis of Pancreatic Ductal Adenocarcinomas Identifies Genetic Alterations That Might Be Targeted With Existing Drugs or Used as Biomarkers. Gastroenterology *156*, 2242-2253.e4.

Sørensen, C.S., Syljuåsen, R.G., Falck, J., Schroeder, T., Rönnstrand, L., Khanna, K.K., Zhou, B.-B., Bartek, J., and Lukas, J. (2003). Chk1 regulates the S phase checkpoint by coupling the physiological turnover and ionizing radiation-induced accelerated proteolysis of Cdc25A. Cancer Cell *3*, 247–258.

Staibano, S., Pepe, S., Lo Muzio, L., Somma, P., Mascolo, M., Argenziano, G., Scalvenzi, M., Salvatore, G., Fabbrocini, G., Molea, G., et al. (2005). Poly(adenosine diphosphate-ribose) polymerase 1 expression in malignant melanomas from photoexposed areas of the head and neck region. Hum. Pathol. *36*, 724–731.

Stokes, M.P., Rush, J., MacNeill, J., Ren, J.M., Sprott, K., Nardone, J., Yang, V., Beausoleil, S.A., Gygi, S.P., Livingstone, M., et al. (2007). Profiling of UV-induced ATM/ATR signaling pathways. Proc. Natl. Acad. Sci. *104*, 19855–19860.

Stracker, T.H., and Petrini, J.H.J. (2011). The MRE11 complex: starting from the ends. Nat. Rev. Mol. Cell Biol. *12*, 90–103.

Ström, C.E., Johansson, F., Uhlén, M., Szigyarto, C.A.-K., Erixon, K., and Helleday, T. (2011). Poly (ADP-ribose) polymerase (PARP) is not involved in base excision repair but PARP inhibition traps a single-strand intermediate. Nucleic Acids Res. *39*, 3166–3175.

Sultana, R., Abdel-Fatah, T., Perry, C., Moseley, P., Albarakti, N., Mohan, V., Seedhouse, C., Chan, S., and Madhusudan, S. (2013). Ataxia Telangiectasia Mutated and Rad3 Related (ATR) Protein Kinase Inhibition Is Synthetically Lethal in XRCC1 Deficient Ovarian Cancer Cells. PLoS ONE *8*.

Sun, L., Wu, J., Du, F., Chen, X., and Chen, Z.J. (2013). Cyclic GMP-AMP Synthase Is a Cytosolic DNA Sensor That Activates the Type I Interferon Pathway. Science *339*, 786–791.

Sun, Q., Guo, Y., Liu, X., Czauderna, F., Carr, M.I., Zenke, F.T., Blaukat, A., and Vassilev, L.T. (2019). Therapeutic Implications of p53 Status on Cancer Cell Fate Following Exposure to Ionizing Radiation and the DNA-PK Inhibitor M3814. Mol. Cancer Res. MCR *17*, 2457–2468.

Sundar, R., Miranda, S., Rodrigues, D.N., Chénard-Poirier, M., Dolling, D., Clarke, M., Figueiredo, I., Bertan, C., Yuan, W., Ferreira, A., et al. (2018). Ataxia Telangiectasia Mutated Protein Loss and Benefit From Oxaliplatin-based Chemotherapy in Colorectal Cancer. Clin. Colorectal Cancer *17*, 280–284.

Suto, M.J., Turner, W.R., Arundel-Suto, C.M., Werbel, L.M., and Sebolt-Leopold, J.S. (1991). Dihydroisoquinolinones: the design and synthesis of a new series of potent inhibitors of poly(ADP-ribose) polymerase. Anticancer. Drug Des. *6*, 107–117.

Swift, M., Morrell, D., Massey, R.B., and Chase, C.L. (1991). Incidence of cancer in 161 families affected by ataxia-telangiectasia. N. Engl. J. Med. *325*, 1831–1836.

Sy, S.M.H., Huen, M.S.Y., and Chen, J. (2009). PALB2 is an integral component of the BRCA complex required for homologous recombination repair. Proc. Natl. Acad. Sci. U. S. A. *106*, 7155–7160.

Syljuåsen, R.G., Sørensen, C.S., Hansen, L.T., Fugger, K., Lundin, C., Johansson, F., Helleday, T., Sehested, M., Lukas, J., and Bartek, J. (2005). Inhibition of human Chk1 causes increased initiation of DNA replication, phosphorylation of ATR targets, and DNA breakage. Mol. Cell. Biol. *25*, 3553–3562.

Takai, H., Tominaga, K., Motoyama, N., Minamishima, Y.A., Nagahama, H., Tsukiyama, T., Ikeda, K., Nakayama, K., Nakanishi, M., and Nakayama, K. (2000). Aberrant cell cycle checkpoint function and early embryonic death in Chk1(-/-) mice. Genes Dev. *14*, 1439–1447.

Thiebaut, F., Tsuruo, T., Hamada, H., Gottesman, M.M., Pastan, I., and Willingham, M.C. (1987). Cellular localization of the multidrug-resistance gene product P-glycoprotein in normal human tissues. Proc. Natl. Acad. Sci. *84*, 7735–7738.

Thomas, A., Redon, C.E., Sciuto, L., Padiernos, E., Ji, J., Lee, M.-J., Yuno, A., Lee, S., Zhang, Y., Tran, L., et al. (2017). Phase I Study of ATR Inhibitor M6620 in Combination With Topotecan in Patients With Advanced Solid Tumors. J. Clin. Oncol. *36*, 1594–1602.

Thomas, A., Vilimas, R., Trindade, C., Erwin-Cohen, R., Roper, N., Xi, L., Krishnasamy, V., Levy, E., Mammen, A., Nichols, S., et al. (2019). Durvalumab in Combination with Olaparib in Patients with Relapsed SCLC: Results from a Phase II Study. J. Thorac. Oncol. Off. Publ. Int. Assoc. Study Lung Cancer *14*, 1447–1457.

Thompson, D., Duedal, S., Kirner, J., McGuffog, L., Last, J., Reiman, A., Byrd, P., Taylor, M., and Easton, D.F. (2005). Cancer Risks and Mortality in Heterozygous ATM Mutation Carriers. JNCI J. Natl. Cancer Inst. *97*, 813–822.

Toledo, L., Neelsen, K.J., and Lukas, J. (2017). Replication Catastrophe: When a Checkpoint Fails because of Exhaustion. Mol. Cell *66*, 735–749.

Toledo, L.I., Murga, M., Zur, R., Soria, R., Rodriguez, A., Martinez, S., Oyarzabal, J., Pastor, J., Bischoff, J.R., and Fernandez-Capetillo, O. (2011). A cell-based screen identifies ATR inhibitors with synthetic lethal properties for cancer-associated mutations. Nat. Struct. Mol. Biol. *18*, 721–727.

Toledo, L.I., Altmeyer, M., Rask, M.-B., Lukas, C., Larsen, D.H., Povlsen, L.K., Bekker-Jensen, S., Mailand, N., Bartek, J., and Lukas, J. (2013). ATR Prohibits Replication Catastrophe by Preventing Global Exhaustion of RPA. Cell *155*, 1088–1103.

Tonotsuka, N., Hosoi, Y., Miyazaki, S., Miyata, G., Sugawara, K., Mori, T., Ouchi, N., Satomi, S., Matsumoto, Y., Nakagawa, K., et al. (2006). Heterogeneous expression of DNA-dependent protein kinase in esophageal cancer and normal epithelium. Int. J. Mol. Med. *18*, 441–447.

Trenz, K., Smith, E., Smith, S., and Costanzo, V. (2006). ATM and ATR promote Mre11 dependent restart of collapsed replication forks and prevent accumulation of DNA breaks. EMBO J. *25*, 1764–1774.

Tsuji, T., Sapinoso, L.M., Tran, T., Gaffney, B., Wong, L., Sankar, S., Raymon, H.K., Mortensen, D.S., and Xu, S. (2017). CC-115, a dual inhibitor of mTOR kinase and DNA-PK, blocks DNA damage repair pathways and selectively inhibits ATM-deficient cell growth in vitro. Oncotarget *8*, 74688–74702.

Uhrhammer, N., Bay, J.-O., and Bignon, Y.-J. (1998). Seventh International Workshop on Ataxia-Telangiectasia. Cancer Res. *58*, 3480–3485.

Vendetti, F.P., Lau, A., Schamus, S., Conrads, T.P., O'Connor, M.J., and Bakkenist, C.J. (2015). The orally active and bioavailable ATR kinase inhibitor AZD6738 potentiates the anti-tumor effects of cisplatin to resolve ATM-deficient non-small cell lung cancer in vivo. Oncotarget *6*, 44289–44305.

Vendetti, F.P., Karukonda, P., Clump, D.A., Teo, T., Lalonde, R., Nugent, K., Ballew, M., Kiesel, B.F., Beumer, J.H., Sarkar, S.N., et al. (2018). ATR kinase inhibitor AZD6738 potentiates CD8+ T cell-dependent antitumor activity following radiation. J. Clin. Invest. *128*, 3926–3940.

Vincent, A., Herman, J., Schulick, R., Hruban, R.H., and Goggins, M. (2011). Pancreatic cancer. Lancet Lond. Engl. *378*, 607–620.

Vo, Q.N., Kim, W.J., Cvitanovic, L., Boudreau, D.A., Ginzinger, D.G., and Brown, K.D. (2004). The ATM gene is a target for epigenetic silencing in locally advanced breast cancer. Oncogene *23*, 9432–9437.

Von Hoff, D.D., Ervin, T., Arena, F.P., Chiorean, E.G., Infante, J., Moore, M., Seay, T., Tjulandin, S.A., Ma, W.W., Saleh, M.N., et al. (2013). Increased survival in pancreatic cancer with nab-paclitaxel plus gemcitabine. N. Engl. J. Med. *369*, 1691–1703.

Waddell, N., Pajic, M., Patch, A.-M., Chang, D.K., Kassahn, K.S., Bailey, P., Johns, A.L., Miller, D., Nones, K., Quek, K., et al. (2015). Whole genomes redefine the mutational landscape of pancreatic cancer. Nature *518*, 495–501.

Wallez, Y., Dunlop, C.R., Johnson, T.I., Koh, S.-B., Fornari, C., Yates, J.W.T., Fernández, S.B. de Q., Lau, A., Richards, F.M., and Jodrell, D.I. (2018). The ATR Inhibitor AZD6738 Synergizes with Gemcitabine In Vitro and In Vivo to Induce Pancreatic Ductal Adenocarcinoma Regression. Mol. Cancer Ther. *17*, 1670–1682.

Wang, H., Yang, H., Shivalila, C.S., Dawlaty, M.M., Cheng, A.W., Zhang, F., and Jaenisch, R. (2013). One-step generation of mice carrying mutations in multiple genes by CRISPR/Cas-mediated genome engineering. Cell *153*, 910–918.

Wang, X.Q., Redpath, J.L., Fan, S.T., and Stanbridge, E.J. (2006). ATR dependent activation of Chk2. J. Cell. Physiol. *208*, 613–619.

Warren, N.J.H., and Eastman, A. (2019). Inhibition of checkpoint kinase 1 following gemcitabine-mediated S phase arrest results in CDC7- and CDK2-dependent replication catastrophe. J. Biol. Chem. *294*, 1763–1778.

Weber, A.M., Drobnitzky, N., Devery, A.M., Bokobza, S.M., Adams, R.A., Maughan, T.S., and Ryan, A.J. (2016). Phenotypic consequences of somatic mutations in the ataxia-telangiectasia mutated gene in non-small cell lung cancer. Oncotarget *7*, 60807–60822.

Wengner, A.M., Siemeister, G., Lücking, U., Lefranc, J., Wortmann, L., Lienau, P., Bader, B., Bömer, U., Moosmayer, D., Eberspächer, U., et al. (2020). The Novel ATR Inhibitor BAY 1895344 Is Efficacious as Monotherapy and Combined with DNA Damage–Inducing or Repair–Compromising Therapies in Preclinical Cancer Models. Mol. Cancer Ther. *19*, 26–38.

Westphal, C.H., Rowan, S., Schmaltz, C., Elson, A., Fisher, D.E., and Leder, P. (1997). atm and p53 cooperate in apoptosis and suppression of tumorigenesis, but not in resistance to acute radiation toxicity. Nat. Genet. *16*, 397–401.

Williamson, C.T., Miller, R., Pemberton, H.N., Jones, S.E., Campbell, J., Konde, A., Badham, N., Rafiq, R., Brough, R., Gulati, A., et al. (2016). ATR inhibitors as a synthetic lethal therapy for tumours deficient in ARID1A. Nat. Commun. *7*, 13837.

Wise, H.C., Iyer, G.V., Moore, K., Temkin, S.M., Gordon, S., Aghajanian, C., and Grisham, R.N. (2019). Activity of M3814, an Oral DNA-PK Inhibitor, In Combination with Topoisomerase II Inhibitors in Ovarian Cancer Models. Sci. Rep. *9*, 18882.

Witkiewicz, A.K., McMillan, E.A., Balaji, U., Baek, G., Lin, W.-C., Mansour, J., Mollaee, M., Wagner, K.-U., Koduru, P., Yopp, A., et al. (2015). Whole-exome sequencing of pancreatic cancer defines genetic diversity and therapeutic targets. Nat. Commun. *6*, 6744.

Xia, B., Sheng, Q., Nakanishi, K., Ohashi, A., Wu, J., Christ, N., Liu, X., Jasin, M., Couch, F.J., and Livingston, D.M. (2006). Control of BRCA2 cellular and clinical functions by a nuclear partner, PALB2. Mol. Cell *22*, 719–729.

Xiao, Z., Chen, Z., Gunasekera, A.H., Sowin, T.J., Rosenberg, S.H., Fesik, S., and Zhang, H. (2003). Chk1 Mediates S and G2 Arrests through Cdc25A Degradation in Response to DNA-damaging Agents. J. Biol. Chem. *278*, 21767–21773.

Yadav, B., Wennerberg, K., Aittokallio, T., and Tang, J. (2015). Searching for Drug Synergy in Complex Dose–Response Landscapes Using an Interaction Potency Model. Comput. Struct. Biotechnol. J. *13*, 504–513.

Yanai, M., Makino, H., Ping, B., Takeda, K., Tanaka, N., Sakamoto, T., Yamaguchi, K., Kodani, M., Yamasaki, A., Igishi, T., et al. (2017). DNA-PK Inhibition by NU7441 Enhances Chemosensitivity to Topoisomerase Inhibitor in Non-Small Cell Lung Carcinoma Cells by Blocking DNA Damage Repair. Yonago Acta Med. *60*, 9–15.

Yap, T.A., Luken, M.J. de M., O'Carrigan, B., Roda, D., Papadatos-Pastos, D., Lorente, D., Tunariu, N., Lopez, R.P., Gayle, S., Riisnaes, R., et al. (2015). Abstract PR14: Phase I trial of first-in-class ataxia telangiectasia-mutated and Rad3-related (ATR) inhibitor VX-970 as monotherapy (mono) or in combination with carboplatin (CP) in advanced cancer patients (pts) with preliminary evidence of target modulation and antitumor activity. Mol. Cancer Ther. *14*, PR14–PR14.

Yazinski, S.A., Comaills, V., Buisson, R., Genois, M.-M., Nguyen, H.D., Ho, C.K., Kwan, T.T., Morris, R., Lauffer, S., Nussenzweig, A., et al. (2017). ATR inhibition disrupts rewired homologous recombination and fork protection pathways in PARP inhibitor-resistant BRCA-deficient cancer cells. Genes Dev. *31*, 318–332.

You, Z., Shi, L.Z., Zhu, Q., Wu, P., Zhang, Y.-W., Basilio, A., Tonnu, N., Verma, I.M., Berns, M.W., and Hunter, T. (2009). CtIP Links DNA Double-strand Break Sensing to Resection. Mol. Cell *36*, 954–969.

Yu, X., and Chen, J. (2004). DNA damage-induced cell cycle checkpoint control requires CtIP, a phosphorylation-dependent binding partner of BRCA1 C-terminal domains. Mol. Cell. Biol. *24*, 9478–9486.

Yun, M.H., and Hiom, K. (2009). CtIP-BRCA1 modulates the choice of DNA double-strand-break repair pathway throughout the cell cycle. Nature *459*, 460–463.

Yurgelun, M.B., Chittenden, A.B., Morales-Oyarvide, V., Rubinson, D.A., Dunne, R.F., Kozak, M.M., Qian, Z.R., Welch, M.W., Brais, L.K., Da Silva, A., et al. (2019). Germline cancer susceptibility gene variants, somatic second hits, and survival outcomes in patients with resected pancreatic cancer. Genet. Med. *21*, 213–223.

Zeman, M.K., and Cimprich, K.A. (2014). Causes and Consequences of Replication Stress. Nat. Cell Biol. *16*, 2–9.

Zhang, F., Fan, Q., Ren, K., and Andreassen, P.R. (2009). PALB2 functionally connects the breast cancer susceptibility proteins BRCA1 and BRCA2. Mol. Cancer Res. MCR *7*, 1110–1118.

Zhao, Y., Thomas, H.D., Batey, M.A., Cowell, I.G., Richardson, C.J., Griffin, R.J., Calvert, A.H., Newell, D.R., Smith, G.C.M., and Curtin, N.J. (2006). Preclinical evaluation of a potent novel DNA-dependent protein kinase inhibitor NU7441. Cancer Res. *66*, 5354–5362.

Zhou, J., Enewold, L., Stojadinovic, A., Clifton, G.T., Potter, J.F., Peoples, G.E., and Zhu, K. (2010). Incidence rates of exocrine and endocrine pancreatic cancers in the United States. Cancer Causes Control *21*, 853–861.

Zhou, J.X., Feng, L.J., and Zhang, X. (2017). Risk of severe hematologic toxicities in cancer patients treated with PARP inhibitors: a meta-analysis of randomized controlled trials. Drug Des. Devel. Ther. *11*, 3009–3017.

Ziv, Y., Bielopolski, D., Galanty, Y., Lukas, C., Taya, Y., Schultz, D.C., Lukas, J., Bekker-Jensen, S., Bartek, J., and Shiloh, Y. (2006). Chromatin relaxation in response to DNA double-strand breaks is modulated by a novel ATM- and KAP-1 dependent pathway. Nat. Cell Biol. *8*, 870–876.

Zou, L., and Elledge, S.J. (2003). Sensing DNA Damage Through ATRIP Recognition of RPA-ssDNA Complexes. Science *300*, 1542–1548.